A THEORETICAL STUDY OF THE QUADRATIC ZEEMAN EFFECT

by

BERNARD ANTHONY KELLY

A thesis presented for the Degree of
Doctor of Philosophy of the University of London
and the Diploma of Membership of Imperial College

The Blackett Laboratory
Imperial College
London SW7

January 1982

ACKNOWLEDGEMENTS

The work presented in this thesis was carried out between September 1974 and August 1977 in the Physics Department of Imperial College, London, under the supervision of Dr. A.R. Edmonds. I offer Dr. Edmonds my most sincere thanks for his encouragement and guidance throughout the duration of this research. I am grateful to Professor W.R.S. Garton for access to his unpublished experimental results. My thanks are also due to Dr. E. Ortiz of the Mathematics Department of Imperial College for advice regarding the use of Chebyshev approximations. Finally, I wish to thank the Northern Ireland Department of Education for the award of a Postgraduate Studentship.

ABSTRACT

Recent experimental work on the quadratic Zeeman effect has indentified previously unobserved phenomena in certain atomic spectra. A theoretical investigation of these phenomena in the context of the Coulomb approximation requires the computation of large numbers of radial quadrupole integrals involving large principal quantum numbers and non-zero quantum defects. The well-known method of Bates and Damgaard breaks down in these circumstances, and alternative methods become unreliable.

This thesis describes a new method of computing the required radial integrals. The radial wavefunctions are evaluated very efficiently by means of recurrence relations and Chebyshev approximations; the integrals themselves are computed by means of Gauss-Laguerre quadrature. Although it was developed for use in calculations associated with the quadratic Zeeman effect, the new method has a much wider domain of applicability. It is effective with large or small principal quantum numbers; error bounds may be adjusted simply by setting a few parameters, and the speed of computation compares favourably with other methods in current use. In addition, the possibility of varying the lower limit of integration allows the testing of the validity of the Coulomb approximation itself, e.g. the effect of the deviation of the radial functions from Coulombic form in the region of the atomic core. In particular, the new computational method was used to investigate the reason for the breakdown of the Bates-Damgaard method at large principal quantum numbers; the results of this research are presented in this thesis.

Finally, the results of numerical calculations of the quadratic Zeeman effect in the spectra of Ba I are compared with experimental observations obtained by Garton and Tomkins. Very good agreement is obtained provided inter-n mixing is not too strong. Some of the previously unexplained features of the experimental spectra are reproduced.

CONTENTS PAGE

CONTENTS PAGE

LIST OF FIGURES

LIST OF TABLES

CHAPTER 1

INTRODUCTION

The search for a theoretical explanation of the magnetic structures of atomic spectra has been of interest to atomic spectroscopists ever since Zeeman's historic discovery in 1896 of the broadening of spectral lines when a sodium light source was placed between the poles of an electromagnet. In an attempt to explain Zeeman's observations, Lorentz developed the classical theory of the motion of a bound electron in a magnetic field. However, this theory failed to explain later investigations of the Zeeman effect carried out by Preston in 1898 and Paschen and Back in 1902. A more accurate account came in 1905 with Landé's development of the vector model of the atom. Later, when quantum mechanics was developed, these phenomena were treated more rigourously, and the (linear) Zeeman effect became an important tool in atomic physics.

In these early experiments the magnetic field $\underline{B}$ was sufficiently weak so that all observed Zeeman patterns were symmetrical about the field-free spectral lines, and the width of each pattern was proportional to B. Thus, in the early theoretical studies of the Zeeman effect, calculations were carried out to first order in B. Although it was well known that the Hamiltonian describing an atom in the presence of a uniform magnetic field contained a term proportional to B^2, this quadratic or diamagnetic term was usually dismissed as being of little practical significance (Condon and Shortley 1963, p150).

The influence of the diamagnetic term becomes observable only if very strong magnetic fields or highly excited atomic states are present. Under these circumstances the associated "quadratic Zeeman effect" can be studied.

1.1 HISTORICAL BACKGROUND

Since the introduction of Bohr's atomic theory various authors have discussed the importance of the diamagnetic term in the atomic Hamiltonian. The possibility of a quadratic Zeeman effect was pointed out by Herzfeld (1914) and discussed by Burgers (1919) in the framework of the old quantum theory. The first calculations by the methods of modern quantum mechanics were reported by Guth (1929), Halpern and Sexl (1929), and Van Vleck (1932). Using perturbation theory, these calculations showed that the first order energy shift due to the diamagnetic term was proportional to

$$\frac{n^2[5n^2 + 1 - 3l(l+1)][l(l+1) - 1 + m_l^2]}{(2l-1)(2l+3)} B^2, \qquad (1.1)$$

and would be appreciable only for highly excited states and magnetic fields large compared with those required to produce the Paschen-Back effect (Van Vleck 1932, p178).

Investigation of the quadratic Zeeman effect with reasonable field strengths thus required the development of long spectral series. Consequently the most extensive experimental studies have concerned long absorption series of alkalis and alkaline earths. The first quantitative measurements were given by Jenkins and Segrè (1939), who studied the effect in the principal series of Na I and K I. In the absence of a magnetic field they observed the sodium series in absorption up to n = 51 and the potassium series up to n = 43. When a transverse magnetic field of 27 kilogauss (kG) was applied the Zeeman effects were observed. For low n ($n \sim 10$) each line split into a triplet - the Paschen-Back triplets formed by the splitting of the very narrow $^2S - n^2P$ doublets, with the magnetic splitting much larger than the spin-orbit splitting of the n^2P term. For values of n from about 12 upwards the quadratic Zeeman shifts became measurable.

Up to about n = 20 the observed shifts agree well with the simple theoretical formula

$$\Delta \nu_a \ (cm^{-1}) = 4.98 \times 10^{-15} Z^{-2} n^4 (1 + m_\ell^2) B^2, \qquad (1.2)$$

obtained by specializing the more general formula (1.1). For the $\sigma^\pm$ components of transitions of the type $^2S - n^2P$, $m_p = \pm 1$, and for the π components $m_p = 0$. Beyond $n \sim 20$ a new perturbation appeared, ascribable to l-mixing, which caused broadening of the components and produced shifts which increased faster than the n^4 behaviour of (1.2).

Jenkins and Segrè also reported the onset of n-mixing, that is the overlap of the Zeeman patterns of adjacent n-values, and concluded that both σ and π components merged into an apparent continuum considerably before the free-field series limit was reached. Some of these observations were interpreted quantum mechanically by Schiff and Snyder (1939). They took the inter-l mixing between the ^2P and ^2F terms into account using perturbation theory. This mixing allowed $^2S - n^2P$ transitions, and the perturbations between the ^2P and ^2F terms lead to additional level shifts. Beyond n = 28, however, this approach was inadequate due to the onset of inter-n mixing. To account for n-mixing, Schiff and Snyder invoked the adiabatic approximation. However, this provided only a qualitative explanation of the observed phenomena.

The correctness of (1.1) was further tested by Harting and Klinkenberg (1949) who observed the principal series of K I, Rb I and Cs I in a magnetic field of 26 kG over a similar range of n-values. The agreement with theory was excellent; the separations between the higher P and F states are relatively larger in Rb I and Cs I than Na I, so that inter-l perturbations are less important - in agreement with observation.

The most recent, and to date the most detailed, investigation of the quadratic Zeeman effect was carried out by Garton and Tomkins. Aided by

significant improvements in experimental techniques, they were able to study the spectra of highly excited atoms of several species, including Ba I and Sr I, in fields ranging from 10 - 47 kG. A remarkably detailed set of absorption spectra were obtained. Moreover, transverse observations were made, separating the σ and π components by means of a Wollaston prism. Only a small part of this work has been published, namely that on the spectra of Ba I; measurements of all their plates are not yet available.

A series of observations on the $6s^2\,{}^1S_0 - 6snp\,{}^1P_1$ principal series of Ba I was reported in Garton and Tomkins (1969a). In the absence of the magnetic field the series could be observed up to n = 75. When a field of 24kG was applied the σ components were clearly observable in pairs. Up to about n = 31 inter-l mixing is negligible. Beyond that many additional lines appear due to inter-l mixing, their strengths rapidly increasing as n increases.

Above about n = 37 inter-n mixing sets in, and above n = 40 there is little trace of the free-field (Rydberg) structure. There are, however, striking regularities in the spectra in this region. In two distinct regions of the σ spectrum we observe sequences of regularly spaced lines at intervals of approximately $\frac{1}{2}\hbar\omega$, ω being the cyclotron frequency. Another system of very broad lines extends from just below the free-field series limit into the continuum; the spacing is again uniform and roughly equal to $\frac{3}{2}\hbar\omega$. Other regularities exist in the π spectrum, but these are still under investigation.

The theory of the quadratic Zeeman effect received negligible attention from atomic spectroscopists between the important experiments of Jenkins and Segrè in 1939 and those of Garton and Tomkins in 1969. Understandably, the novelty of the phenomena exhibited by the spectra of Garton and Tomkins has lead to a revival of interest in the subject. As

well as conventional quantum mechanical methods (Edmonds 1973), semi-classical methods have also been employed (Edmonds 1970, Starace 1973, Connerade 1974). However, the fact that the system of atom and magnetic field is inherently non-separable renders the computation of energies, wavefunctions and intensities very difficult, and little progress has been made to date.

1.2 RELATED STUDIES OF THE QUADRATIC ZEEMAN EFFECT

The quadratic Zeeman effect is also of interest to research workers in solid state physics and astrophysics.

The importance of strong magnetic fields in solid state phenomena has been recognised for some time. Soon after the discovery of magneto-optical phenomena (Haidemenakis 1969) in the early 1950's it became apparent that the structure of energy bands in solids could be studied by means of resonance spectroscopy - analogous to the approach used in the investigation of atomic structure. As in atomic spectroscopy, the application of a magnetic field lowers the symmetry of the system and permits the examination of resonance spectra by means of new theoretical models of the energy bands.

Of particular interest to solid state theorists has been the effect of very strong magnetic fields on the low spectral terms of the Balmer series of hydrogen. The reason is that, to a good approximation, the behaviour of excitons and impurities in semiconductors in the presence of magnetic fields may be inferred from calculations on an isolated hydrogen atom. In these hydrogen models the normal electron mass is replaced by the effective mass of the electron in the crystal and the normal hydrogen potential is decreased by the dielectric constant of the solid (Kohn and Luttinger 1955). For materials in which the effective electron mass is small and the dielectric constant is large, the effect

of the magnetic field is greatly magnified. Consequently, the quadratic Zeeman effect becomes appreciable, even in the low-lying energy levels, and results in an increase in the ionization energy at high fields (Yafet et al. 1956).

In view of the very strong effective magnetic fields which may arise in this way, most solid state theorists have concentrated on the so-called Landau regime, where the Coulomb interaction is small compared to the magnetic interactions. In these circumstances oscillations in the direction of the magnetic field are much slower than the cyclotron frequency. Thus the adiabatic approximation, introduced by Schiff and Snyder (1939), is appropriate. This approach was developed by Yafet et al. (1956) and extended by later authors, including Elliot and Loudon (1960), Hasegawa and Howard (1961), Zhilich and Monozon (1967), Larsen (1968) and Baldereschi and Bassani (1970). The magnetic fields involved in these calculations lie in the range 10^3 - 10^9 kG. For further details and references to this research see Haidemenakis (1969) or the review by Garstang (1977).

In astrophysics the behaviour of atoms in magnetic fields has been of interest ever since 1908, when Hale discovered the presence of magnetic fields in sunspots. However, a revival of interest in the subject has been stimulated by the discovery (Kemp et al. 1970) of circularly polarized continuum radiation from a white dwarf star. These observations have been interpreted as being due to a magnetic field of 10^4 kG at the surface of the star. Other observations (Landstreet and Angel 1971, Angel and Landstreet 1971, 1972) have indicated fields in excess of 10^3 kG in a number of white dwarfs. It is now believed that fields of the order of 10^9 kG may exist in neutron stars and pulsars (Lamb and Sutherland 1974). This follows from the suggestion that magnetic flux is conserved during stellar evolution (see, for example, Preston 1970) and this suggests that

any magnetic field in a star would vary as the square of the stellar radius.

Because of the intense magnetic fields and the abundance of hydrogen thought to be present in these stellar objects, further attention has been devoted to the study of the Landau regime in hydrogen. As in the solid state theory, the adiabatic approximation is widely used (Smith et al. 1972, Praddaude 1972, Canuto and Kelly 1972, Sturmelian et al. 1974). The other most commonly used approach is to express the wavefunctions of the system in terms of the free-field states and then determine the energy levels by diagonalizing a truncated Hamiltonian matrix. The results of such calculations for the low energy levels of hydrogen and helium have been reported by Garstang and Kemic (1972, 1974) and Kemic (1974). In these calculations magnetic fields in the range of 10^3 - 10^7 kG were assumed. Kemic (1975) has also studied the quadratic Zeeman effect in Ca II using perturbation theory.

Further references to the astrophysical literature may be found in the reviews by O'Connell (1974), Lamb and Sutherland (1974) and Garstang (1977).

1.3 SUMMARY OF THESIS

The research reported in this thesis began as an attempt to gain a theoretical understanding of the remarkably detailed absorption spectra obtained by Garton and Tomkins. Most of these spectra lie between the ranges of validity of the two main types of theory previously used to study the quadratic Zeeman effect, namely perturbation theory and the adiabatic method. The presence of a magnetic field and such high excitations makes the analysis of such spectra extremely difficult; the problem is inherently non-separable.

Following guidance from Dr. A.R. Edmonds the present author adopted

the approach of Schiff and Snyder, extending it to incorporate n-mixing. This involved the diagonalization of a Hamiltonian matrix, using basis functions taken from the Coulomb approximation, together with experimental quantum defects. Although this basis had the disadvantage of incompleteness (since the continuum states were ignored) it did not pose such formidable computational problems as some alternative bases. In any case, it was interesting to investigate when the neglect of the continuum states is permissible. The theory associated with this approach is described in Chapter 2.

The construction of the Hamiltonian matrix using free-field basis functions entails the computation of large numbers of radial quadrupole matrix elements with large principal quantum numbers and non-zero quantum defects. The well-known method of Bates and Damgaard (1949) breaks down in these circumstances. Earlier calculations by Dr. Edmonds (unpublished) obtained the required integrals by extrapolation from smaller principal quantum numbers (cf. Burgess and Seaton 1960, Peach 1965, 1967). However, the method was of doubtful validity, and the accuracy of the computed quadratic Zeeman spectra was difficult to assess.

Thus, before the effectiveness of the free-field basis could be investigated, it was first necessary to overcome the problem of computing the required radial integrals. A major part of the present author's contribution to this research area was the development of a suitable computational method for computing these integrals. In this method the radial Coulomb wavefunctions are evaluated very efficiently using recurrence relations and Chebyshev approximations, and the integrals are computed by means of Gauss-Laguerre quadrature. The associated numerical analysis is reported in Chapters 3 and 4.

Although the new method of computing radial integrals was first devised for use in calculations associated with the quadratic Zeeman effect,

it has a much wider domain of application. The analysis of Chapter 5 demonstrates that the method is effective with large or small principal quantum numbers; error bounds may be adjusted simply by setting a few parameters, and the speed of computation compares favourably with other methods in current use. As reported in Section 5.3, the possibility of varying the lower limit of integration has enabled the author to investigate why the Bates-Damgaard method breaks down at large principal quantum numbers.

In Chapter 6 we assess the validity of the theoretical approach proposed in Chapter 2. The energy levels and associated intensities of Ba I in the presence of magnetic fields in the range of 10 - 70 kG are obtained by diagonalizing a truncated Hamiltonian matrix. The physical significance of these results is discussed in the context of the experimental spectra of the $6s^2\ ^1S_0 - 6snp\ ^1P_1$ principal series of Ba I obtained by Garton and Tomkins. The computed results are in good agreement with the experimental spectra provided inter-n mixing is not too strong. Some previously unexplained regularities of the σ spectra are reproduced.

CHAPTER 2

FORMULATION OF THE QUADRATIC ZEEMAN PROBLEM

As outlined in the previous Chapter we shall confine our attention to the quadratic Zeeman effect on the spectra of alkali and alkaline-earth atoms. In the range of magnetic fields to be considered here we can ignore the effects of relativity and spin-orbit interactions, since these will be small in comparison with the Zeeman shifts. Indeed, since optical transitions occur without a change of spin, the spin angular momentum of the electron effectively does not enter our calculations at all.

In the non-hydrogenic species experimental data is available only for moderate magnetic fields, so that the quadratic Zeeman effect is appreciable only in highly excited states of the optical electron. The influence of the other electrons may be taken into account when using a one-electron approximation by including the empirical quantum defects in the calculation, or by modifying the radial electrostatic potential in the region of the atomic core. The consequences of configuration interaction (e.g. 5d8p interaction in Ba I) are more difficult to deal with. In general, however, interactions between the optical and 'core' electrons will be important only in the lower part of the energy spectrum and will have little effect on the local behaviour of the higher regions.

2.1 THE SCHRODINGER EQUATION

We will therefore consider the Hamiltonian of a spinless non-relativistic electron of mass μ and charge $-e$ in the presence of an attractive electrostatic potential $V(r)$ and a uniform magnetic field $\underline{B}$. If the direction of $\underline{B}$ is taken as the $\theta = 0$ axis of the usual polar co-ordinate system (r, θ, ϕ),

this Hamiltonian operator has the form

$$\mathcal{H} = \frac{p^2}{2\mu} + V(r) + \frac{eB}{2\mu c} l_z + \frac{e^2 B^2}{8\mu c^2} r^2 \sin^2\theta, \qquad (2.1)$$

where l_z is the operator for the component of orbital angular momentum along the magnetic field.

Since $\mathcal{H}$ commutes with l_z, the linear Zeeman term $\frac{eB}{2\mu c} l_z$ is a constant of the motion. It may therefore be omitted from our calculations provided the associated energy shift $\frac{eB}{2\mu c} m_l \hbar$ is taken into account, $m_l \hbar$ being the eigenvalue of the operator l_z. Our calculations are further simplified if atomic units are used. Thus we put

$$e = \hbar = \mu = 1, \quad c = 137.17.$$

In these units the cyclotron frequency, $\frac{eB}{\mu c}$, takes the value

$$\omega \text{ (a.u.)} = 4.2543 \times 10^{-10} B \text{ (Gauss)}, \qquad (2.2)$$

and the unit of energy is twice the ionization energy of hydrogen.

With these simplifications the basic Hamiltonian reduces to

$$\mathcal{H}(\omega) = \frac{p^2}{2} + V(r) + \frac{\omega^2}{8} r^2 \sin^2\theta. \qquad (2.3)$$

We note that the effect of the quadratic or diamagnetic term $\frac{\omega^2}{8} r^2 \sin^2\theta$ is to render $\mathcal{H}(\omega)$ inherently non-separable. It is this inseparability that gives rise to the interesting and difficult theoretical problems in the study of the quadratic Zeeman effect.

Since the quadratic term in (2.3) commutes with neither the free-field Hamiltonian $\mathcal{H}(0)$ nor the total orbital angular momentum operator L^2, it follows that n and l, the usual principal and orbital angular momentum quantum numbers of the free-field states, are no longer exactly defined; the only remaining 'good' quantum numbers in the presence of the magnetic field are the eigenvalues of the operators l_z and parity,

namely m_ℓ and $\tilde{\omega}$. The eigenstates of $\mathcal{H}$ may therefore be designated $\psi^{m_\ell \tilde{\omega}}(\underline{r})$, and the appropriate time-independent Schrodinger equation is

$$\left\{-\tfrac{1}{2}\nabla^2 + V(r) + \frac{\omega^2}{8} r^2 \sin^2\theta\right\} \psi^{m_\ell \tilde{\omega}} = E \psi^{m_\ell \tilde{\omega}} \qquad (2.4)$$

For given m_ℓ and $\tilde{\omega}$ the solution of (2.4) may be expanded in an infinite series of spherical harmonics. Thus we may write

$$\psi^{m_\ell \tilde{\omega}}(r, \theta, \phi) = \frac{1}{r} \sum_{\ell \geq |m|}^{(\tilde{\omega})} \phi_\ell^{m_\ell \tilde{\omega}}(r)\, Y_{\ell, m_\ell}(\theta, \phi), \qquad (2.5)$$

where $\Sigma^{(\tilde{\omega})}$ indicates that the sum is to be taken over even or odd ℓ according as the parity $\tilde{\omega}$ is even or odd. The spherical harmonic $Y_{\ell,m}(\theta,\phi)$ is defined by the equation

$$Y_{\ell,m}(\theta,\phi) = \sqrt{\frac{(2\ell+1)(\ell-m)!}{4\pi\,(\ell+m)!}}\, P_\ell^m(\cos\theta)\, e^{im\phi}, \qquad (2.6)$$

where P_ℓ^m denotes the associated Legendre polynomial (see Abramowitz and Stegun 1964).

On substituting (2.5) into (2.4) we obtain an infinite set of coupled differential equations for the radial functions $\phi_\ell^{m_\ell \tilde{\omega}}(r)$, namely

$$\sum_{\ell' \geq |m|}^{(\tilde{\omega})} \mathcal{H}_{\ell,\ell'} \phi_{\ell'}(r) = E \phi_\ell(r), \qquad \ell \geq |m|, \qquad (2.7)$$

where $\mathcal{H}_{\ell,\ell'}$ is the differential operator

$$\mathcal{H}_{\ell,\ell'} = \left\{-\frac{1}{2}\frac{d^2}{dr^2} + \frac{\ell(\ell+1)}{2r^2} + V(r)\right\} \delta_{\ell,\ell'} + Q_{\ell,\ell'} \qquad (2.8)$$

and

$$Q_{\ell,\ell'} = \frac{\omega^2}{8} r^2 \langle \ell\, m | \sin^2\theta | \ell'\, m \rangle. \qquad (2.9)$$

We note that the matrix elements $Q_{\ell,\ell'}$ are zero unless $|\ell - \ell'| = 0$ or 2, and may be computed easily by means of angular momentum algebra (see, for example, Edmonds 1968).

Cabib et al. (1971) obtained an approximate solution of (2.7) for

the ground state of hydrogen. They reduced (2.7) to a finite matrix eigenvalue equation by first truncating the infinite summation and then approximating the differential equations by difference equations. However, this approach is ill-suited when highly excited states are required, since the wave-functions which describe highly excited states are strongly oscillatory and have a large spatial extent. Thus they require large numbers of grid points for their discrete representation, and consequently lead to matrix equations of very high order.

2.2 EXPANSION OF THE RADIAL FUNCTIONS

An alternative approach is to reduce (2.7) to a set of algebraic equations by expanding $\phi_\ell(r)$. Although, in principle, any complete set of functions defined on the interval $(0, \infty)$ is valid for this purpose we should try to choose a basis which produces the greatest simplification of the corresponding matrix of $\mathcal{H}_{\ell,\ell'}$. In physical terms, this means that we should seek a separable Hamiltonian which closely approximates to $\mathcal{H}_{\ell,\ell'}$; the radial functions of this (separable) Hamiltonian, if they can be computed without too much difficulty, should then be used as a basis for $\phi_\ell(r)$.

We therefore try to split the effective potential $V(r) + \frac{\omega^2}{8} r^2 \sin^2\theta$ into the form $V_1(r) + V_2(r,\theta)$, and then consider the radial Schrodinger equation

$$\left\{ \frac{1}{2}\frac{d^2}{dr^2} - \frac{\ell(\ell+1)}{2r^2} - V_1(r) + \epsilon \right\} R(r) = 0. \qquad (2.10)$$

The complete set of solutions of this equation is the required basis.

The simplest splitting of the effective potential is to assign

$$V_1(r) = V(r) \quad \text{and} \quad V_2(r) = \frac{\omega^2}{8} r^2 \sin^2\theta. \qquad (2.11)$$

In this case (2.10) reduces to the radial Schrodinger equation describing the atomic system in the absence of a magnetic field.

If we assume that the energy spectrum of the free-field atom is known from experiment, and that the corresponding radial wavefunctions can be determined, and denote these quantities by $\epsilon_{n\ell}$ and $R_{n\ell}$ respectively, we may then, following Schiff and Snyder (1939), write the radial functions $\phi_\ell^{m\tilde{\omega}}(r)$ of equation (2.7) in the form

$$\phi_\ell^{m\tilde{\omega}}(r) = \sum_{n=\ell+1}^{\infty}(\tilde{\omega})\, C_{n\ell}^{m\tilde{\omega}}\, R_{n\ell}(r). \tag{2.12}$$

We note immediately that the set $R_{n\ell}(r)$, $n = \ell+1, \ell+2, \ldots$ does not form a complete set; the continuous states of the atom (those with positive energy) have been ignored. However, for sufficiently weak magnetic fields neglect of the continuum states is permissible; the extent to which it is permissible when the magnetic field is strong is not known. However, the free-field states will still be used here, since one of the objectives of the present author's research is to establish how important these continuum states are when the magnetic field is relatively strong.

From (2.7) and (2.12) we can easily derive the matrix eigenvalue equation

$$\sum_{n'>\ell'}\sum_{\ell'\geq|m|}(\tilde{\omega})\, H_{n\ell,n'\ell'}\, C_{n'\ell'}^{m\tilde{\omega}} = E\, C_{n\ell}^{m\tilde{\omega}}, \tag{2.13}$$

$$\ell = 0, 1, 2, \ldots \quad ; \quad n = \ell+1, \ell+2, \ldots, \tag{2.14}$$

where

$$H_{n\ell,n'\ell'} = \epsilon_{n\ell}\,\delta_{nn'}\,\delta_{\ell\ell'} + Q_{n\ell,n'\ell'}, \tag{2.15}$$

$$Q_{n\ell,n'\ell'} = \frac{\omega^2}{8}\langle n\ell|r^2|n'\ell'\rangle\langle \ell m|\sin^2\theta|\ell' m\rangle, \tag{2.16}$$

and

$$\langle n\ell|r^2|n'\ell'\rangle = \int_0^\infty R_{n\ell}(r)\, r^2\, R_{n'\ell'}(r)\, dr. \tag{2.17}$$

As remarked earlier $Q_{n\ell,n'\ell'} = 0$ unless $|\ell-\ell'| = 0$ or 2.

2.3 METHOD OF SOLUTION

In order to determine solutions to the eigenvalue equation (2.13) the Hamiltonian matrix $H_{n\ell,n'\ell'}$ must be diagonalized.

Consider first for simplicity the case of a hydrogen atom. In the absence of a magnetic field, the energy levels of a given principal quantum number n are degenerate in ℓ. This degeneracy is removed by Q. If the maximum energy shift produced by this term is small we may compute the effect easily: for any given value of n we compute the eigenvalue spectrum of the sub-matrix $H_{n\ell,n'\ell'}$, where $n = n'$ and $|m| \leq (\ell,\ell') < n$. The transformation which diagonalizes a given sub-matrix mixes states of different ℓ-values. Thus the eigenvectors of the perturbed system are linear combinations of hydrogenic states, each of definite ℓ-value.

If we are studying the principal series of an atom with optical transitions to or from the ground state ($6s^2\ ^1S_0$ in the case of Ba) the selection rule $|\ell - \ell'| = 1$ implies that only excited states with $\ell = 1$ contribute to intensity. Thus, intensities are given by the square moduli of the coefficients of 'p' states in the above eigenvectors.

In the hydrogenic spectra of atoms other than hydrogen (e.g. the principal series of Ba I) we no longer have complete degeneracy in ℓ, even when a magnetic field is not present. Thus the computation of the matrix elements $H_{n\ell,n'\ell'}$ must allow for the relevant quantum defects. In the case of Ba the quantum defects of 'p' states in the range of n values considered in the present study may be written as $4 + \alpha$, where α is a positive or negative quantity small compared with one; the quantum defects of states of higher ℓ-values are assumed to be zero (see Garton and Tomkins 1969b). Thus we may expect to achieve satisfactory results by relabelling 'p' states of different n and applying the procedure described above. This approach was adopted by Schiff and Snyder (1939) in a study of the quadratic Zeeman effect in Na I and K I.

Clearly the sub-matrix approach described above is valid only when the quadratic Zeeman shifts are small in comparison with the energy differences of neighbouring free-field states.

Dr. Edmonds has found that such calculations for the σ spectrum of Ba I give good agreement with the experimental results of Garton and Tomkins for n-values between 26 and 34. The dominance of the lines of maximum shift over their associated groups of satellite lines was well reproduced. We note that the matrix elements of r^2 are roughly proportional to B^2 and n^4.

In an attempt to explain the behaviour of higher members of the Garton-Tomkins spectra the present author adopted the natural extension of the method of Schiff and Snyder, taking into account the sub-matrices of the Hamiltonian matrix (2.14) linking different values of n. In practice this involved truncating the Hamiltonian matrix $H_{nl,n'l'}$ such that only a finite range of n values was included, i.e. $n_{min} \leq n, n' \leq n_{max}$.

However, the entry of quantum defects introduces difficulty into the calculation of the radial integrals $\langle nl | r^2 | n'l' \rangle$ when n, n' become large. The established method of Bates and Damgaard breaks down under these circumstances (Oertel and Shomo 1968), and alternative methods become unreliable or very inefficient.

Before the adopted approach (using free-field Coulomb basis functions) could be fully evaluated a suitable method was required for computing large numbers of radial quadrupole integrals. As described in detail in the next Chapter, the author has developed such a computational method.

In Chapter 6 we describe in detail the methods used to compute the theoretical energy levels and intensities of the principal series of Ba I in magnetic fields in the range of 10 - 70 kG. The computed spectra are compared with the experimental results obtained by Garton and Tomkins (1969a).

CHAPTER 3

COMPUTATION OF RADIAL INTEGRALS IN THE COULOMB APPROXIMATION

Following the discussion of the preceding Chapter it is clear how the present study of the quadratic Zeeman effect gave rise to the problem of computing large numbers of radial integrals of the form

$$\langle n\ell | r^2 | n'\ell' \rangle = \int_0^\infty R_{n\ell}(r)\, r^2\, R_{n'\ell'}(r)\, dr, \qquad (3.1)$$

$\frac{1}{r} R_{n\ell}(r)$ being the radial wavefunction which describes the free-field bound state $|n\ell m\rangle$. In practical calculations the integrals involved states of neutral alkali and alkaline earth atoms with very large principal quantum numbers. In the case of Ba I these states were given in terms of very detailed and accurate tables of experimental quantum defects (Garton and Tomkins 1969b) with n, n′ in the range 25-75.

The large principal quantum numbers involved in these integrals, together with the fact that the quadrupole operator r^2 emphasised the large values of r, implied that the Coulomb approximation for the radial functions might be appropriate. The large principal quantum numbers also implied that the simple normalization convention of Hartree (1928) would be adequate.

Attention was therefore turned to the Bates-Damgaard method (Bates and Damgaard 1949) as a prospective means of computing the required integrals. However, as pointed out by Oertel and Shomo (1968), the computational scheme used in the Bates-Damgaard method breaks down for sufficiently large n, n′, due to the accumulation of rounding errors in the summation of an alternating series. In trial calculations, which were carried out using double precision arithmetic on a CDC 6400 computer (i.e.using about

29 significant decimal digits), the Bates-Damgaard method gave reliable results only for n, n' up to about 25.

Several alternative methods of computing (3.1) were evaluated (Friedrich et al. 1970, Lindgård and Nielsen 1976). Although these methods were designed to overcome limitations of the Bates-Damgaard method they too were found to be ineffective when n, n' became large ($\gtrsim$ 15).

The present author therefore began a search for a new method of computing the required integrals. This research led to the development of a powerful new technique, based upon Gauss-Laguerre quadrature; the Coulomb wavefunctions in the integrand were evaluated by means of convergent Chebyshev expansions and recurrence relations. The details of these techniques are discussed later in this Chapter and in the following Chapter. A discussion of the efficiency and accuracy of the new method is presented in Chapter 5.

As we shall explain in the subsequent discussion, the new method became more than just a means of computing integrals for use in calculations of the quadratic Zeeman effect; it provided a means of investigating the Coulomb approximation itself. In particular, it enabled the author to carry out a thorough investigation of the behaviour of the Bates-Damgaard method when n,n' are large. Although Oertel and Shomo (1968) had established that the Bates-Damgaard method breaks down at large n,n', they did not determine which part of the numerical procedure gives rise to the numerical errors. The results of this application of the new method are reported in Chapter 5.

The problems associated with the computation of radial integrals involving Coulomb wavefunctions with large principal quantum numbers did not arise in previous studies of the quadratic Zeeman effect. In

previous studies either quantum defects did not enter the calculations, so that hydrogenic wavefunctions and associated analytic formulas could be used in the computation of radial integrals; or the quadratic Zeeman effect was only of interest in the low energy states. A brief review of these studies is given in Garstang (1977).

In recent years, interest in the calculation of Coulomb wavefunctions and associated integrals involving large principal quantum numbers has arisen in another context. Recent experiments in laser spectroscopy have required the analysis of empirical data on highly excited atomic systems involving principal quantum numbers in the range of 20-60 (see, for example, Andersen et al. 1975, Ducas et al. 1975, Risley and Jebule 1975, Stebbings et al. 1975, Littman et al. 1976). The new computational schemes proposed in this and the following Chapter should also be applicable in these circumstances.

The remainder of the present Chapter is organised as follows. In Section 3.1 we present a summary of the Coulomb approximation and associated equations. Sections 3.2 and 3.3 contain a brief review of the Bates-Damgaard method, explaining why it is inappropriate in the context of large principal quantum numbers. Alternative methods are reviewed in Section 3.4 Finally, in Section 3.5, we formulate equation (3.1) in terms of Gauss-Laguerre quadrature.

3.1 THE COULOMB APPROXIMATION

We consider a single excited electron is an atomic system with nuclear charge Z and N + 1 electrons, and suppose that this electron moves in a central potential V(r). We assume that V(r) depends on the structure of the atomic core for $r < r_1$, and takes the Coulomb form $-\frac{Z}{r}$

(in atomic units) for $r \geq r_1$, where $z = Z-N$ and r_1 is the core radius of the atomic system (see, for example, Brooks and Ham 1958, for typical values of r_1 for the alkalis). We further assume that the energy spectrum of the system is known from spectroscopic data, but that the form of V(r) for small r is generally not known.

It is well known that the radial wavefunction for the above system can be written in the form $\frac{1}{r} R(r)$, where R(r) satisfies the differential equation

$$\left\{ -\frac{1}{2}\frac{d^2}{dr^2} + \frac{\ell(\ell+1)}{2r^2} + V(r) - E \right\} R(r) = 0, \qquad (3.2)$$

and the normalization condition

$$\int_0^\infty [R(r)]^2 dr = 1. \qquad (3.3)$$

For $E < 0$, solutions of (3.2) which are everywhere bounded and continuous exist only for discrete values of the energy E. For $E \geq 0$, however, such solutions exist for all values of E, forming a continuous spectrum.

Following Seaton (1966) we label the discrete eigenenergies of (3.2) by n and ℓ, the usual principal and angular quantum numbers respectively, and express $E_{n\ell}$ in terms of the effective principal quantum number $\nu_{n\ell}$ and quantum defect $\mu_{n\ell}$ by the equations

$$E_{n\ell} = -\frac{z^2}{2\nu_{n\ell}^2}, \qquad \nu_{n\ell} = n - \mu_{n\ell}, \qquad (3.4)$$

$$n = 1, 2, 3, \ldots \text{ and } \ell = 0, 1, \ldots, n-1.$$

Hartree (1928) showed that if V(r) does not differ appreciably from its asymptotic form $-\frac{z}{r}$, the bound state radial function $R_{n\ell}(r)$ has the approximate form

$$R_{n\ell}(r) \underset{r\to\infty}{\sim} K(\nu,\ell)\, W_{\nu,\ell+1/2}\left(\frac{2Zr}{\nu}\right), \tag{3.5}$$

where W denotes the irregular Whittaker function (Abramowitz and Stegun 1964) and $K(\nu,\ell)$ is a normalization factor.

By analogy with the hydrogenic radial functions Hartree (1928) proposed the assignment

$$K(\nu,\ell) = Z^{1/2}\left[\nu^2\,\Gamma(\nu+\ell+1)\,\Gamma(\nu-\ell)\right]^{-1/2}. \tag{3.6}$$

However, many authors have suggested ways in which this factor should be modified. For instance, Seaton (1958) has shown that, in the context of the quantum defect method, the appropriate normalization factor should be

$$K(\nu,\ell) = Z^{1/2}\left[\nu^2\,\xi(\nu)\,\Gamma(\nu+\ell+1)\,\Gamma(\nu-\ell)\right]^{-1/2}, \tag{3.7}$$

where

$$\xi(\nu) = 1 + \frac{\partial\mu}{\partial\nu} = 1 + \frac{Z^2}{\nu^3}\frac{\partial\mu}{\partial E}. \tag{3.8}$$

Other forms of $K(\nu,\ell)$ have been suggested by Armstrong and Purdum (1966), Foldy (1958) and others. However, if the quantum defect varies slowly with the energy, most of these normalization factors reduce to the Hartree formula (3.6) when ν is large.

We note that the assumptions concerning the one-electron potential governing the interaction between the valence (or optical) electron and the core imply that the following interactions are neglected:

(a) Correlations between different electrons within the core, and between core electrons and the valence electron. This leads to polarization of the core - the induction of

a dipole moment leading to a polarization potential of the asymptotic form $\alpha/2r^4$ $(r \to \infty)$ (see Abramowitz and Stegun 1964).

(b) Spin-orbit interactions .

(c) Configuration interactions.

3.2 THE BATES-DAMGAARD METHOD

The typical radial integral involving the operator r^s is of the form

$$I_s = \langle n\ell | r^s | n'\ell' \rangle = \int_0^\infty R_{n\ell}(r)\, r^s\, R_{n'\ell'}(r)\, dr. \qquad (3.9)$$

The case s = 0 arises in overlap and normalization integrals; in the dipole case (s = 1) we have $|\ell - \ell'| = 1$; in the quadrupole case (s = 2), which arises in the quadratic Zeeman effect, we have $|\ell - \ell'| = 0$ or 2, though $\ell = \ell' = 0$ is excluded. All values of n, n' may arise.

Bates and Damgaard (1949) suggested a method of calculating such radial integrals in the context of the Coulomb approximation. Although their method was developed as a means of computing I_s for the case s = 1, its principles are equally valid for s = 0,1,2,..... The main arguments of Bates and Damgaard are summarized below.

The basic postulate of the Bates-Damgaard method is that, when calculating radial dipole matrix elements, the contribution to the matrix element arising from small radial distances can be neglected. The method utilises the known experimental term values of the active electron to construct an asymptotic Coulomb wavefunction (of the form (3.5)) which is accurate at large radial distances. The radial integral is evaluated using two such wavefunctions.

Thus the Bates-Damgaard approximation to the integrand of I_s is

$$R_{n\ell}(r)\, r^s\, R_{n'\ell'}(r)$$

$$\underset{r\to\infty}{\sim} K(\nu,\ell)\, K(\nu',\ell')\, W_{\nu,\ell+\frac{1}{2}}\left(\frac{2zr}{\nu}\right) r^s\, W_{\nu',\ell'+\frac{1}{2}}\left(\frac{2zr}{\nu'}\right). \quad (3.10)$$

The Whittaker functions can now be replaced by asymptotic expansions of the form

$$W_{\nu,\ell+\frac{1}{2}}\left(\frac{2zr}{\nu}\right)$$

$$\underset{r\to\infty}{\sim} e^{-\frac{zr}{\nu}} \left(\frac{2zr}{\nu}\right)^{\nu} \left\{ \sum_{i=0}^{\infty} \frac{(\ell+1-\nu)_i\,(-\ell-\nu)_i}{i!} \left(-\frac{\nu}{2zr}\right)^i \right\}, \quad (3.11)$$

where the notation $(x)_i$ refers to the Pochhammer symbol, which is defined by the equations

$$(x)_{i+1} = (x+i)\,(x)_i, \quad i = 0, 1, 2, \ldots \text{ and } (x)_0 = 1. \quad (3.12)$$

Using (3.11) the Bates-Damgaard approximation to the integrand of I_s becomes

$$R_{n\ell}(r)\, r^s R_{n'\ell'}(r)$$

$$\underset{r\to\infty}{\sim} f \sum_{i=0}^{\infty}\sum_{j=0}^{\infty} (-1)^{i+j}\, a_i\, a'_j \left(\frac{\nu}{2z}\right)^i \left(\frac{\nu'}{2z}\right)^j e^{-\alpha r}\, r^{\beta-i-j-1}, \quad (3.13)$$

where $$f = K(\nu,\ell)\, K(\nu',\ell') \left(\frac{2z}{\nu}\right)^{\nu} \left(\frac{2z}{\nu'}\right)^{\nu'}, \quad (3.14)$$

$$\alpha = z\left(\frac{1}{\nu} + \frac{1}{\nu'}\right), \quad (3.15)$$

$$\beta = \nu + \nu' + s + 1, \quad (3.16)$$

$$a_i = \frac{(\ell+1-\nu)_i\,(-\ell-\nu)_i}{i!}, \quad (3.17)$$

and $a_i = a'_i$ with ν, ℓ replaced by ν', ℓ' respectively.

Bates and Damgaard ignored all terms in (3.13) containing r^k $(k < 2)$ and performed term-byterm integration over the range (o, ∞) on the remaining terms, giving the approximation

$$I_s^{BD} =$$

$$f \sum_{i=o}^{i+j \le k_m} \sum_{j=o} (-1)^{i+j} a_i a'_j \left(\frac{\nu}{2z}\right)^i \left(\frac{\nu'}{2z}\right)^j \alpha^{i+j-\beta} \Gamma(\beta - i - j), \quad (3.18)$$

where $$k_m = [\nu + \nu'] + s - 2. \quad (3.19)$$

The reason given by Bates and Damgaard for choosing $k_m = [\nu+\nu'] + s - 2$ was that this truncation criterion was equivalent to neglecting the singularity in the Whittaker function at $r = 0$; although (3.13) was integrated over the entire range (o, ∞), it was argued (Bates and Damgaard 1949, p104) that, since the maxima of all terms in the integrand having the form $\tau^{\beta - i - k}$ lie within the "core radius" if $k > k_m$, truncating (3.13) at $k = k_m$ was equivalent to neglecting the contribution to I_s which arises from the region of $0 \le \tau \le \tau_m$, where

$$\tau_m = \frac{\xi \nu \nu'}{z(\nu + \nu')}, \qquad 1 < \xi < 2. \quad (3.20)$$

The Bates-Damgaard method has been widely used and has achieved considerable success, often yielding results which agree with experiment better than those calculated by self-consistent-field methods. It is particularly effective for non-equivalent electrons and for highly excited states, since in these cases the contribution to the integral from large radial distances is enhanced. However, as we shall discuss later in this Section, it breaks down for numerical reasons when n, n' become sufficiently large.

Clearly the Bates-Damgaard approximation is equivalent to

$$I_s(n\ell, n'\ell') \approx J_s(\nu\ell; \nu'\ell'; r_0),$$

where

$$J_s(\nu\ell; \nu'\ell'; r_0) = K(\nu,\ell)K(\nu',\ell')\int_{r_0}^{\infty} W_{\nu,\ell+\frac{1}{2}}\left(\frac{2zr}{\nu}\right) r^s W_{\nu',\ell'+\frac{1}{2}}\left(\frac{2zr}{\nu'}\right) dr. \quad (3.21)$$

We note however that the lower limit of integration, r_0, is not introduced explicitly into the computational algorithm of the Bates-Damgaard method.

The validity of the Coulomb approximation and the Bates-Damgaard method have been discussed by several authors, including Layzer and Garstang (1968), Crossley (1969) and Sobel'man (1972). The important question of polarization of the core has been studied by Norcross (1973) and that of normalization by Seaton (1958). These analyses have shown that if n and n' exceed the principal quantum numbers of the core electrons, we may expect, for $s > 0$, that the Coulomb approximation (3.21) is acceptable. More precisely, we expect a small relative variation of J_s when r_0 varies between the "core radius", r_1, and the inner turning points of the states $|n\ell\rangle$ and $|n'\ell'\rangle$. However, as remarked by Layzer and Garstang (1968,pp472-82), for a given species certain values of $n\ell$, $n'\ell'$ may exist for which strong cancellation occurs in the outer part of the integral. In such cases the relative error given by the Coulomb approximation may be high, though it may be perfectly adequate for neighbouring $n\ell$, $n'\ell'$ where such cancellation does not occur.

3.3 INTEGRALS WITH LARGE PRINCIPAL QUANTUM NUMBERS

As regards the calculation of radial quadrupole integrals in the context of the quadratic Zeeman effect, the assumptions of the Coulomb

approximation and the Bates-Damgaard method seemed appropriate: the large principal quantum numbers involved and the presence of the quadrupole operator r^2 both emphasised the contribution from the large values of r. Moreover, the quantum defects of the atomic states of Ba I were available from the experimental results of Garton and Tomkins (1969b). In view of the highly excited states involved it seemed reasonable to assume that the simple normalization convention of Hartree (1928) would be adequate, and that polarization effects could be neglected.

However, as pointed out by Oertel and Shomo (1968), the Bates-Damgaard method breaks down if the principal quantum numbers n, n' are sufficiently large. This is due to the accumulation of rounding errors in the summation of the series (3.18), whose terms increase in magnitude and alternate in sign as n, n' increase. Oertel and Shomo found that the domain of validity of the Bates-Damgaard method depends upon the word length of the computer used to evaluate (3.18) and upon the desired accuracy of the required integrals: when $n + n \leq 10$ dipole transitions integrals could be computed with an accuracy of four significant figures using a computer with a precision of fourteen decimal digits. The present author has found that when double precision arithmetic is used on a CDC 6000 series computer (i.e. using 29 significant decimal digits) results which are accurate to within four significant figures can be obtained provided $n, n' \lesssim 25$.

Thus the Bates-Damgaard method was of little practical value in the present study of the quadratic Zeeman effect, where integrals involving n, n' up to about 60 were required. An alternative method of computation was essential.

We note that extrapolation of the Bates-Damgaard results to higher n, n' is possible in principle (see, for example, Seaton 1958, Burgess and

Seaton 1960, Peach 1965, 1967) and has been tried by Dr. A.R. Edmonds. He found that the accuracy of the calculations was difficult to assess and the method seemed ill-suited to the task of computing automatically very large numbers of integrals.

3.4 CHOICE OF NUMERICAL QUADRATURE

In view of the numerical difficulties associated with the Bates-Damgaard method the author began a search for a satisfactory method of numerical quadrature for computing the required radial integrals. In judging the numerical methods tested the following criteria were adopted:

(i) The method (assuming appropriate adjustment of such parameters as the number of abscissae in the quadrature formula) should be capable of computing accurately and efficiently integrals involving n, n' up to about 60, and should accomodate any reasonable values of quantum defects, angular quantum numbers ℓ, ℓ' and positive powers of r.

(ii) It should be possible to choose parameters so that the accuracy of computation is high enough to exclude errors other than those due to experimental uncertainties in the quantum defects, or inadequacies in the physical assumptions (for example, that of the "frozen core" approximation). In particular, it should be possible to vary the lower cut-off point, which is inherent in the Coulomb approximation, and study the effect on the computed integrals.

(iii) In the region of n, n' where the Bates-Damgaard method is effective the new method should, when set for comparable

accuracy, have a similar or faster speed of execution. In general, the computing time should not increase too fast with increase of n, n'.

(iv) The method should, if possible, give accurate results for small as well as large n, n' and allow for modification of the radial functions or the operator r^s due, for example, to taking polarization effects into account.

Previous work aimed at an accuracy of computation superior to that of the Bates-Damgaard method failed to meet these criteria.

Friedrich et al. (1970) computed I_s by equal-interval quadrature, using asymptotic series of the form (3.11) to evaluate the Whittaker functions in the integrand. But (3.11) becomes invalid when r is small, due to truncation errors. It also breaks down when r is large due to the very large absolute values attained by terms of the series; the associated numerical cancellations lead to disastrous rounding errors. Our calculations have shown that this method of equal-interval quadrature becomes very inefficient when $n, n' \gtrsim 20$, due to the large number of abscissae required (see Section 5.2.5).

Lindgård and Nielsen (1975) had the same aim as our own, namely to extend the computation of radial integrals to large n, n'. They used a method of equal-interval quadrature in which the Whittaker functions were evaluated by integrating the defining radial differential equation

$$\left\{ \frac{d^2}{d\tau^2} - \frac{\ell(\ell+1)}{\tau^2} + \frac{2z}{\tau} - \frac{z^2}{\nu^2} \right\} W_{\nu,\ell+\frac{1}{2}}\left(\frac{2z\tau}{\nu}\right) = 0 \qquad (3.21a)$$

using the Numerov method. This approach failed to meet our criteria for several reasons: many steps are needed in the integration, particularly for large values of n, n' ; each determination of the radial function requires a normalization computation. Furthermore, the accuracy of

computation of the radial function at small r may be inadequate unless great care is taken. Finally the range of integration (r_o, r_{max}) must increase roughly as $n \times n'$, if $n, n' \gtrsim 10$, in order to maintain a given accuracy. Thus this method becomes very inefficient when n, n' become large.

It should be emphasised that it was not possible to investigate fully the numerical behaviour of either of the quadrature methods outlined above, since all existing methods become unreliable as soon as n, n' exceed 15 or so. As we shall discuss in Chapter 5, their behaviour could only be investigated fully when a method existed which adequately satisfied the criteria outlined at the beginning of this Section. Such a method, based upon Gauss-Laguerre quadrature, has been developed by the author: it is introduced in the following Section. In Chapter 5 this new method is compared with those of Friedrich et al. and Lindgård and Nielsen.

3.5 INTEGRATION BY GAUSS-LAGUERRE QUADRATURE

Because of the form of the integrand (3.10) a search for a quadrature formula for computing I_s leads naturally to that of Gauss-Laguerre (Stroud and Secrest 1966). To help explain why this is so it is convenient to introduce the auxiliary function, $F_{\kappa,m}(x)$, defined by the equation (cf. Miller 1966)

$$F_{\kappa,m}(x) = e^{x/2} x^{-\kappa} W_{\kappa,m}(x). \qquad (3.22)$$

$F_{\kappa,m}(x)$ has slower variation and simpler asymptotic behaviour than $W_{\kappa,m}(x)$. In terms of auxiliary functions (3.21) may be written in the form

$$J_s = u \int_{r_0}^{\infty} e^{-\alpha r} r^{\beta-1} F_{\nu,\ell+\frac{1}{2}}\left(\frac{2zr}{\nu}\right) F_{\nu',\ell'+\frac{1}{2}}\left(\frac{2zr}{\nu'}\right) dr, \tag{3.23}$$

where we have used the substitution

$$u = K(\nu,\ell)\, K(\nu',\ell') \left(\frac{2z}{\nu}\right)^{\nu} \left(\frac{2z}{\nu'}\right)^{\nu'}. \tag{3.24}$$

α and β have been defined by equations (3.15) and (3.16) respectively.

In order to put (3.23) into the correct form for the application of Gauss-Laguerre we change the variable of integration to $x = \alpha(r - r_0)$. (3.23) then reduces to

$$J_s = u \int_0^{\infty} e^{-x} q(x)\, dx, \tag{3.25}$$

where

$$q(x) = \frac{e^{-\alpha r_0}}{\alpha} r^{\beta-1} F_{\nu,\ell+\frac{1}{2}}\left(\frac{2zr}{\nu}\right) F_{\nu',\ell'+\frac{1}{2}}\left(\frac{2zr}{\nu'}\right). \tag{3.26}$$

Application of the Mth order of G-L quadrature formula now gives (see Erdélyi 1953, Krylov 1962, or Stroud and Secrest 1966)

$$J_s = u \left\{ \sum_{i=1}^{M} \lambda_{iM}\, q(x_{iM}) + R_M(q) \right\}. \tag{3.27}$$

The zeros x_{iM} and weights λ_{iM} of the Laguerre polynomial $L_M(x)$ are defined by the equations

$$\lambda_{iM} = \frac{1}{x_{iM} [L'_M(x_{iM})]^2}, \tag{3.28}$$

$$L_M(x_{iM}) = 0, \qquad i = 1, 2, \ldots, M. \tag{3.29}$$

In equation (3.27) the term $R_M(g)$ is a remainder term which tends to zero as M tends to infinity: $R_M(g)$ is given by the well-known formula

$$R_M(g) = \frac{1}{(2M)!} \frac{d^{2M}}{d\xi^{2M}} g(\xi). \qquad (3.30)$$

In practical calculations M must be chosen sufficiently large such that $R_M(g)$ is sufficiently small. J_s is then computed using the approximation

$$J_s \approx u \sum_{i=1}^{M} \lambda_{iM} g(x_{iM}). \qquad (3.31)$$

Clearly any numerical evaluation of J_s using (3.31) involves the computation of 2M values of the auxiliary function F or the Whittaker function W. When ν, ν' are large ($\gtrsim$ 15) the computation of these functions leads to numerical problems similar to those which arise in the method of Lindgård and Nielsen (see Section 3.4 above). However, as described in the next Chapter, the author has developed a new method of computing these functions which is particularly effective when ν, ν' are large.

In Chapter 5 we return to a discussion of the accuracy and efficiency of the Gauss-Laguerre approximation (3.31).

CHAPTER 4

COMPUTATION OF THE WHITTAKER FUNCTION $W_{k,m}(x)$

The discussion of the previous Chapter focussed upon the choice of quadrature formula for computing $I_s(\nu l; \nu' l'; t_0)$. However, in practice, the most difficult aspect of any numerical method of integration is the evaluation of the integrand at the quadrature points. In the present case the integrand involves the irregular Whittaker function $W_{k,m}(x)$ which is well-known to be a difficult function to evaluate, especially when the parameter k is large and the argument x spans a wide range of values. In these circumstances existing computational techniques become inaccurate or require excessive computing time. Although there are many theoretical approximations of $W_{k,m}(x)$ (Slater 1960), very few of them are of any value in practical calculations.

A considerable part of the present author's research was therefore devoted to a search for a suitable numerical method for computing $W_{k,m}(x)$ when $x > 0$ and $15 \leq k \leq 60$. The outcome of this work was the development of a very powerful numerical technique, based upon the use of a recurrence relation involving three contiguous Whittaker functions, together with Chebyshev expansions of the starting functions. This technique, and the computational algorithms developed for its implementation, are the subject of this Chapter. As we will discuss in the next Chapter, the existence of such an accurate and efficient technique for computing $W_{k,m}(x)$ was of crucial importance in enabling the development of a method of numerical quadrature which satisfied the criteria stipulated in Section 3.4.

4.1 INTRODUCTION

In the context of the Coulomb approximation and the quadratic Zeeman effect the parameter k of $W_{k,m}(x)$ corresponds to the effective principal quantum number, labelled ν in the previous Chapter; it may take any value in the range 15-60. The parameter m corresponds to $\ell + \frac{1}{2}$, where ℓ is the angular momentum quantum number and takes the integer values 0,1,2,..... When ℓ is greater than 2 or 3 the quantum defect is usually negligible; in this case k differs little from an integer and the Whittaker function simplifies to a polynomial. The proposed algorithm takes this case into account.

Although the techniques described in this Chapter have been developed primarily for the calculation of radial wavefunctions in the Coulomb approximation, their use is not limited to the range of parameters described above. For example, restriction of the parameter m to half-odd-integer values is not necessary; neither is the restriction $k > 15$.

The importance of the wide domain of applicability of the proposed technique arises from the fact that the Whittaker function appears in other contexts of physical interest; for example in line broadening theory (see Lisitsa and Sholin 1972, Tran-Minh et al. 1976), when k may take negative values, although the magnitudes of k and m are not large. $W_{k,m}(x)$ also appears in calculations of multichannel electron scattering (Dourneuf and Ky Lan 1977) in which m, k and x satisfy the conditions

$$-4 < k < 100 , \qquad \tfrac{1}{2} \leq m \leq \tfrac{3}{2} \quad \text{and} \quad 0 < x < 50.$$

The applicability of the proposed algorithms in these contexts is discussed in Section 4.7.

The remainder of this Chapter is organised as follows. In the next Section we present some of the background theory and properties of the Whittaker function $W_{k,m}(x)$; this will be used in the later discussion.

A critique of existing methods of computing $W_{k,m}(x)$ is presented in Section 4.3. Then, in Sections 4.4, 4.5 and 4.6 we present the proposed algorithms for computing $W_{k,m}(x)$. Section 4.5 also contains a discussion of the accuracy and efficiency of the new algorithm.

4.2 RELEVANT PROPERTIES

Before discussing the details of the proposed computational procedures we introduce some of the relevant properties of the Whittaker function. These properties will be used in the subsequent discussion. For a discussion of the associated theory the reader should consult Erdélyi (1953), Slater (1960), Abramowitz and Stegun (1964), or Whittaker and Watson (1946). Only a summary of useful results is presented here.

(i) Defining Equation

The functions $M_{k,m}(x)$ and $W_{k,m}(x)$ are solutions of Whittaker's equation (Slater 1960, p9):

$$\frac{d^2y}{dx^2} + \left[-\frac{1}{4} + \frac{k}{x} + \left(\frac{1}{4} - m^2\right)/x^2\right] y = 0. \qquad (4.1)$$

In the present discussion we shall normally be concerned with non-negative real values of k, m and x.

The turning points x_a, x_p of (4.1) are given by

$$\left.\begin{matrix} x_p \\ x_a \end{matrix}\right\} = 2k\left\{1 \mp \left[1 + \left(\tfrac{1}{4} - m^2\right)/k^2\right]^{1/2}\right\}. \qquad (4.2)$$

The solutions of (4.1) are oscillatory in the region $x_p < x < x_a$ and monotonic in the regions $0 < x \leq x_p$, $x_a \leq x < \infty$. We note that if $k \gg m$ then $x_p \approx m^2/k$ and $x_a \approx 4k$.

(ii) Integer Case

If $k-m-\frac{1}{2}$ is a positive integer, equal to p, say, then $W_{k,m}(x)$ and $M_{k,m}(x)$ are related to the associated Laguerre polynomial $L_p^{2m}(x)$ by the equations (Slater 1960, p95):

$$W_{k,m}(x) = (-1)^p p!\, e^{-x/2} x^{m+\frac{1}{2}} L_p^{2m}(x), \qquad (4.3)$$

$$M_{k,m}(x) = \frac{p!}{(1+2m)_p} e^{-x/2} x^{m+\frac{1}{2}} L_p^{2m}(x). \qquad (4.4)$$

In this case only $W_{k,m}(x)$ and $M_{k,m}(x)$ are both polynomials of degree k (apart from the exponential factor $e^{-x/2}$), having $(k-m-\frac{1}{2})$ zeros in the range $0 < x < \infty$. Furthermore, both functions tend to zero as $x \to 0$ and as $x \to \infty$; they behave as $x^{m+\frac{1}{2}}$ as $x \to 0$ and as $e^{-x/2} x^k$ as $x \to \infty$.

(iii) Limiting Behaviour

If $k-m-\frac{1}{2}$ is not an integer

$$M_{k,m}(x) = e^{-x/2} x^{m+\frac{1}{2}} [1 + O(x)] \text{ as } x \to 0, \qquad (4.5)$$

$$= \frac{\Gamma(1+2m)}{\Gamma(\frac{1}{2}+m-k)} e^{x/2} x^{-k} [1 + O(x^{-1})] \text{ as } x \to \infty, \qquad (4.6)$$

while, as $x \to 0$

$$W_{\kappa,m}(x) = e^{-x/2}\left[\frac{\Gamma(2m)\,x^{-m+\frac{1}{2}}}{\Gamma(\frac{1}{2}+m-\kappa)} + O(x^{3m-\frac{1}{2}})\right], \text{ if } m > \tfrac{1}{2},$$

$$= e^{-x/2}\left[\frac{1}{\Gamma(1-\kappa)} + O(|\log x|)\right], \text{ if } m = \tfrac{1}{2}, \quad (4.7)$$

and as $x \to \infty$

$$W_{\kappa,m}(x) = e^{-x/2}\, x^{\kappa}\,[\,1 + O(x^{-1})\,]. \quad (4.8)$$

(iv) Asymptotic Expansion

A useful asymptotic expansion of $W_{\kappa,m}(x)$ is

$$W_{\kappa,m}(x) \underset{x\to\infty}{\sim} e^{-x/2}\, x^{\kappa} \sum_{i=0}^{\infty} \frac{(\frac{1}{2}+m-\kappa)_i\,(\frac{1}{2}-m-\kappa)_i}{i!}\left(-\frac{1}{x}\right)^{i} \quad (4.9)$$

Thus

$$W_{\kappa,m}(x) = e^{-x/2}\, x^{\kappa}\, {}_2F_0\left(\tfrac{1}{2}+m-\kappa, \tfrac{1}{2}-m-\kappa; -\frac{1}{x}\right). \quad (4.10)$$

(v) Confluent Hypergeometric Functions

The Whittaker functions may be expressed in terms of the confluent hypergeometric functions of Kummer and Tricomi:

$$W_{k,m}(x) = e^{-x/2} x^{c/2} \Psi(a, c; x), \tag{4.11}$$

$$M_{k,m}(x) = e^{-x/2} x^{c/2} \Phi(a, c; x). \tag{4.12}$$

where $a = \frac{1}{2} + m - k$ and $c = 2m + 1$.

The functions Φ and Ψ are frequently written as M(a, c; x) and U(a, c; x) respectively.

(vi) Recurrence Relation

$W_{k,m}(x)$ satisfies the recurrence relation (Slater 1960, eq, 2.5.11)

$$(k - m - \tfrac{1}{2})(k + m - \tfrac{1}{2}) W_{k-1,m}(x)$$

$$+ (2k - x) W_{k,m}(x) + W_{k+1,m}(x) = 0. \tag{4.13}$$

4.3 EXISTING METHODS OF COMPUTING $W_{k,m}(x)$

Although there are many approximations and expansions of $W_{k,m}(x)$ in terms of simpler functions (Slater 1960), very few of these are of any value in numerical calculations. A brief review of some of the more useful approximations is presented below.

For small x Kummer's function Φ may be computed by means of the equation

$$\Phi(a, c; x) = \sum_{i=0}^{\infty} \frac{(a)_i}{(c)_i \; i!} x^i,$$

and Tricomi's function Ψ (for integer c and non-zero x) may be computed by means of the equation

$$\psi(a,n+1;x) = \frac{(-1)^{n-1}}{n!\,\Gamma(a-n)}\left\{\phi(a,n+1;x)\log x\right.$$

$$\left.+\sum_{r=0}^{\infty}\frac{(a)_r}{(n+1)_r}\left[\psi(a+r)-\psi(1+r)-\psi(1+n+r)\right]\frac{x^r}{r!}\right\}$$

$$+\frac{(n-1)!}{\Gamma(a)}\sum_{r=0}^{n-1}\frac{(a-n)_r}{(1-n)_r}\frac{x^{r-n}}{r!}, \qquad (4.14)$$

where the last sum should be omitted if n = 0, and where

$$\psi(z) = \frac{\Gamma'(z)}{\Gamma(z)}.$$

See Erdélyi 1953, eqs. 6.5(7) and 6.7(13), for further details.

Equation (4.14) can be used to compute $W_{\kappa,m}(x)$ to any desired accuracy provided x is sufficiently small. However, in the context of the Coulomb approximation, the values of x involved are not small enough to ensure rapid convergence; we note that $x > x_1$, where $x_1 = 2z\tau_1/\nu$, τ_1 being the core radius (see Section 3.1). Thus (4.14) is of little practical value.

When x is large the asymptotic approximation (4.9) provides a useful computational scheme. After an initial increase, the magnitudes of the terms decrease rapidly to a minimum term and then increase indefinitely. In order to compute $W_{\kappa,m}$ equation (4.9) should be truncated so as to include one half of the minimum term; subsequent terms should be neglected. The magnitude of the minimum term provides an estimate of the truncation error (see Olver 1974). This method was used by Friedrich et al. (1970)

for computing radial Coulomb wavefunctions. Unfortunately, as regards calculations of the quadratic Zeeman effect, it becomes inaccurate if k is large and m is small, due to the accumulation of rounding errors in the series summation; the individual terms of the series become large and alternate in sign, inducing numerical cancellation. The onset of rounding errors can be delayed by using double precision arithmetic, but at the expense of increased computer time.

The author's experience has shown that even when k and m are relatively small ($\lesssim 10$) it is impossible to evaluate $W_{k,m}(x)$ with sufficient accuracy over the entire range of values of x: $x_1 < x < \infty$ using the methods mentioned above. Although the extreme values of x can be computed effectively it is necessary to find other computational schemes for the intermediate values. This need becomes greater as k increases.

Lindgård and Nielsen (1975) attempted inward integration of the defining differential equation (4.1) using the Numerov method. They found this approach to be effective for $k \lesssim 10$. However, uncertainties were raised regarding the accuracy of the numerical procedures when x became small. This approach has not been applied to cases involving large values of k.

Previous tabulations of $W_{k,m}(x)$ or related functions have been very restricted in scope. For example Curtis (1964) tabulated a function, which is equivalent to $W_{k,m}(x)$ for $0{\cdot}707 < k < 2{\cdot}24$, $m = \frac{1}{2}, \frac{3}{2}, \frac{5}{2}$. One computer library program is known for the $M_{k,m}(x)$, which could, in principle, be used to calculate $W_{k,m}(x)$ (CERN library C325 and Luke 1959). However, this program is valid only for a very restricted range of values of parameters and argument.

The above analysis, together with extensive numerical calculations, have shown that all of the methods reviewed above give rise to numerical

problems whenever the number of zeros in $W_{k,m}(x)$, which is given by $[k-m-\frac{1}{2}]$, becomes greater than about 5. Furthermore, even if $[k-m-\frac{1}{2}] \lesssim 5$, no existing technique can adequately represent $W_{k,m}(x)$ throughout the range of values of x and k which arise in calculations of the quadratic Zeeman effect.

In the remainder of this Chapter we describe a new numerical technique for computing $W_{k,m}(x)$ when k is large. This technique, which is based upon the use of the recurrence relation (4.13), together with Chebyshev expansions of the starting functions, overcomes most of the limitations of existing techniques.

4.4 USE OF RECURRENCE RELATIONS

Luke (1959), Gautschi (1967, 1975) and Wimp (1970) have demonstrated that recurrence relations can often provide an effective means of computing recalcitrant special functions. In particular, Gautschi (1967)* has illustrated, using the example of the Miller algorithm for the Bessel functions, how recursion can be used in circumstances in which the proportion of the wanted solution to the unwanted solution increases progressively; in this case a normalization relation makes it possible to commence the recursion with arbitrary starting values and, after a few steps, produce a close approximation to the function required.

As we shall demonstrate presently, recurrence relations can also be very effective in the computation of $W_{k,m}(x)$ with large k. However, the numerical procedures are not as straightforward as those used in the case of the Bessel function or the other functions described by Gautschi (loc. cit.).

---

* This review article provides an excellent introduction to the numerical analysis of recurrence relations; knowledge of this introduction is assumed in the following discussion.

4.4.1 Recurrence Relation for $W_{k,m}(x)$

Several recurrence relations exist which link three Whittaker functions with contiguous parameters (see Slater 1960, Chapter 2). An examination of these has shown that there is only one which is useful in the present context, namely that in which only the parameter k varies (Slater 1960, eq. 2.5.11), i.e.

$$(k - m - \tfrac{1}{2})(k + m - \tfrac{1}{2})\,W_{k-1,m}(x) + (2k - x)\,W_{k,m}(x) + W_{k+1,m}(x) = 0. \qquad (4.15)$$

We note that (4.15) is also satisfied by $M_{k,m}(x)/\Gamma(\tfrac{1}{2} - m - k)$.

It can be shown that when $x > 4k$, $W_{k,m}(x)$ is the dominant solution (see Gautschi loc. cit.) of (4.15) as k increases; otherwise both solutions oscillate. Thus, when (4.15) is used in numerical calculations of $W_{k,m}(x)$ we should use forward recursion on the parameter k, i.e. we should compute $W_{k_0+2,m}(x)$, $W_{k_0+3,m}(x)$, ..., $W_{k,m}(x)$ by repeated application of (4.15), starting from $W_{k_0,m}(x)$ and $W_{k_0+1,m}(x)$. In this way, inaccuracies in the starting functions, or rounding errors introduced during the recursion process, do not grow to an intolerable level. Of course, if $x > 4k$, such errors are attenuated by the recursion process.

Thus (4.15) seems well suited to our requirements, provided we can establish an effective means of determining the starting functions $W_{k_0,m}(x)$ and $W_{k_0+1,m}(x)$. Unfortunately, it is not possible to adopt arbitrary starting values, as in the cases cited by Gautschi (loc. cit.). There are two reasons why this is so. Firstly, we cannot assume that a sufficient number of steps of the recursion will fall in the region where $W_{k_0+i,m}(x)$ is dominant (i.e. where $k_0 + i < x/4$, $i = 1, 2, \ldots$). Thus attenuation of the unwanted solution cannot be assured. Secondly,

there is no normalization relation of the form

$$\theta = \sum_{i=0}^{\infty} \alpha_i W_{k_0+i,m}(x),$$

where θ and α_i are known constants (cf. Gautschi loc. cit. p160). Hence at least one accurate fiduciary computation of a $W_{k_0+i,m}$ is needed, even if attenuation of the unwanted solution does take place, i.e. even if $x > 4k$.

In view of the above remarks, which were substantiated by extensive trial calculations, it was decided that the best approach was to start the recursion with <u>two</u> accurately computed starting functions. This approach became practical following the author's development of a new numerical technique for computing the starting functions. Using this approach it is necessary only to ensure that rounding errors, propagated by the recursion formula (4.15) as components of the unwanted solution $M_{k,m}(x)/\Gamma(\frac{1}{2}-k-m)$, should remain small in relation to $W_{k_0,m}(x), W_{k_0+1,m}(x), \cdots, W_{k,m}(x)$. Therefore, in practical calculations, the required function $W_{k,m}(x)$ need not be the dominant solution of (4.15). Instead, it is only necessary that $M_{k,m}(x)/\Gamma(\frac{1}{2}-k-m)$ should <u>not</u> be the dominant solution. Trial calculations over the range of parameters of interest in the present context have shown that this condition is usually satisfied.

We shall return to a discussion of the effectiveness of the above approach in Section 4.6, following a presentation of the method used to compute the starting functions.

4.5 COMPUTATION OF THE STARTING FUNCTIONS

We have already remarked (Section 4.3) on the inadequacy of existing methods of computing $W_{k,m}(x)$, even when $k-m-\frac{1}{2}$ is small.

Therefore, in the search for a numerical method of computing the starting functions, I investigated the potential of several theoretical approximations involving simpler special functions. The most important of these were Chebyshev polynomials, Laguerre polynomials and Bessel functions (see Erdélyi 1953, Clenshaw 1962, Luke and Wimp 1963 and Luke 1969). Of these three representations the Chebyshev expansion was most effective; the Bessel and Laguerre expansions lead to series containing many terms and computation of the co-efficients was frequently laborious. The Chebyshev expansion and its numerical properties are discussed below.

4.5.1 Chebyshev Expansion of the Auxiliary Function

Miller (1966) suggested that in numerical calculations involving the Whittaker function $W_{\kappa,m}(x)$ it is useful to introduce the auxiliary function $F_{\kappa,m}(x)$, defined by the equation

$$F_{\kappa,m}(x) = e^{x/2} x^{-\kappa} W_{\kappa,m}(x), \tag{4.16}$$

$$= x^{a} \Psi(a, c; x), \tag{4.17}$$

where $a = \frac{1}{2}+m-k$, $c = 2m+1$ and Ψ is Tricomi's function (see Section 4.2(v)). $F_{\kappa,m}(x)$ has slower variation and simpler asymptotic behaviour than $W_{\kappa,m}(x)$. If a and b ($= a+1-c$) are both negative, which is usually the case in calculations of physical interest, the number of zeros of $F_{\kappa,m}(x)$ is ent ($-a+1$) or ent ($-b+1$), whichever is the smaller. It follows from (4.9) and (4.10) that

$$F_{\kappa,m}(x) \underset{x\to\infty}{\sim} {}_2F_0\left(\tfrac{1}{2}+m-k, \tfrac{1}{2}-m-k; -\tfrac{1}{x}\right), \tag{4.18}$$

i.e. $$\lim_{x\to\infty} F_{\kappa,m}(x) = 1. \tag{4.19}$$

A convergent Chebyshev expansion of $F_{k,m}(x)$ can be derived very easily from a result due to Luke and Wimp (1963). They showed that

$$(\lambda x)^a \Psi(a,c;\lambda x) = \sum_{i=0}^{\infty} c_i(\lambda)\, T_i^*\left(\frac{1}{x}\right), \qquad (4.20)$$

where $1 \le x \le \infty$, neither a nor $a+1-c$ equals zero or a negative integer, and $\lambda \neq 0$. T_i^* represents the shifted Chebyshev polynomial of order i and is defined by the equations (Abramowitz and Stegun 1964)

$$T_i^*(z) = \cos(i\theta), \qquad (4.21)$$

$$2z - 1 = \cos\theta. \qquad (4.22)$$

(For further details regarding the derivation of equation (4.20) see also Wimp 1967 and Luke 1969, Sections 9.2, 12.4 and 12.5).

We can obtain a convergent Chebyshev expansion of $F_{k,m}(x)$ for $0 < x_0 \le x \le \infty$ simply by replacing λ by x_0 and x by x/x_0 in (4.20). Thus, noting (4.17), we find that if $\frac{1}{2}+m-k$ and $\frac{1}{2}-m-k \neq 0,-1,\ldots$ then

$$F_{k,m}(x) = \sum_{i=0}^{\infty} c_i(x_0)\, T_i^*\left(\frac{x_0}{x}\right), \quad 0 < x_0 \le x \le \infty. \qquad (4.23)$$

Since (4.23) converges we may use a truncated form of it in numerical calculations. Thus

$$F_{k,m}(x) \approx \sum_{i=0}^{n} c_i(x_0)\, T_i^*\left(\frac{x_0}{x}\right), \qquad (4.24)$$

where n is chosen large enough to ensure that $F_{k,m}$ can be evaluated with sufficient accuracy. As we shall discuss below, if k and m are small ($\lesssim 5$) and $x_0 > x_\rho$ (see equation 4.2), (4.23) converges very rapidly indeed; in typical cases only five or six terms are required to achieve an accuracy of four significant figures.

4.5.2 Computation of the Chebyshev Coefficients

Before (4.24) can be used in practical calculations the Chebyshev coefficients $C_i(x_0)$, $i = 0, 1, \ldots, n$ must be computed. There are several ways in which this may be carried out. Some of these methods are discussed by Fox and Parker (1968) and by Clenshaw (1962). However, the most appropriate method for our present purpose has been found to be that of Luke (1969). He has given a procedure for computing $C_i(x_0)$, $i = 0, 1, \ldots$ using backward recursion on a four-term recurrence relation for which $C_i(x_0)$ is the minimal solution. The associated computational algorithm, described in the notation of Luke (loc. cit., p25), is presented below.

The Chebyshev coefficients $C_i(x_0)$ satisfy the four-term recurrence relation

$$\frac{2C_i(x_0)}{\epsilon_i} = 2(i+1)\left\{1 - \frac{(2i+3)(i+a+1)(i+b+1)}{2(i+2)(i+a)(i+b)} - \frac{2x_0}{(i+a)(i+b)}\right\} C_{i+1}(x_0)$$

$$+ \left\{1 - \frac{2(i+1)(2i+3-2x_0)}{(i+a)(i+b)}\right\} C_{i+2}(x_0)$$

$$- \frac{(i+1)(i+3-a)(i+3-b)}{(i+2)(i+a)(i+b)} C_{i+3}(x_0), \quad (4.25)$$

where $\epsilon_0 = 1$, $\epsilon_i = 2$ if $i > 0$; $a = \frac{1}{2} + m - k$, $b = \frac{1}{2} - m - k$.

The algorithm for computing $C_i(x_o)$ is expressed as follows (Luke 1969, Section 12.5):

1. Define

$$\varphi_{N+\tau}^{(N)} = 0, \quad \tau = 2, 3,$$

$$\varphi_{N+1}^{(N)} = 1.$$

2. Compute

$$\varphi_i^{(N)}, \quad i = N, N-1, \ldots, 0.$$

by backward recursion using equation (4.25) with C_i replaced by $\varphi_i^{(N)}$.

3. Define

$$\theta_N = \sum_{i=0}^{N+1} (-1)^i \varphi_i^{(N)}.$$

4. Compute

$$B_i^{(N)} = \varphi_i^{(N)} / \theta_N, \quad i = 0, 1, \ldots, N.$$

Luke (loc. cit.) has proven that:

(i) $\text{Lim}_{N \to \infty} B_i^{(N)} = C_i(x_o), \quad i = 0, 1, \ldots$ (4.26)

(ii) For any $\epsilon > 0$ and integer N_1 we can always find N such that

$$|B_i^{(N)} - C_i(x_o)| < \epsilon, \quad i = 0, 1, \ldots, N_1. \qquad (4.27)$$

At Step 1 $\varphi_{N+r}^{(N)}$, r = 1, 2, 3 are assigned arbitrary values; they therefore contain arbitrary combinations of the three linearly independent solutions of (4.25). However, since $C_i(x_0)$ is the minimal solution of (4.25) (see Gautschi 1967), the components of the unwanted solutions are attenuated by the recursion process. Thus N should be chosen sufficiently large to ensure that the two unwanted solutions of (4.25) make a negligible contribution to $\varphi_i^{(N)}$, $i \leq N_1$. With an appropriate choice of N, therefore, $\varphi_i^{(N)}$, $i \leq N_1$, differ from the corresponding Chebyshev coefficients of $F_{k,m}(x)$ by a multiplicative factor.

The normalization factor is determined by considering the limiting case of (4.23) as $x \to \infty$, together with equation (4.19). This leads to the normalization relation

$$1 = \sum_{i=0}^{\infty} C_i(x_0)\, T_i^*(0) = \sum_{i=0}^{\infty} (-1)^i C_i(x_0). \qquad (4.28)$$

This relation is used to compute the normalization factor at Step 3 of the above algorithm. The normalized coefficients, $B_i^{(N)}$, are computed at Step 4.

There is no analytical method of determining the appropriate choice of N, N_1 or ϵ when using the above algorithm in numerical calculations. Neither is there any analytical method of determining an appropriate value of n to ensure a specified accuracy in the computed values of $F_{k,m}(x)$. In common with many other algorithms of this type (Gautchi loc. cit.), n, N and N_1 can only be determined by trial calculations.

The present research therefore involved an extensive scheme of numerical experiments, which were designed to:

(a) determine whether the above algorithm was of practical value in the context of the Coulomb approximation;

(b) determine the behaviour of the Chebyshev coefficients of $F_{k,m}(x)$, and thereby develop guidelines regarding the choice of N and n.

A discussion of these experiments, together with some typical results, are presented below.

4.5.3 Numerical Calculations

Chebyshev coefficients, $B_i^{(N)}$, were computed for many sets of parameters k, m and x_o. For each set $B_i^{(N)}$ was computed for several values of N, typically 4, 8, 12,..... Table 4.1 illustrates the behaviour of $B_i^{(N)}$ when k = 6.125, m = 1.5 and x_o = 3.25 for the two cases N = 12 and N = 20. The behaviour of the associated auxiliary function, $F_{k,m}(x)$, is illustrated in Fig. 4.1.

When using (4.24) to compute the values of $F_{k,m}(x)$ displayed in Fig. 4.1 the degree of truncation (i.e. the value of n) was determined by inspection of the Chebyshev coefficients, $B_i^{(N)}$. In order to achieve an accuracy of four significant figures in the computed value of $F_{k,m}(x)$, n = 6 was found to be the appropriate choice.

It should be emphasised that, if the desired accuracy of $F_{k,m}(x)$ had never been greater than four significant figures, less accurate Chebyshev coefficients than those displayed in Table 4.1 would have been acceptable; numerical calculations have shown that the appropriate choice would have been N = 8. Either set of coefficients displayed in Table 4.1 is sufficiently accurate to enable $F_{k,m}(x)$ to be evaluated with an accuracy of ten significant figures!

Fig. 4.1 also shows the behaviour of $F_{k,m}(x)$, k = 5.5, m = 1.5.

i	$B_i^{(20)}$	$B_i^{(12)}$
0	$.184402 \times 10^{-1}$	$.184402 \times 10^{-1}$
1	$-.611291 \times 10^{0}$	$-.611291 \times 10^{0}$
2	$.131839 \times 10^{-1}$	$.131839 \times 10^{-1}$
3	$-.289970 \times 10^{0}$	$-.289970 \times 10^{0}$
4	$.756997 \times 10^{-1}$	$.756997 \times 10^{-1}$
5	$-.651061 \times 10^{-3}$	$-.651061 \times 10^{-3}$
6	$-.153971 \times 10^{-4}$	$-.153971 \times 10^{-4}$
7	$-.278781 \times 10^{-6}$	$-.278781 \times 10^{-6}$
8	$-.631274 \times 10^{-9}$	$-.631276 \times 10^{-9}$
9	$.104188 \times 10^{-10}$	$.104206 \times 10^{-10}$
10	$-.371801 \times 10^{-12}$	$-.371943 \times 10^{-12}$
11	$.202002 \times 10^{-13}$	$.188227 \times 10^{-13}$
12	$-.145611 \times 10^{-14}$	
13	$.129357 \times 10^{-15}$	
14	$-.135294 \times 10^{-16}$	
15	$.161529 \times 10^{-17}$	
16	$-.215407 \times 10^{-18}$	
17	$.315882 \times 10^{-19}$	
18	$-.496455 \times 10^{-20}$	
19	$.707461 \times 10^{-21}$	

Table 4.1 Chebyshev Coefficients of $F_{k,m}(x)$, $x = 3.25$, $k = 6.125$ and $m = 1.5$

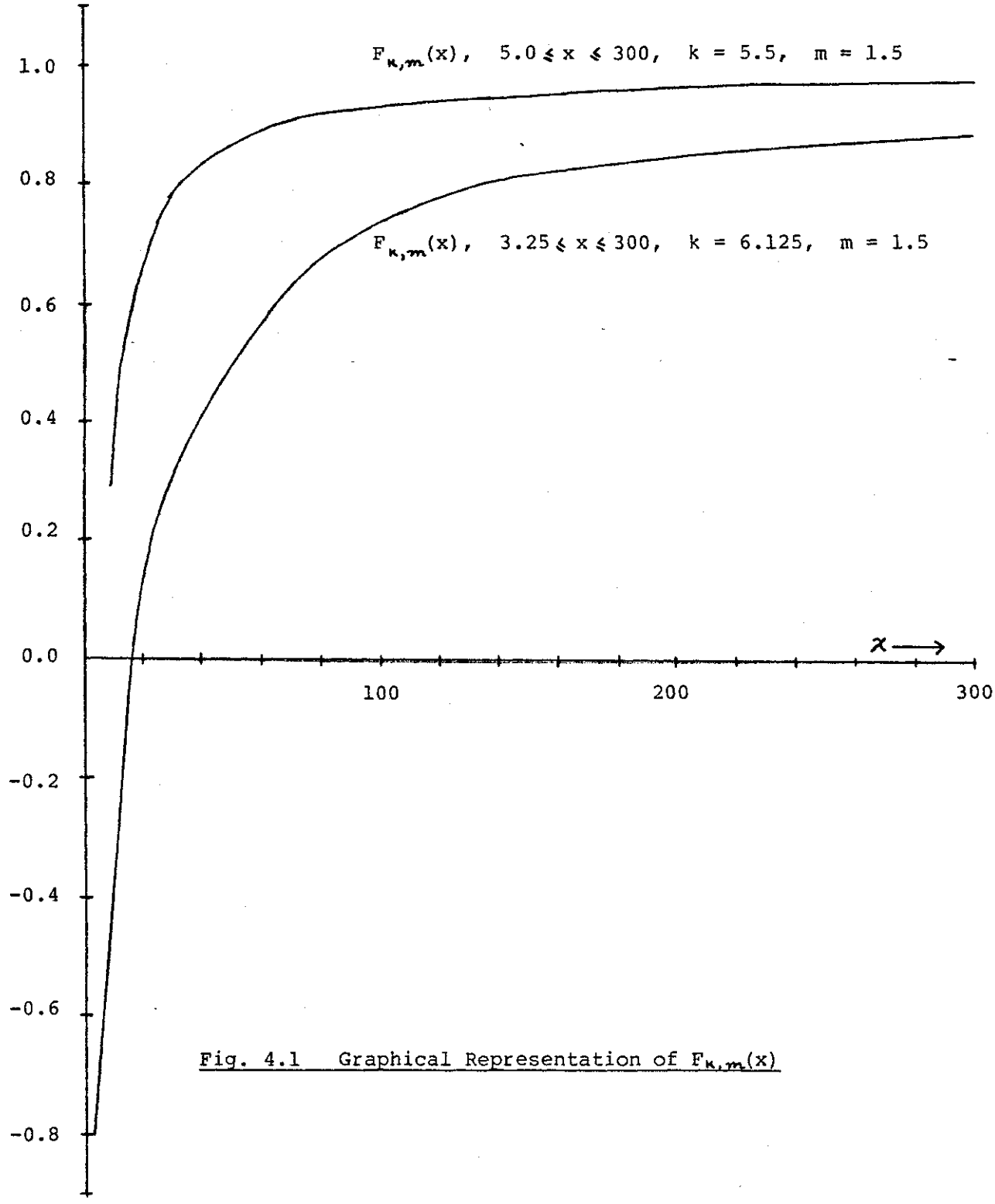

Fig. 4.1 Graphical Representation of $F_{k,m}(x)$

This graph illustrates clearly the smooth asymptotic behaviour of the auxiliary function as x becomes large. Of course, the highly oscillatory behaviour of $F_{k,m}(x)$ which occurs when $x \to 0$, is not shown on this graph.

Fig. 4.2 shows how $F_{k,m}(x)$ compares with $W_{k,m}(x)$, in the case k = 3.5, m = 1.5 and $0.5 \leq x \leq 28.5$. When $x \gtrsim 3.0$ the smoother variation of the auxiliary function becomes significant.

In order to illustrate the effect of x_0 on the rate of convergence of the Chebyshev expansion of $F_{k,m}(x)$, the coefficients, $B_i^{(N)}$, corresponding to the case k = 6.125, m = 1.5, were computed with $x_0 = 0.325$. These coefficients, which are displayed in Table 4.2, should be compared with those of Table 4.1, which correspond to the case $x_0 = 3.25$. These, and similar calculations, have shown that the rate of convergence decreases as x_0 approaches the auxiliary function's singularity at x = 0. Moreover, the magnitudes of the coefficients (and hence the magnitudes of the terms in 4.24) increase as $x_0 \to 0$, thereby introducing the possibility of rounding errors in the summation of (4.24).

The dependence of the Chebyshev coefficients on x_0 is further illustrated in Table 4.3(a). In this case the results are presented in terms of the parameters ν and ℓ, and argument $\frac{2zr}{\nu}$, which arise in the context of the Coulomb approximation (see Section 3.1). Table 4.3(a) shows the computed Chebyshev coefficients $B_i^{(12)}$ corresponding to $F_{\nu,\ell+1/2}\left(\frac{2zr}{\nu}\right)$ for the case $\nu = 5.5$, $\ell = 1$, z = 1. Two ranges of r are considered, namely $r \geq r_0 = 10.0$ and $r \geq r_0 = 1.0$ (note $x_0 = 2zr_0/\nu$). Samples of values of the associated auxiliary functions, computed using (4.24), are displayed in Table 4.3(b). As a check of the accuracy of these values the calculations were repeated using $B_i^{(N)}$ with N = 20. These results showed that the figures displayed in Table 4.3(b) for the case $r_0 = 10$ are all correct.

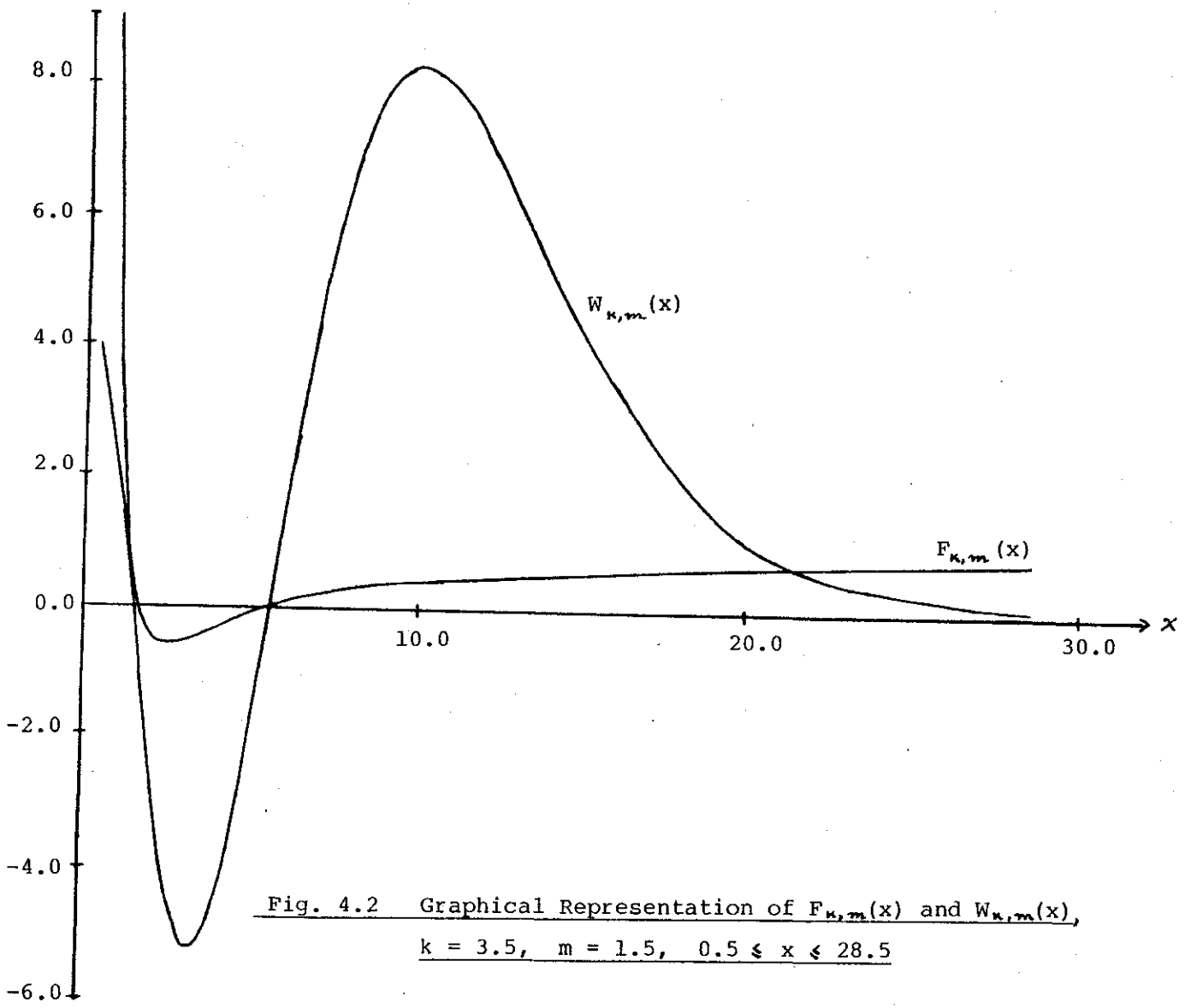

Fig. 4.2 Graphical Representation of $F_{\kappa,m}(x)$ and $W_{\kappa,m}(x)$, $k = 3.5$, $m = 1.5$, $0.5 \leq x \leq 28.5$

i	$B_i^{(20)}$	$B_i^{(12)}$
0	$.771683 \times 10^{4}$	$.771005 \times 10^{4}$
1	$.508379 \times 10^{4}$	$.507793 \times 10^{4}$
2	$.276976 \times 10^{3}$	$.273237 \times 10^{3}$
3	$-.204415 \times 10^{4}$	$-.204586 \times 10^{4}$
4	$-.150126 \times 10^{4}$	$-.150179 \times 10^{4}$
5	$-.457458 \times 10^{3}$	$-.457558 \times 10^{3}$
6	$-.541833 \times 10^{2}$	$-.541942 \times 10^{2}$
7	$-.324902 \times 10^{1}$	$-.324980 \times 10^{1}$
8	$-.203629 \times 10^{-1}$	$-.203331 \times 10^{-1}$
9	$.838365 \times 10^{-3}$	$.824043 \times 10^{-3}$
10	$-.696275 \times 10^{-4}$	$-.628485 \times 10^{-4}$
11	$.837017 \times 10^{-5}$	$.519213 \times 10^{-5}$
12	$-.128389 \times 10^{-5}$	
13	$.235142 \times 10^{-6}$	
14	$-.493295 \times 10^{-7}$	
15	$.114925 \times 10^{-7}$	
16	$-.288301 \times 10^{-8}$	
17	$.744601 \times 10^{-9}$	
18	$-.181283 \times 10^{-9}$	
19	$.327389 \times 10^{-9}$	

Table 4.2 Chebyshev Coefficients of $F_{k,m}(x)$, $k = 6.125$, $m = 1.5$, $x = 0.325$

i	$B_i^{(12)}$, $\tau_0 = 10.0$	$B_i^{(12)}$, $\tau_0 = 1.0$
0	.554997 x 10^{0}	.782678 x 10^{4}
1	-.232077 x 10^{0}	.671885 x 10^{4}
2	.314654 x 10^{0}	.418384 x 10^{4}
3	-.167650 x 10^{0}	.179641 x 10^{4}
4	.827548 x 10^{-2}	.484147 x 10^{3}
5	.157967 x 10^{-3}	.711565 x 10^{2}
6	.352046 x 10^{-5}	.621121 x 10^{1}
7	.311426 x 10^{-7}	.169337 x 10^{0}
8	-.292660 x 10^{-9}	-.429577 x 10^{-2}
9	.838982 x 10^{-11}	.299213 x 10^{-3}
10	-.397774 x 10^{-12}	-.295296 x 10^{-4}
11	.225109 x 10^{-13}	.260387 x 10^{-5}

Table 4.3(a) Chebyshev Coefficients of $F_{\nu,\ell+\frac{1}{2}}\left(\frac{2\tau}{\nu}\right)$, $\nu = 5.5$, $\ell = 1$

τ	$F_{\nu,\ell+\frac{1}{2}}\left(\frac{2\tau}{\nu}\right)$, $\tau_0=10$	$F_{\nu,\ell+\frac{1}{2}}\left(\frac{2\tau}{\nu}\right)$, $\tau_0=1$
10	.200863	.200811
110	.523566	.523558
210	.728119	.728112
310	.810249	.810243
410	.854339	.854334

Table 4.3(b) Computed Values of $F_{\nu,\ell+\frac{1}{2}}\left(\frac{2\tau}{\nu}\right)$, $\nu = 5.5$, $\ell = 1$

Hence the choice of N = 12 is too small if $F_{k,m}\left(\frac{2z^2}{\nu}\right)$, k = 5.5, m = 1.5, z = 1, r $\geq$ 1.0, is to be computed with an accuracy of six significant figures. On the other hand, if only four significant figures of $F_{k,m}\left(\frac{2z^2}{\nu}\right)$ are required, N = 12 is adequate, even if $r_0 = 1.0$.

We note that the truncated Chebyshev series (4.24) can be evaluated very efficiently by means of the following procedure, developed by Clenshaw (1955):

1. Define $t = x_0/x$, $c_i = B_i^{(N)}$, $(i = 1, 2, \ldots, n)$

   and $S_{n+1} = S_{n+2} = 0.$

2. Compute $S_i = 2(2t-1)S_{i+1} - S_{i+2} + \epsilon_i c_i$

   for $i = n, n-1, \ldots, 0$

   where $\epsilon_i = 2$ if $i = 0$ and $\epsilon_i = 1$ if $i > 0$.

Clenshaw (loc. cit.) has proved that

$$\tfrac{1}{2}(S_0 - S_2) = \sum_{i=0}^{n} c_i T_i^*(t).$$

This algorithm avoids explicit calculation of the Chebyshev polynomials $T_i^*(t)$ by making implicit use of the recurrence relation

$$T_{i+1}^*(t) - 2(2t-1)T_i^*(t) + T_{i-1}^*(t) = 0$$

(see Abramowitz and Stegun 1964).

The author's numerical experiments have shown that the value of N required to enable the computation of $F_{k,m}(x)$ to a specified accuracy increases as a (= ½ + m - k) and b (= ½ - m - k) increase in magnitude, and as x_0 decreases. If $x_0 \gtrsim x_p$, the inner turning point of the associated Whittaker function (see equation 4.2), and $|a|, |b| \leq 5$, the

Chebyshev expansion converges rapidly; in general $F_{k,m}(x)$ can be computed with an accuracy of six significant figures provided N lies in the range 10-20. However, if $x_0 < x_p$ or $|a|, |b| \gtrsim 5$ the series converges slowly; the number of terms required increases roughly as k if $m = \frac{1}{2}$ or $\frac{3}{2}$. These results confirmed an intuitive belief that the Chebyshev expansion alone would not provide an effective means of computing $F_{k,m}(x)$ when k is large.

Numerical calculations have also shown that the speed of convergence of the Chebyshev series increases rapidly as a or b approach zero or a negative integer. However, the difference must be smaller than about 10^{-3} before a substantial reduction in N can be achieved.

We note that many of the characteristics observed in the numerical calculations discussed above can be explained by reference to an asymptotic estimate of $C_i(x_0)$, which states

$$C_i(x_0) = \frac{4(-1)^i (\frac{\pi}{3})^{1/2} \exp[-3x_0^{1/3} i^{2/3} + x_0/3]}{\Gamma(a)\Gamma(b) x_0^{\frac{4K-1}{6}} i^{\frac{4K+2}{3}}}$$

$$\times [1 + O(i^{-2/3})]. \qquad (4.29)$$

This result, which is due to Miller (1966), is more accurate than the corresponding estimate given by Luke (Luke 1969, equation 9.2(28)).

Numerical calculations have shown that (4.29) is accurate to within 30% if $i \gtrsim 10$. The form of this equation helps to explain the way in which the convergence of the Chebyshev expansion depends upon a, b and x_0. Clearly, if $x_0 \gg 1$ we expect rapid convergence due to the term $\exp(-3x_0^{1/3} i^{2/3})$. Rapid convergence is also expected when a and b are small and negative, since, in these cases the gamma functions in the

denominator become large (see Abramowitz and Stegun 1964). The fact that $\Gamma(z)$ becomes infinite if $z = 0, -1, -2, \ldots$ explains why the Chebyshev series converges very rapidly when a or b are close to zero or negative integers.

4.5.4 Truncation Errors

The maximum truncation error in the approximation (4.24) is $\sum_{i=n+1}^{\infty} |c_i(x_0)|$, since $|T_i^*| \leq 1$. If the Chebyshev expansion converges rapidly we expect that the truncation error is dominated by the first neglected term. Thus we expect

$$\sum_{i=n+1}^{\infty} |c_i(x_0)| \leq R\,|c_{n+1}(x_0)|, \qquad (4.30)$$

where R is a constant and not too large. Numerical calculations, such as those referred to in Section 4.5.3, have illustrated that provided x_0 is not taken much smaller than unity, and provided the desired accuracy in $F_{k,m}(x)$ is not so large that n becomes greater than about 15, then (4.30) is true and R is about 20.

Thus n may be determined by examining successive terms of the Chebyshev series and truncating when $|c_i(x_0)|$ is less than $\frac{1}{20}$th of the permissible error in $F_{k,m}(x)$. In the context of the Coulomb approximation, in which $F_{k,m}(x)$ is required with an accuracy of four significant figures, the appropriate truncation point is usually in the range n = 6 to n = 10, provided $|a|, |b| \lesssim 5$; the corresponding choice of N is N = 8 to N = 12. If $|a|$ or $|b|$ exceed 5 the rate of convergence of the Chebyshev series decreases. We note that, since m usually takes the values $\frac{1}{2}, \frac{3}{2}, \frac{5}{2}$ in calculations of physical interest, the cases $|a|, |b| \gtrsim 5$ arise when k becomes large.

4.5.5 Choice of Starting Functions

Numerical calculations, such as those presented above, have demonstrated that the Chebyshev expansion provides the basis of a very powerful algorithm for computing the auxiliary function, $F_{k,m}(x)$, and hence the Whittaker function $W_{k,m}(x)$. The fact that the expansion converges rapidly only when $|a|$ and $|b|$ are small does not present a problem, since we have already established (see Section 4.4) that when k is large the required function $W_{k,m}(x)$ can be computed by recursion from two starting functions $W_{k_0,m}(x)$ and $W_{k_0+1,m}(x)$.

Clearly, k_0 should be chosen such that the conditions for rapid convergence are achieved in the Chebyshev expansions of the auxiliary starting functions $F_{k_0,m}(x)$, $F_{k_0+1,m}(x)$. We therefore choose k_0 such that $|a_0| = |\frac{1}{2} + m - k_0|$ is small (i.e. ≤ 5). Since m is small in calculations of physical interest and takes the values $\frac{1}{2}$, $\frac{3}{2}$, $\frac{5}{2}$, $b_0 = \frac{1}{2} - m - k_0$ is automatically small if a_0 is small.

Of course k_0 must differ from k by an integer to facilitate the use of the recurrence relation (4.15). The author's extensive numerical calculations have indicated that the best choice is such that $-1 < a_0 \leq 0$. In this way $F_{k_0,m}(x)$ and $F_{k_0+1,m}(x)$ have no zeros and one zero respectively. We note that if $k-m-\frac{1}{2}$ is an integer, then $a_0 = 0$; in this case (4.9) terminates, giving the exact formulas

$$F_{k_0,m}(x) = 1, \tag{4.31a}$$

$$F_{k_0+1,m}(x) = 1 - \frac{2m+1}{x}. \tag{4.31b}$$

4.6 ALGORITHM FOR COMPUTING $W_{k,m}(x)$

Having established the efficiency of the recurrence relation (4.15), together with the Chebyshev expansion for the starting functions, we can now specify the algorithm for computing $W_{k,m}(x)$, k being large and m small.

1. Define $\quad k_0 = k - [k] + m + 1/2 .$

2. Define $\quad M = k - k_0 .$

3. Compute $\quad P_0 = W_{k_0,m}(x) = e^{-x/2} x^{k_0} F_{k_0,m}(x),$

$$P_1 = W_{k_0+1,m}(x) = e^{-x/2} x^{k_0+1} F_{k_0+1,m}(x),$$

using the procedure described in Section 4.5 for computing the auxiliary functions $F_{k_0,m}(x)$ and $F_{k_0+1,m}(x)$.

4. Define $\quad A_0 = x - 2(k_0+1),$

$$B_0 = (\tfrac{1}{2} + m + k_0)(m - k_0 - 1/2).$$

5. Compute P_M using the recursion formula

$$\left.\begin{aligned} P_{i+1} &= A_i P_i + B_i P_{i-1} \\ A_{i+1} &= A_i + 2 \\ B_{i+1} &= B_i + A_i + 1 \end{aligned}\right\} \quad i = 1, 2, \ldots, M-1.$$

Step 1 sets the value of k_0 such that $-1 < a_0 \leq 0$, while Step 2 computes the number of steps in the recursion process, used at Step 5. Step 3 involves the computation of two sets of Chebyshev coefficients, one for $F_{k_0,m}(x)$ and one for $F_{k_0+1,m}(x)$. These are computed using the backward

recurrence algorithm described in Section 4.5.2 above. This algorithm contains a test for the case in which $k_o - m - \frac{1}{2}$ differs from zero by a small quantity (e.g. 10^{-4}); if this test is satisfied the starting functions are computed by means of the simple formulas (4.31).

From equation (4.15) it follows that the value of P_M computed at Step 5 is equal to $W_{k,m}(x)$. The subsidiary recurrence relations $A_{i+1} = A_i + 2$ and $B_{i+1} = B_i + A_i + 1$ improve the efficiency of execution of (4.15).

For example, suppose we wish to evaluate $W_{\nu,\ell+\frac{1}{2}}\left(\frac{2\tau}{\nu}\right)$, $\nu = 20.5$, $\ell = 1$, $z = 1$ and $\tau \geq 10.0$. In this case $k_o = 2.5$ and $M = 18$. Thus computation of P_0 and P_1 involves the evaluation of the auxiliary functions $F_{2.5,1.5}\left(\frac{2\tau}{20.5}\right)$, $F_{3.5,1.5}\left(\frac{2\tau}{20.5}\right)$. The latter function and the associated Whittaker function are illustrated in Fig. 4.2 above.

If $W_{k,m}(x)$ must be evaluated for several values of x, the Chebyshev coefficients of the starting functions can be computed once and stored for repeated use; x_o is chosen to be equal to the smallest x for which $W_{k,m}(x)$ is required.

For each set of Chebyshev coefficients the appropriate truncation point (i.e. value of n in equation 4.24) is determined using the procedure described in Section 4.5; a test in the algorithm detects the case in which no sufficiently small coefficient is found, and the algorithm indicates an error condition.

4.7 CONCLUSION

A computational method of evaluating $W_{k,m}(x)$ which is well-suited to the cases in which k is large, m is small and $x \geq x_o > 0$ has been presented. Numerical experiments have demonstrated that the proposed

method is accurate and efficient, and overcomes many of the limitations of existing algorithms. The method's main drawback is that trial calculations may be required to determine the appropriate settings of the parameters n and N in the Chebyshev expansions of the auxiliary functions.

In this Chapter attention has been concentrated on the computation of $W_{k,m}(x)$ when the parameters k, m and x_0 take values appropriate to the Coulomb approximation. In these circumstances the parameters k_0, k_1, m, and to some extent x_0, are of closely bounded variation. When evaluating dipole and quadrupole radial integrals in this context the contributions to the integrals come mainly from the large radial distances, and so there is no need to compute values of $W_{k,m}(x)$ involving very small values of x. Thus the parameter x_0 can be kept relatively large with a corresponding reduction in the number of terms in the Chebyshev series of $F_{k,m}(x)$. In the context of the quadratic Zeeman effect ℓ $(= m - \frac{1}{2})$ is usually small (= 0, 1, 2) and τ_0 (= $\frac{\nu x_0}{2z}$) is approximately equal to $\frac{5\nu^2}{20z}$; under these circumstances, if $\nu \gtrsim 15$ then N = 9 is usually adequate to enable the radial wavefunctions to be determined with an accuracy of four significant figures.

CHAPTER 5

NUMERICAL ACCURACY OF COMPUTED INTEGRALS

In this Chapter we discuss the procedure used to assess the accuracy and efficiency of the Gauss-Laguerre quadrature formula (3.31). The criteria upon which this evaluation is based have been specified in Section 3.4 of Chapter 3. It is therefore assumed that the following limitations are imposed upon the parameters:

- $\ell, \ell' = 0, 1, 2, \ldots$
- $\nu \geq \ell + 1, \quad \nu' \geq \ell' + 1$
- $\nu, \nu' \leq 60$
- $r_o, z > 0$
- $s \geq 0$

We note that, in practical calculations, the condition $\ell, \ell' \leq 3$ is usually valid since the quantum defects associated with larger ℓ-values are usually negligible, i.e. the associated value of ν is an integer. Moreover, s normally takes the values 0, 1 or 2: in the normalization case $s = 0$ and $\ell = \ell'$; in the dipole case $s = 1$ and $|\ell - \ell'| = 1$; in the quadrupole case $s = 2$ and $|\ell - \ell'| = 0$ or 2, though $\ell = \ell' = 0$ is excluded.

There are two sources of numerical errors in the evaluation of equation (3.31):

(i) errors resulting from the numerical procedures used to compute the Whittaker functions in the integrand;

(ii) errors resulting from the use of the Gauss-Laguerre quadrature formula.

The errors referred to in (i) are governed by the accuracy of the Chebyshev expansions used to compute the Whittaker functions; the accuracy

of these expansions was fully discussed in the previous Chapter. In this Chapter, therefore, we examine the behaviour of the errors referred to in (ii).

During the early stages of the evaluation of the author's method of computing radial integrals, it became apparent that this method would be applicable across a much wider range of applications that the particular case of the quadratic Zeeman effect, for which it was originally intended. It was important, therefore, that the performance of the associated numerical procedures, in terms of accuracy and efficiency, should be thoroughly understood throughout the range of parameters mentioned above.

The major difficulties in the evaluation arose when ν, ν' were large ($\gtrsim 15$). At smaller values of ν, ν' the computed integrals could be compared with results obtained by the Bates-Damgaard method or alternative numerical methods, as discussed in Section 5.1. However, at large ν, ν' no alternative methods existed, and the evaluation had to be based upon a systematically designed set of numerical experiments. These results are reported in Section 5.2.

In addition to computing radial integrals in the quadratic Zeeman effect, the author has used the new computational scheme in an investigation of the performance of the Bates-Damgaard method at large and small ν, ν' . The outcome of this investigation is discussed in Section 5.3.

Throughout this Chapter it is assumed that the required accuracy of the computed integrals is never greater than four significant figures. This limitation is imposed by the accuracy of the quantum defects and the errors inherent in the physical assumptions of the Coulomb approximation (see Crossley 1969). In the context of the quadratic Zeeman effect four significant figures is commensurate with the accuracy of the experimental results of Garton and Tomkins (see Chapter 6).

All of the author's numerical calculations were performed on a CDC 6400 computer at Imperial College, using 14 significant decimal digits in single precision arithmetic and 28 significant decimal digits in double precision arithmetic.

5.1 PERFORMANCE OF GAUSS-LAGUERRE QUADRATURE: SMALL ν, ν'

One of the criteria (iv) stipulated in Section 3.4 was that the new method of computing radial integrals should be valid at small as well as large principal quantum numbers. An extensive series of calculations was therefore carried out to compare its performance with that of the methods of Bates and Damgaard (1949), Lindgård and Nielsen (1975), and Friedrich et al. (1970).

5.1.1 Results for Mg II

The method of Lindgård and Nielsen (1975) (see Section 3.4) provided the most reliable basis for this comparison when $\nu, \nu' \lesssim 10$. Like the new method, it takes account of the lower limit of integration; the integral is evaluated by means of equal-interval quadrature, and the Whittaker functions in the integrand are computed by inward integration of the defining differential equation (3.21a) using the Numerov method. Lindgard and Nielsen assessed the validity of this approach by comparing their results with the Bates-Damgaard Tables (Bates and Damgaard 1949), and with experimentally determined values of spontaneous transition probabilities of Mg II (Risberg 1955) and Be II (Johanson 1961).

The present author computed the same ns - n'p spontaneous transition probabilities for Mg II and Be II using two methods: (a) Gauss-Laguerre quadrature, using the procedures described in Chapters 3 and 4 above; and (b) a computer-based version of the Bates-Damgaard algorithm. Some of the

results for Mg II are presented in Table 5.1. This shows four values corresponding to each ns - n'p spontaneous transition probability of Mg II ($3 \leq n,n' \leq 9$) obtained by:

(i) Lindgård and Nielsen's method;

(ii) Gauss-Laguerre quadrature;

(iii) Bates-Damgaard tables;

(iv) Bates-Damgaard program.

All results are expressed in atomic units of $10^8\ s^{-1}$, as defined by Lindgård and Nielsen.

The results quoted for methods (i) and (iii) were taken from Table 3 of Lindgård and Nielsen (1975, p1191), the value for (i) corresponding to their lower cut-off radius $r_c = 0.5$. The results quoted for methods (ii) and (iv) were determined using computer programs developed by the author; in the case of (ii) r_c was set to 0.5. The quantum defects of the transition states of Mg II were obtained from the experimental results of Risberg (1955). Where fine structure splitting occurred the level corresponding to the maximum value of total angular momentum (i.e. maximum j-value) was chosen.

All physical parameters in methods (i) and (ii) are identical, and so the corresponding entries in Table 5.1 are directly comparable. From a computational viewpoint these two methods differ: (a) in the technique used to determine the normalization of the radial wavefunctions; (b) in the technique used to evaluate the radial functions at the quadrature points; and (c) in the choice of quadrature formula.

Table 5.1 shows that the results of Gauss-Laguerre quadrature and those obtained by the Lindgård-Nielsen method always agree to within about 2% if $n,n' \geq 6$ and within about 10% otherwise, except when the absolute value of the transition probability is less than about 10^{-4}.

n \ n'	3	4	5	6	7	8	9
3	2.730	0.00307	0.0206	0.0181	0.0133	0.00956	0.00743
	2.572	0.00268	0.0194	0.0171	0.0126	0.00908	0.00664
	2.52	0.0034	0.018	0.0212	------	-------	-------
	2.473	0.01001	0.0369	0.036	0.0246	0.01825	0.01365
4	3.423	0.366	0.00220	0.000239	0.000790	0.000866	0.000773
	3.246	0.359	0.00215	0.000239	0.000770	0.000841	0.000775
	3.23	0.358	0.0016	0.0012	--------	--------	--------
	3.333	0.357	0.00149	0.000641	0.00144	0.00151	0.001340
5	1.166	0.792	0.0887	0.00179	2.7×10^{-5}	2.6×10^{-5}	7.7×10^{-5}
	1.110	0.779	0.0882	0.00189	4.5×10^{-5}	1.6×10^{-5}	5.6×10^{-5}
	1.062	0.778	0.0872	0.0014	0.0001	--------	--------
	1.205	0.786	0.0879	0.0017	1.6×10^{-5}	4.9×10^{-5}	11.3×10^{-5}
6	0.559	0.316	0.255	0.0294	0.00111	0.000127	1.3×10^{-5}
	0.5334	0.3078	0.253	0.0294	0.00110	0.000107	0.65×10^{-5}
	0.510	0.299	0.251	------	-------	--------	---------
	0.6063	0.3177	0.254	0.0294	0.00106	0.000087	0.20×10^{-5}
7	0.313	0.167	0.111	0.101	0.0119	0.000590	7.6×10^{-5}
	0.299	0.164	0.109	0.100	0.0119	0.000616	9.6×10^{-5}
	0.295	0.164	0.105	0.100	------	--------	--------
	0.353	0.173	0.111	0.101	0.0119	0.000603	8.8×10^{-5}
8	0.194	0.101	0.0633	0.0458	0.0461	0.00555	0.000363
	0.185	0.099	0.0625	0.0462	0.0459	0.00556	0.000355
	-----	0.098	0.065	0.046	0.046	-------	--------
	0.224	0.106	0.0642	0.0466	0.0460	0.00556	0.000350
9	0.128	0.0665	0.0401	0.0275	0.0225	0.0233	0.00286
	0.1226	0.0649	0.0398	0.0284	0.0221	0.0233	0.00286
	------	------	-----	------	------	------	-------
	0.1515	0.0705	0.0414	0.0282	0.223	0.0234	0.00286

Table 5.1 ns - n'p Spontaneous Transition Probabilities for Mg II

Results are expressed in atomic units of $10^{8} s^{-1}$

Of course, disagreement is expected when the transition is very small, since the assumptions of the Coulomb approximation are not valid, due to numerical cancellations in the outer part of the integral, as discussed in Section 5.2.3. However, some of the discrepancy at small ν, ν' may be due to numerical errors resulting from Lindgård and Nielsen's use of the Numerov method to compute the radial wavefunctions at small radial distances, although this has not been fully investigated. We note also that when $|n - n'| \gtrsim 3$, or either n or $n' \lesssim 4$, the Bates-Damgaard results often differ from those obtained by the two methods of numerical quadrature by more than 10%. As we shall discuss further in Section 5.3, the Bates-Damgaard method does not provide a good basis for assessing the accuracy of the Coulomb approximation when the effective principal quantum numbers ν, ν' are either large ($\gtrsim 15$) or small ($\lesssim 4$).

5.1.2 Results of Heckmann

Prof. Dr. P.H. Heckmann of Ruhr-Universitat, Bochum, has compared results obtained for a series of transition probabilities using a computer program based upon the author's method with a corresponding set of results obtained using a program of O. Bely. In Bely's program wavefunctions of Burgess were employed which were non-divergent at r = 0, and the radial integral was evaluated by means of equal-integral quadrature. Both sets of results were then compared with the tabulated values of atomic transition probabilities (in atomic units) given in the NBS tables (Wiese et al. 1969)

The results obtained by Heckmann for H I, Li I, O VII and Si XII, together with the associated computer timings (in seconds of CPU time) are displayed in Table 5.2. Clearly, the author's approach is superior to that of Bely both in terms of accuracy and efficiency, requiring only 10-20% of Bely's CPU time.

Species	Transition	G-L Quadrature		Bely		NSRDS
		S(a.u.)	Time (secs)	S(a.u.)	Time (secs)	S(a.u.)
H I	1s - 2p	3.33	0.45	3.29	3.1	3.33
	2p - 3s	1.759	0.54	1.759	5.0	1.761
	2p - 3s	17.74	0.66	17.71	5.0	18.5
Li I	2p - 6s	0.1596	0.63	0.1591	5.0	0.156
	2p - 3d	77.8	0.40	75.8	5.5	80.4
	3d - 4p	11.54	0.54	11.37	6.0	11.7
	3d - 4f	625.0	0.47	617.0	5.0	625.0
O VII	$2^3S - 3^3P$	0.409	0.48	0.413	3.0	0.413
	$2^3S - 7^3P$	0.0085	0.48	0.0087	3.0	-----
	$3^3S - 3^3P$	9.49	0.47	9.52	2.0	-----
Si XII	3d - 4f	4.38	0.39	4.28	3.0	-----

Table 5.2 Results of Heckmann

5.2 PERFORMANCE OF GAUSS-LAGUERRE QUADRATURE: LARGE ν, ν'

As remarked earlier, when the author's method of computing radial integrals was being developed, there were no reliable alternative methods available for comparison when $\nu, \nu' \geq 15$. The assessment of the performance of the new method was therefore based upon numerical experimentation, as described below. We note that efficiency was particularly important in this assessment, in view of the large number of radial integrals required in calculations associated with the quadratic Zeeman effect (see Chapters 2 and 6).

5.2.1 Integer Case

The discussion of the accuracy and efficiency of the Gauss-Laguerre quadrature formula (3.31) at large ν, ν' is best begun by considering the special case in which ν, ν' are integers, equal to n, n', say. In this case the function $g(x)$ is a polynomial of degree $n + n' + s$ (see equation 3.26). It therefore follows from the well-known properties of Gaussian quadrature formulas (Krylov 1962, Stroud and Secrest 1966) that (3.31) is exact if the order of the quadrature formula, M, is chosen such that $2M - 1 \geq n + n' + s$, i.e. $M \geq M_0$, where M_0 is the smallest integer satisfying the inequality.

$$M_0 \geq \tfrac{1}{2}(n + n' + s + 1). \qquad (5.1)$$

In order to check the validity of the computer programs used to implement the Gauss-Laguerre quadrature formula, a variety of integrals (involving integer ν, ν') was computed using (3.31) with $r_0 = 0$, and the results compared with those obtained by evaluating the analytical expressions due to Gordon (1929). These tests also verified the accuracy

of the recurrence relations used in the computation of the integrand. The associated results showed that rounding errors did not grow any faster that the required Whittaker functions (see Section 4.4).

5.2.2 Non-Integer Case

When ν and ν' are not integers there is no analytical technique for determining the appropriate order of the quadrature formula. Unfortunately, the expression for the remainder term of (3.27), which is defined by (3.30), is of no practical value in numerical calculations. The appropriate choice of M can only by determined empirically.

By analogy with the integer case we define M_o as the smallest integer which satisfies the inequality

$$M_o \geq \tfrac{1}{2}(\nu + \nu' + s + 1). \qquad (5.2)$$

For a given integral, the amount by which M must exceed M_o to achieve a specified accuracy gives an indication of the effectiveness of the quadrature formula.

A series of calculations of $J_s(\nu\ell, \nu'\ell', \tau_o)$ was performed in which (3.31) was evaluated for a sequence of values of M. We chose $M = M_o$, $M_o + 1, \ldots$ increasing until the computed value of the integral converged to within four significant figures. These calculations were performed for a wide range of values of the parameters $\nu, \nu', \ell, \ell', \tau_o, s$. In each case great care was taken to ensure that errors in the integral arising from the computation of the Whittaker functions in the integrand were minimized by choosing unusually large values of N and n (see Section 4.5). The results of five typical cases are illustrated in Table 5.3.

The examples in Table 5.3 demonstrate that, as M increases beyond M_o,

Case I		Case II		Case III		Case IV		Case V	
$\nu = 17.23$, $\nu' = 32.27$ $\ell = 1$, $\ell' = 2$, $s = 1$, $r_0 = 7.42$		$\nu = 25.4$, $\nu' = 22.5$ $\ell = 1$, $\ell' = 1$, $s = 2$, $r_0 = 25.31$		$\nu = 31.7$, $\nu' = 29.8$ $\ell = 1$, $\ell' = 2$, $s = 2$, $r_0 = 44.4$		$\nu = 35.5$, $\nu' = 35.5$ $\ell = 1$, $\ell' = 1$, $s = 2$, $r_0 = 63.02$		$\nu = 17.23$, $\nu' = 32.27$ $\ell = 1$, $\ell' = 2$, $s = 0$, $r_0 = 7.42$	
M	$J_s \times 10^{-1}$	M	$J_s \times 10^{-5}$	M	$J_s \times 10^{-6}$	M	$J_s \times 10^{-7}$	M	$J_s \times 10^{2}$
25	.26291	24	-.94858	31	-.30001	35	.25564	25	.35574
26	.25897	25	-.18390	32	-.15557	36	.38932	26	.36043
27	.25868	26	.20934	33	-.15476	37	.39674	27	.36526
28	.25865	27	.20935	34	-.15476	42	.39674	28	.36555
29	.25863	28	.20935	36	-.15476	45	.39674	29	.36564
30	.25862	29	.20935	38	-.15476			30	.36567
32	.25862	48	.20935	41	-.15476			31	.36568
34	.25862							32	.36568
48	.25862							33	.36568
$M_o = 26$, $M_* = 29$		$M_o = 26$, $M_* = 27$		$M_o = 33$, $M_* = 33$		$M_o = 37$, $M_* = 37$		$M_o = 26$, $M_* = 30$	

Table 5.3. Convergence of the Computed Integral as M Increases

the value of the computed integral converges rapidly. An empirical analysis of a large volume of similar calculations has shown that the appropriate choice of M depends primarily on r_o and $\nu + \nu'$. In general, if we denote this choice of M by M_*, and adopt the empirical rule $r_o = \frac{s\nu\nu'}{2oz}$ (see Section 5.2.3), we find that if s = 1 or 2, the assignment

$$M_* = M_o + 3 \qquad (5.3)$$

usually ensures an accuracy of four significant figures.

Exceptions to this "rule of thumb" frequently appear. For instance, if $\nu + \nu'$ differs from an integer by less than about 0.1 (see Cases II and IV of Table 5.3) we need only put $M_* = M_o + 1$ or even M_o. On the other hand, if s = 0 (e.g. in normalization integrals) we may need to put $M_* = M_o + 5$ to achieve the same accuracy.

5.2.3 Choice of Lower Limit of Integration

When using the approximation (3.21) to compute the radial integral (3.9) the lower limit of integration, r_o, should be chosen such that the contribution to the required integral, I_s, arising from the interval $(0, r_o)$ can be neglected. However, we note that even if such a value of r_o cannot be found, i.e. if the Coulomb approximation is not valid, the proposed numerical method can still be used to compute the contribution arising from (r_o, ∞), where Coulomb wavefunctions are valid, provided an appropriate method is used to compute the contribution arising from $(0, r_o)$, e.g. Thomas-Fermi or self-consistent-field method.

A series of numerical calculations was performed to investigate the stability of the radial integral $J_s(\nu l; \nu' l'; r_o)$ with respect to variation of r_o. Some typical results are shown in Table 5.4. In the example illustrated here r_o was varied between 10.0 and 150.0 (a.u.) keeping

r_o	$J_1 \times 10^{-2}$	$e_1 \times 10^{-2}$	$J_2 \times 10^{-6}$	$e_2 \times 10^{-6}$
10	.42905	.00000	.10670	.00000
20	.42903	-.00002	.10670	.00000
30	.42898	-.00007	.10670	.00000
40	.42898	-.00007	.10670	.00000
50	.42878	-.00027	.10669	-.00001
60	.42911	.00006	.10670	.00000
70	.42911	.00006	.10670	.00000
80	.43023	.00118	.10670	.00000
90	.43039	.00134	.10671	.00001
100	.43272	.00367	.10673	.00003
110	.43319	.00414	.10673	.00003
120	.43552	.00647	.10676	.00006
130	.43808	.00903	.10679	.00009
140	.43862	.00960	.10680	.00010
150	.44245	.01340	.10686	.00016

Table 5.4 Variation of $J_s(34.1, 1; 37.2, 0; r_o)$ with r_o

$\nu = 34.1$, $\nu' = 37.2$, $\ell = 1$, $\ell' = 0$ and $z = 1$. The variation of the integral with respect to r_o, which is represented by $e_s = J_s(r_o) - J_s(10)$ was computed for the two cases $s = 1$ and $s = 2$. The results show that, provided r_o is sufficiently small, J_s is relatively insensitive to variation of r_o.

Other calculations involving a wide range of parameters ν, ν', ℓ, ℓ' $(\nu, \nu' \gtrsim 10)$ have confirmed this behaviour. In each case there is a broad range of values of r_o over which $J_s(r_o)$ is relatively stable; any value of r_o chosen from this stable region yields a meaningful value for the associated radial integral $J_s(r_o)$. Wherever possible this value was verified using the Bates-Damgaard method (see Section 5.2.4)

In order to gain further insight into the behaviour of $J_s(r_o)$, a series of integrals was computed in which $\nu - \nu'$ was fixed and ν and r_o varied. We chose $\ell = 0$ and set $\ell' = 1$ in the dipole case ($s = 1$) and $\ell' = 2$ in the quadrupole case ($s = 2$). The relative variation of J_s with respect to r_o was then determined by computing the quantity $v_s(r_o, r_*)$, defined by the equation

$$v_s(r_o, r_*) = \left| \frac{J_s(r_o) - J_s(r_*)}{J_s(r_*)} \right| . \qquad (5.4)$$

The representative value of r_o, lying within the stable region of a set of computed integrals and denoted by r_*, was chosen by inspection. The results of two such sets of calculations, one dipole case and one quadrupole case, are illustrated in Tables 5.5. In this example $\nu - \nu' = 6.89$, ν varied between 26.2 and 43.7, and r_o varied between 5.0 and 90.0. By inspection we chose $r_* = 15.0$ if $s = 1$ and $r_* = 40.0$ if $s = 2$. The relative variations, which are displayed in column 2 of Table 5.5, give an indication

ν	$U_s(r_0, r_*)$	N	M	Time	$J_s(r_*) \times 10^{-2}$
26.2	.100	5	27	.115	.8299
29.7	.025	5	32	.142	.1128
33.2	.020	5	35	.180	.1471
36.7	.010	5	37	.219	.1858
40.25	.005	6	42	.225	.2289
43.7	.005	6	45	.280	.2764

(a) Dipole Case: $s = 1$, $\ell = 0$, $\ell' = 1$, $\nu - \nu' = 6.89$

ν	$U_s(r_0, r_*)$	N	M	Time	$J_s(r_*) \times 10^{-5}$
26.2	.020	4	28	.121	.01957
29.7	.010	4	31	.138	.03555
33.2	.005	5	34	.169	.5959
36.7	.001	5	37	.205	.9402
40.25	.001	5	41	.220	.1414
43.7	.000	5	45	.262	.2047

(b) Quadrupole Case: $s = 2$, $\ell = 0$, $\ell' = 2$, $\nu - \nu' = 6.89$

Table 5.5 Behaviour of $U(r_0, r_*)$

of the contribution to the integral arising from small radial distances; thus they indicate the physical significance of the computed integrals.

The third column of Table 5.5 indicates the smallest value of N (see Section 4.5) which can be used in the computation of the Whittaker functions in the integrand without introducing errors in the fourth significant figure of $J_s(r_*)$. The fourth column indicates the corresponding smallest order of quadrature formula. The fifth column gives the time (in seconds) required to compute $J_s(r_*)$, ignoring the time required to compute the weights and zeros of the quadrature formula. The computed value of the integral $J_s(r_*)$ is given in column 6.

An analysis of a large volume of numerical results describing the behaviour of $\mathcal{V}_s(r_o, r_*)$ has lead to a very simple empirical rule for estimating the appropriate choice of lower cut-off radius when computing a radial integral in the context of the Coulomb approximation: r_o should be chosen according to the rule

$$r_o = \frac{\nu\nu'}{z\eta_s}, \qquad (5.5)$$

where $10 < (\eta_0, \eta_1) < 20$ and $6 < \eta_2 < 10$. This formula usually produces a reliable value of $J_s(r_o)$ if $10 \lesssim (\nu, \nu') \lesssim 60$, $(\ell, \ell') \lesssim 3$ and s = 0, 1 or 2. However, it should be emphasised that, before (5.5) is used in practical calculations, it is advisable to verify that the Coulomb approximation is actually applicable in the case under study. In particular, it is important to ensure that "quenching" does not occur in the outer part of the integral (see Layzer and Garstang 1968).

The quenching phenomenon is illustrated in Fig. 5.1, which shows J_s as a function of $(\nu - \nu')$, $(\nu + \nu')$ being fixed. These integrals were computed using $r_o = 4.0$, $\nu + \nu' = 20.0$, s = 1, $\ell = 0$, $\ell' = 1$ and z = 1. Clearly, the validity of the Coulomb approximation is doubtful when ν, ν' are such

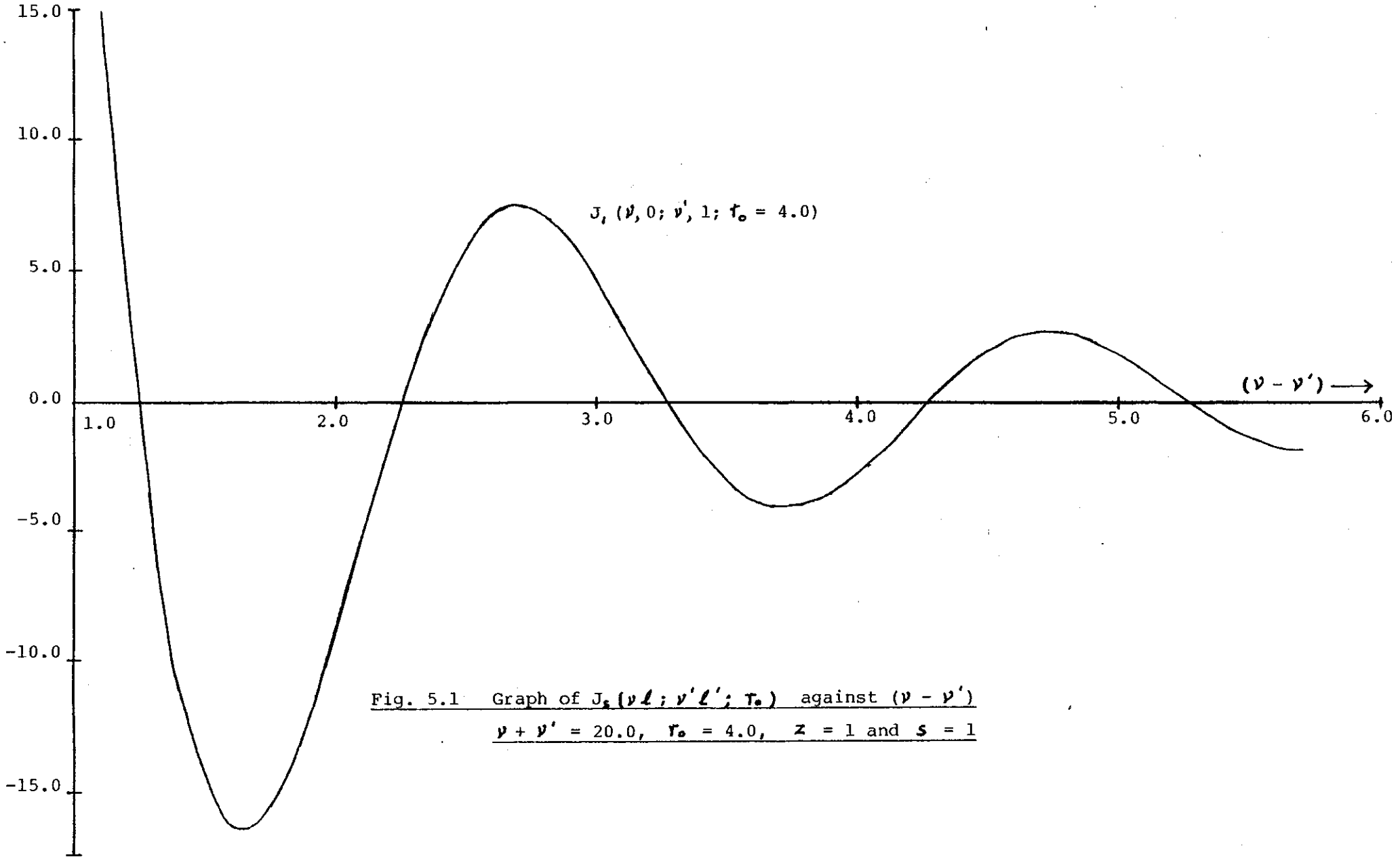

Fig. 5.1 Graph of $J_s(\nu\ell; \nu'\ell'; \tau_0)$ against $(\nu - \nu')$

$\nu + \nu' = 20.0$, $\tau_0 = 4.0$, $z = 1$ and $s = 1$

that the resulting graph lies close to the $(\nu - \nu')$ axis.

We note that the data presented in Table 5.5(b) gives a good indication of the choice of parameters r_o , N and M for typical integrals in the context of the quadratic Zeeman effect. In the examples shown N never exceeds 5, confirming the effectiveness of the Chebyshev expansions for the computation of the Whittaker functions in the integrand.

5.2.4 Comparison with the Bates-Damgaard Method

For non-integer ν, ν' the radial integrals obtained using the author's method have been compared with those obtained using the Bates-Damgaard method. Of course, these checks could only be made for a limited range of ν, ν' since the Bates-Damgaard method fails when ν, ν' become sufficiently large. Using double precision arithmetic (i.e. about 28 significant decimal digits) this limit was $\nu, \nu' \lesssim 25$ (see Section 5.3).

Table 5.6 shows a set of radial integrals computed by the Bates-Damgaard method and Gauss-Laguerre quadrature. $\nu + \nu'$ was fixed (=23.7) and ν varied between 12.2 and 17.1, keeping $\ell = 1$, $\ell' = 2$, s = 1 and z = 1. Using the quadrature method J_s was computed with $r_o = 1.0, 2.0, \ldots\ldots, 10.0$, this range of r_o encompassing the stable region of all the computed integrals. r_* was then chosen by inspection. We note, however, that in some cases there was no clear choice of r_* , since J_s was very sensitive to variations in r_o . These cases, which occurred when $|\nu - \nu'|$ was relatively large or when the computed integral was relatively small, are indicated by an asterisk in Table 5.6. In all calculations using Gauss-Laguerre quadrature we chose M = 15, and set N = 9 if $r_* \lesssim 4.0$ and N = 8 if $r_* > 4.0$.

Table 5.6 also shows the computer (CPU) time required to compute the

ν	T_*	Gauss-Laguerre	Time (secs)	Bates-Damgaard	Time (secs)
12.2	4.0	$.9819 \times 10^{2}$	.059	$.9824 \times 10^{2}$	.028
12.55	5.0	$-.1478 \times 10^{1}$	.060	$-.1478 \times 10^{1}$	.025
12.9	7.0	$-.6733 \times 10^{1}$	.059	$-.6701 \times 10^{1}$	.026
13.25	6.0	$.9199 \times 10^{1}$	.057	$.9243 \times 10^{1}$	.026
14.3	8.0	$.2980 \times 10^{1}$	.056	$.3016 \times 10^{1}$	.026
14.65	4.0	$.2376 \times 10^{1}$	.058	$.2380 \times 10^{1}$	.025
15.0	2.0^{*}	.4109	.050	.4583	.022
15.35	6.0^{-}	$.1113 \times 10^{1}$	.050	$.1114 \times 10^{1}$	.016
15.7	2.0	$-.1343 \times 10^{1}$	.053	$-.1344 \times 10^{1}$	.028
16.05	2.0^{*}	.5675	.060	.6187	.027
16.4	4.0^{*}	.3882	.056	.3640	.026
16.75	2.0^{*}	-.7291	.060	-.7240	.026
17.1	4.0^{*}	.4865	.060	.5314	.025

Table 5.6 Comparison of Author's Method with Bates-Damgaard Method, $\nu + \nu' = 23.7$, $\ell = 1$, $\ell' = 2$, $s = 1$, $z = 1$.

The time specified for Gauss-Laguerre Quadrature does not include the time required to compute the weights and zeros.

radial integrals. Clearly the author's method requires 2-3 times as much computing time as the Bates-Damgaard method. It should be noted that the time specified for Gauss-Laguerre quadrature does not include the time required to compute the weights and zeros (see Section 5.2.6).

5.2.5 Comparison with Other Quadrature Formulas

In order to assess Gauss-Laguerre quadrature in relation to other methods of numerical integration, J_S was evaluated using Romberg and Clenshaw-Curtis quadrature. Before applying either of these methods the infinite interval of integration (r_o, ∞) must be replaced by a finite interval of integration (r_o, r_{max}). An appropriate choice of r_{max} was found to be

$$r_{max} = r_c + \alpha (r_c - r_d), \qquad (5.6)$$

where r_c is the classical turning point of $W_{\tilde{\nu}, \tilde{l}+\frac{1}{2}}\left(\frac{2zr}{\tilde{\nu}}\right)$, r_d is the largest zero of $W_{\tilde{\nu}, \tilde{l}+\frac{1}{2}}\left(\frac{2zr}{\nu'}\right)$, $\tilde{\nu} = \max(\nu, \nu')$ and α is a constant lying in the range 1.5 - 3.5. If ν, ν' are large then r_d is given by (Abramowitz and Stegun 1964)

$$r_d = \frac{1}{2z}\left[\tilde{\nu}\sqrt{2} - 2^{-1/6}\,\tilde{\nu}^{1/3}\,|a_1|\right]^2, \qquad (5.7)$$

where $|a_1| = 2.3381074$, a_1 being the smallest zero of the Airy function Ai(a). This choice of upper limit ensures that r_{max} lies well beyond the outer turning points of the radial wavefunctions in the integrand.

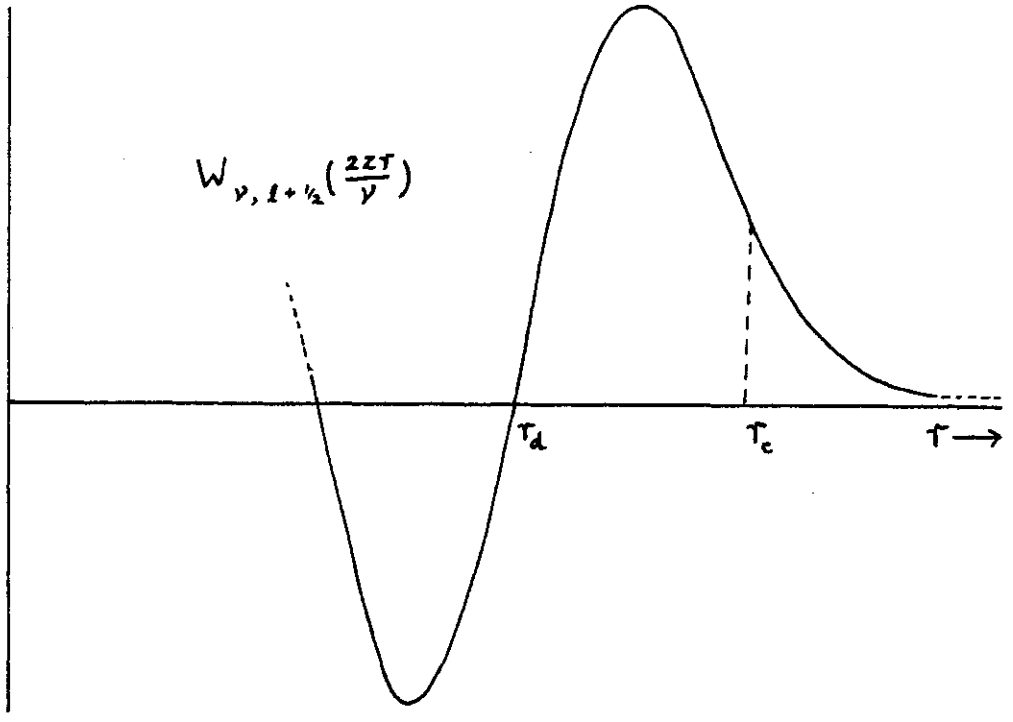

Fig. 5.2 Graphical Description of r_c and r_d

Using (5.5) to determine r_o, these calculations demonstrated that, for ν, ν' in the range 30-40, the Romberg method usually required 512 quadrature points and about 2.4 seconds of computing time per integral. Changing the variable of integration to $\sqrt{r}$ did not reduce the number of quadrature points. The Clenshaw-Curtis method, on the other hand, usually required about 100 points and 0.8 seconds of computing time per integral. By contrast Gauss-Laguerre quadrature never required more than 43 points and 0.3 seconds of computing time, assuming that the weights and zeros were already available. The additional computing time needed to compute a set of weights and zeros (M = 30-40) was usually about 0.5 secs.

5.2.6 Computation of the Weights and Zeros

The method employed to compute the weights and zeros for a particular order of Gauss-Laguerre quadrature (see equations 3.28, 3.29) was a variation of that described by Shao et al. (1963). Since the time needed to compute x_{iM}, λ_{iM}, $i = 1, 2, \ldots, M$ was often greater that the time required to compute the radial integral (assuming x_{iM}, λ_{iM} were given), it was found more economical to specify a value of M large enough to deal satisfactorily with a group of radial integrals having neighbouring parameters. The appropriate set of weights and zeros could then be computed and stored for repeated use. All computer programs have been written to facilitate this procedure.

5.3 ANALYSIS OF THE BATES-DAMGAARD METHOD

In view of their wide domain of applicability, the numerical methods proposed in this thesis provided an effective means of assessing the performance of other methods of computing radial integrals in the Coulomb approximation. In particular, they enabled the author to conduct a detailed analysis of the Bates-Damgaard method. As remarked earlier (Section 3.3), the Bates-Damgaard method breaks down when ν, ν' becomes sufficiently large, and previous analyses have never given an adequate explanation of this phenomenon. Even Oertel and Shomo only concluded that the cause "probably lies in numerical cancellations" (Oertel and Shomo 1968, p177).

The present author's analysis of the Bates-Damgaard method falls into two parts:

(a) an investigation of the numerical cancellations which arise in the evaluation of the equation (3.18);

(b) an investigation of the criterion used to truncate the infinite series (3.13).

We note that (b) was the subject of a limited study by Friedrich et al. (1970), as we shall discuss in Section 5.3.2.

5.3.1 Numerical Cancellations

This part of the investigation was begun by repeating some of the calculations of Oertel and Shomo (loc. cit.), using single and double precision arithmetic. These calculations confirmed that numerical cancellations (i.e. rounding errors) give rise to a loss of accuracy in the computed integrals whenever ν, ν' become sufficiently large. The point at which the method actually breaks down was found to depend upon the number of significant figures used in the numerical calculations, and upon the desired accuracy of the required integrals, e.g. in order to ensure an accuracy of four significant figures when using 14 significant decimal digits, ν, ν' must not exceed 12; the corresponding limit when using 28 significant decimal digits is $\nu, \nu' \lesssim 25$. However, disastrous rounding errors can still occur if $\nu, \nu' \lesssim 25$ due to the "quenching phenomenon" (see Section 5.2.3). It should of course be emphasised that the main purpose of the present investigation was not to establish precise numerical limits regarding the validity of the Bates-Damgaard method, but to identify the underlying causes of the errors which arise when ν, ν' become large.

In order to provide an adequate theoretical basis for this analysis it is useful to return to equation (3.18) and express it in this form

$$I_s^{BD} = f \sum_{i=0,\, j=0}^{i+j \leq k_m} (-1)^{i+j} a_i a_j' \left(\frac{\nu + \nu'}{2\nu'} \right)^i \left(\frac{\nu + \nu'}{2\nu} \right)^j \times \left[\frac{\nu \nu'}{2(\nu + \nu')} \right]^\beta \Gamma(\beta - i - j). \qquad (5.8)$$

On putting

$$e_i = a_i \left(\frac{\nu+\nu'}{2\nu'}\right)^i, \quad e_i' = a_i' \left(\frac{\nu+\nu'}{2\nu}\right)^i, \tag{5.9}$$

and re-arranging (5.8) we find that

$$I_s^{SD} = h \sum_{K=0}^{K_m} (-1)^K \Gamma(\beta - K) \sum_{i=0}^{K} e_i e'_{K-i}, \tag{5.10}$$

where

$$h = f \left[\frac{\nu\nu'}{z(\nu+\nu')}\right]^{\beta}. \tag{5.11}$$

Now, on substituting

$$b_K = \sum_{i=0}^{K} e_i \acute{e}_{K-i}, \tag{5.12}$$

we find that I_s^{SD} can be expressed in the simple form

$$I_s^{SD} = h \sum_{K=0}^{K_m} (-1)^K \Gamma(\beta - K)\, b_K. \tag{5.13}$$

It follows from equation (5.13) that there are two potential sources of rounding errors in the evaluation of $I_S^{(8)}$:

(i) errors which arise during the computation of b_κ using (5.12);

(ii) errors which arise during the summation of (5.13).

Since a very effective asymptotic expansion for $\log_e \Gamma(x)$ $(x \to \infty)$ is available (see Abramowitz and Stegun 1964, equation 6.1.41), there is no practical danger of excessive rounding errors arising during the computation of the multiplying factor, h.

The extent to which errors of types (i) or (ii) arise depends upon the existence of terms of relatively large magnitude and alternating sign in the corresponding series (5.12) and (5.13). If either series contains terms which are large compared with the sum of series, even the leading digits of the computed sum may not be significant. An estimate of the number of significant digits, $\bar{p}$, in the computed sum is given by the expression

$$\bar{p} \approx p - \log_{10}[|\text{max. term}|/|\text{sum}|], \qquad (5.14)$$

where p is the number of significant decimal digits used in the computation (see Wilkinson 1963 for details). Unfortunately, this estimate of $\bar{p}$ cannot be utilized in computer programs since, if rounding errors are present, the computed sum may not be an accurate estimate of the actual sum of the series.

We now consider errors of types (i) and (ii) in more detail.

(i) Errors of Type (i)

From equations (3.17) and (5.9) it follows that e_i satisfies the recurrence relation:

$$e_i = \left(\frac{\nu+\nu'}{2\nu'}\right)\frac{1}{i}(\nu-\ell-i)(\nu+\ell+1-i)\,e_{i-1}\,, \qquad (5.15)$$

where $e_0 = 1$. Thus the terms of the sequence $\{e_i\}_{i=0}^{\infty}$ are positive if $i \leq [\nu] - \ell$, negative if $i \geq [\nu] + \ell + 1$, and alternate in sign if $[\nu] - \ell < i < [\nu] + \ell + 1$. The sequence terminates only if ν is an integer ($\geq \ell$), in which case $e_i = 0$ if $i \geq \nu - \ell$.

In order to assess the possibility of rounding errors in the computation of b_k it is necessary to investigate the signs and relative magnitudes of the individual terms of equation (5.12). This investigation is simplified if these terms, $e_i e'_j$, are represented by points on a two-dimensional plane whose axes are labelled by i and j, as illustrated in Fig. 5.3. The products $e_i e'_j$ which arise in (5.12) are then represented by those points (i, j) which lie along the line $i + j = k$.

It follows from the above remarks that the signs of the terms of $\{e_i e'_{k-i}\}_{i=0}^{k}$ are governed by the following rules:

(a) $\{e_i e_{k-i}\}_{i=0}^{k}$ is positive

if $i \leq [\nu] - \ell$ and $j \leq [\nu'] - \ell'$,

or if $i \geq [\nu] + \ell + 1$ and $j \geq [\nu'] + \ell' + 1$.

(b) $\{ e_i e'_{k-i} \}_{i=0}^{k}$ is negative

if $i \geq [\nu] + \ell + 1$ and $j \leq [\nu'] - \ell'$

or if $i \geq [\nu'] + \ell' + 1$ and $j \leq [\nu] - \ell$.

(c) $\{ e_i e'_{k-i} \}_{i=0}^{k}$ alternate in sign

if $i \leq [\nu] - \ell$ and $[\nu'] - \ell' < j < [\nu'] + \ell' + 1$

or if $i \geq [\nu] + \ell + 1$ and $[\nu'] - \ell' < j < [\nu'] + \ell' + 1$

or if $j \leq [\nu'] - \ell'$ and $[\nu] - \ell < i < [\nu] + \ell + 1$

or if $j \geq [\nu'] + \ell' + 1$ and $[\nu] - \ell < i < [\nu] + \ell + 1$.

(d) $\{ e_i e'_{k-i} \}_{i=0}^{k}$ have the same sign

if $[\nu] - \ell < i < [\nu] + \ell + 1$ and $[\nu'] - \ell' < j < [\nu'] + \ell' + 1$

the sign alternating as k $(= i + j)$ varies

between $[\nu] + [\nu'] - \ell - \ell'$ and $[\nu] + [\nu'] + \ell + \ell' + 2$.

The four regions of the (i , j) plane defined by (a), (b), (c) and (d) are illustrated in Fig. 5.3.

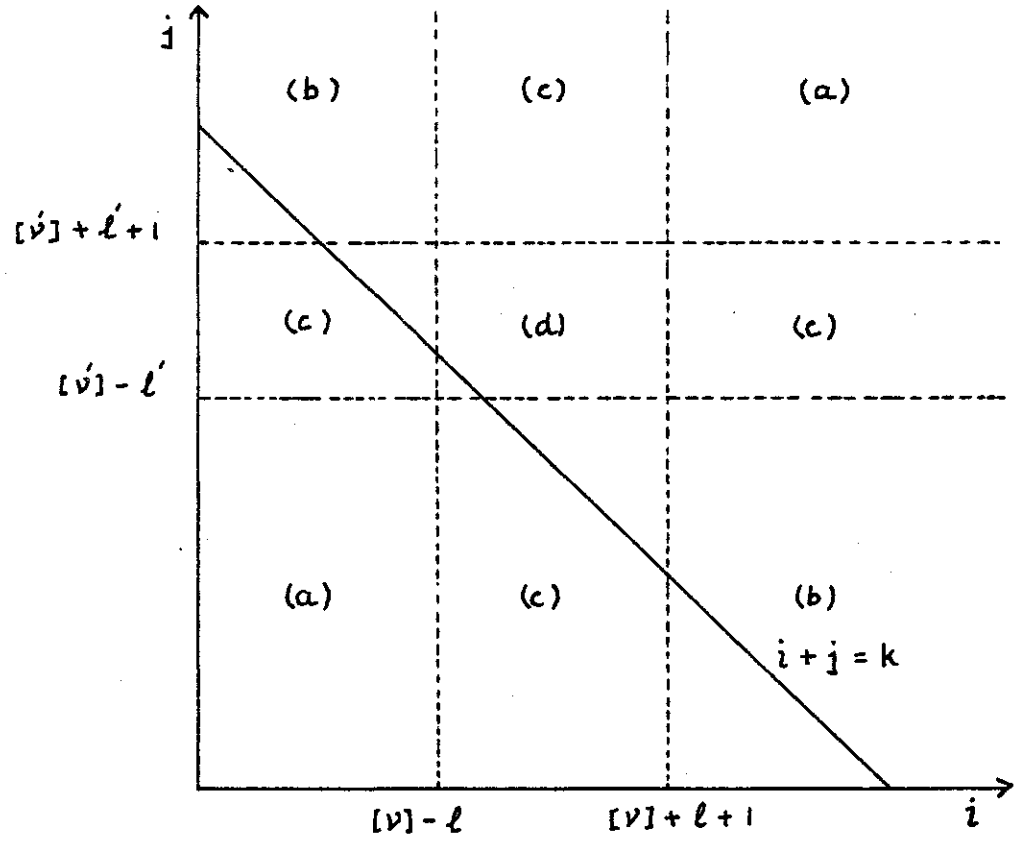

Fig. 5.3 Graphical Representation of $e_i e'_j$

It is clear from the above discussion that there is no possibility of numerical cancellations arising in the computation of b_k until

$$k \geq \min([\nu] - \ell, [\nu'] - \ell').$$

For smaller values of k all of the terms of (5.12) are positive. At larger values of k numerical cancellation is possible in principle. However, in practice, it is only when k lies close to k_m that negative terms $e_i e'_j$

arising from (b), (c) or (d) (see Fig. 5.3) are large enough to cancel the large positive terms which arise from region (a).

Numerical calculations have shown that, in the context of the quadratic Zeeman effect, b_k is normally positive except when $k_m - k \leq 4$. These calculations have also shown that not more than 2 or 3 significant figures of b_k are lost due to numerical cancellation. These rounding errors are negligible when compared with the severe errors which arise during the summation of the main series (5.13), as we shall discuss below.

Further confirmation of the above conclusions was provided by the observation that the values of ν, ν' at which the breakdown of the Bates-Damgaard method occurs does not depend upon whether ν or ν' are integers: in the integer case all terms of (5.12) are positive, and so there is no possibility of cancellation errors arising in the computation of b_k.

(ii) Errors of Type (ii)

Let us denote the term $(-1)^k \Gamma(\beta - k)$ of (5.13) by g_k. From the properties of the Gamma function (Abramowitz and Stegun 1964) it follows that g_k satisfies the recurrence relation

$$g_{k-1} = -(\beta - k) g_k , \qquad k \geq 1 , \tag{5.16}$$

where

$$g_0 = \Gamma(\beta).$$

Since $\beta - k$ is positive if $0 \leq k \leq k_m$ (see equations 3.16 and 3.19), and therefore $\Gamma(\beta - k)$ is always positive, the terms of the sequence $\{ g_k \}_{k=0}^{k_m}$ alternate in sign and decrease in magnitude as k increases. Therefore the individual terms, $g_k b_k$, of (5.13) alternate in sign if all b_k, $(0 \leq k \leq k_m)$, are of the same sign.

The behaviour of a typical sequence $\{q_k b_k\}$ is illustrated in Table 5.7. The sequence $\{q_k b_k / q_0 b_0\}$, together with the partial sums $c_k = \sum_{i=0}^{k} q_i b_i / q_0 b_0$ are given for the case $\nu = 20.25$, $\ell = 2$, $\nu' = 19.25$, $\ell' = 1$, $s = 1$, $z = 1$. Clearly, the signs of $\{q_k b_k / q_0 b_0\}$ and c_k alternate until $k = 35$. We note also that c_k increases in absolute value until $k = 12$, and then decreases as k increases further. In view of the alternation in sign of $q_k b_k$, and the existence of terms of very large magnitude (in relation to the total sum, c_{km}), it is clear that numerical cancellation would give rise to intolerable rounding errors unless a sufficient number of digits is used in the computation. In this example the calculations were performed using 28 significant decimal digits, 16 of which were lost due to cancellations. Only the most significant eight digits are displayed in Table 5.7.

Calculations similar to those of Table 5.7, involving ν, ν' in the range 20 - 35 and $\ell, \ell' = 0$, 1, 2 or 3, have shown that the magnitudes of the terms $q_k b_k$, and hence the severity of numerical cancellations, increases rapidly as ν, ν' increase. When ν, ν' lie in the range 25 - 30 only 2 or 3 figures of the computed value of c_{km} may be significant.

This investigation has not produced any rules, either empirical or analytical, which might give practical guidance to users of the Bates-Damgaard method regarding onset of numerical errors as ν, ν' increase. The only advice which can be given is that if one is in any doubt about the domain of validity of the Bates-Damgaard method, then one should examine the behaviour of the sequence $\{q_k b_k\}$ for a few typical sets of parameters ν, ν', ℓ, ℓ'. Equation (5.14) can then be applied manually to give an estimate of the severity of the numerical cancellation.

k	$g_k b_k / g_0 b_0$	c_k	k	$g_k b_k / g_0 b_0$	c_k	k	$g_k b_k / g_0 b_0$	c_k
0	1.0000000	1.0000000	13	-322109.62	-150564.27	26	4.9588979	.78620611
1	-18.135040	-17.135040	14	268021.58	117457.30	27	-.91359362	-.12738752
2	159.95078	142.81574	15	-199141.41	-81684.103	28	.14487591	$.17488388 \times 10^{-1}$
3	-914.08031	-771.26457	16	132429.50	50745.393	29	$-.19481330 \times 10^{-1}$	$-.19929419 \times 10^{-2}$
4	3804.3975	3033.1329	17	-78943.069	-28197.676	30	$.21759444 \times 10^{-2}$	$.18300255 \times 10^{-3}$
5	-12289.015	-9255.8817	18	42219.935	14022.259	31	$-.19593331 \times 10^{-3}$	$-.12930757 \times 10^{-4}$
6	32061.090	22805.208	19	-20261.359	-6239.0999	32	$.13579971 \times 10^{-4}$	$.64921452 \times 10^{-6}$
7	-69414.016	-44608.808	20	8720.5796	2481.4797	33	$-.66878636 \times 10^{-6}$	$-.19571842 \times 10^{-7}$
8	127171.64	80562.834	21	-3362.1706	-880.69086	34	$.19779826 \times 10^{-7}$	$.20798339 \times 10^{-9}$
9	-200043.17	-119480.34	22	1158.8643	278.17339	35	$-.19645580 \times 10^{-9}$	$.11527610 \times 10^{-10}$
10	273199.72	153719.38	23	-356.08460	-77.911212	36	$-.19718997 \times 10^{-11}$	$.95557102 \times 10^{-11}$
11	-326752.28	-173032.90	24	97.166918	19.255706	37	$-.60792006 \times 10^{-13}$	$.94949182 \times 10^{-11}$
12	344578.25	171545.35	25	-23.428398	-4.1726918	38	$-.45200129 \times 10^{-14}$	$.94903982 \times 10^{-11}$

Table 5.7 Terms of the Bates-Damgaard Series (5.13)

$\nu = 20.25$, $\ell = 2$, $\nu' = 19.25$, $\ell' = 1$,

$s = 1$, $z = 1$, $r_0 = 10.0$

5.3.2 Truncation Criterion

The second major aspect of the Bates-Damgaard method which was investigated was the criterion used to truncate the infinite series (3.13). In the following discussion we examine the validity of this criterion by developing an asymptotic expansion of the radial integral (3.21) which takes account of the lower cut-off radius, r_o.

(i) Asymptotic Expansion of the Radial Integral

For a general introduction to asymptotic series and their properties see Olver (1974) or Jeffreys (1962). A detailed discussion of the asymptotic properties of Whittaker functions is given in Slater (1960).

An asymptotic expansion of $J_s(\nu\ell;\nu'\ell';r_o)$ can be obtained from (3.21) by invoking asymptotic expansions of the form (3.11) for the two Whittaker functions in the integrand. These two asymptotic expansions can be multiplied to produce an asymptotic expansion of the integrand in terms of $\frac{1}{r}$. Thus we have

$$R_{n\ell}(r)\,r^{s}\,R_{n'\ell'}(r)$$

$$\underset{r\to\infty}{\sim} f\sum_{k=0}^{N-1}(-1)^k e^{-\alpha r}\,r^{\beta-k-1}\,c_k + O[e^{-\alpha r}r^{\beta-N-1}], \qquad (5.17)$$

where

$$c_k = \sum_{i=0}^{k} a_i\,a'_{k-i}\left(\frac{\nu}{2z}\right)^{i}\left(\frac{\nu'}{2z}\right)^{k-i}. \qquad (5.18)$$

On integrating (5.17) over the range (r_0, ∞) with respect to r we find

$$J_s(\nu l; \nu' l'; r_0) = \int_{r_0}^{\infty} R_{nl}(r)\, r^s\, R_{n'l'}(r)\, dr, \tag{5.19}$$

$$\underset{r_0 \to \infty}{\sim} f \sum_{K=0}^{N-1} (-1)^K \int_{r_0}^{\infty} \left\{ e^{-\alpha r} r^{\beta-K-1} C_K + O\left[e^{-\alpha r} r^{\beta-N-1}\right] \right\} dr, \tag{5.20}$$

$$\underset{r_0 \to \infty}{\sim} f \sum_{K=0}^{N-1} (-1)^K C_K \frac{1}{\alpha^{\beta-K}} \Gamma(\beta-K, \alpha r_0) + O\left[\Gamma(\beta-N, \alpha r_0)\right], \tag{5.21}$$

$$\underset{r_0 \to \infty}{\sim} h \sum_{K=0}^{N-1} (-1)^K b_K \Gamma(\beta-K, \alpha r_0) + O\left[\Gamma(\beta-N, \alpha r_0)\right], \tag{5.22}$$

where

$$f = h\, b_K\, \alpha^{\beta-K} / C_K . \tag{5.23}$$

The terms h and b_k have been defined earlier (see equations 5.11 and 5.12) and $\Gamma(x,y)$ is the complementary incomplete Gamma function, defined by the equation (Abramowitz and Stegun 1964)

$$\Gamma(x,y) = \int_y^\infty e^{-t}\, t^{x-1}\, dt. \qquad (5.24)$$

Equation (5.22) is the desired asymptotic expansion of J_s. We note that its form closely resembles that of the Bates-Damgaard expansion (5.13). We also note that, although (5.22) suggests that r_o should be large, in practical calculations quite accurate results can be obtained when r_o is relatively small, as illustrated by the following example.

Let us denote $(-1)^k\, \Gamma(\beta-k, \alpha r_o)$ by d_k. Table 5.8 illustrates the behaviour of the terms $d_k b_k$ of (5.22) for the typical case $\nu = 5.85$, $\nu' = 4.85$, $\ell = 2$, $\ell' = 1$, $s = 1$, $r_o = 1.0$ and $z = 1$. In this example the terms $d_k b_k$, together with the partial sums $s_k = \sum_{i=0}^{k} d_i b_i$, $k \leq 17$, are displayed. These results show that the sequence $\{d_k b_k\}$ exhibits the classical asymptotic behaviour, i.e. after an initial increase, the terms of the sequence $\{|d_k b_k|\}$ decrease to a minimum (at $k = 12$) and thereafter increase indefinitely.

Thus, when using (5.22) to compute $J_1(5.85, 2; 4.85, 1; 1.0)$, the asymptotic expansion should be truncated at the smallest term, $k = 12$; hs_{12} is then the appropriate approximation to J_1, involving a minimum truncation error (Jeffreys 1962). Numerical evaluation of (5.22) in this case gives $J_1 = hs_{12} = 0.9044 \times 10^{-1}$. Computation of the same integral using the author's Gauss-Laguerre quadrature method gives $J_1 = 0.9048 \times 10^{-1}$, whereas the Bates-Damgaard method gives $J_1 = 0.9015 \times 10^{-1}$.

k	$d_k\, b_k$	$s_k = \sum_{i=0}^{k} d_i b_i$
0	225322480.396	225322480.396
1	-768916686.366	-543594206.571
2	1100321279.19	556727072.622
3	-844577391.739	-287850319.116
4	364069952.757	76219633.6411
5	-81552760.5209	-5333126.87978
6	6450159.36979	1117032.49001
7	189347.852920	1306380.34293
8	22601.0374188	1328981.38035
9	6521.59202385	1335502.97237
10	3953.40153991	1339456.37391
11	2270.70338740	1341727.07730
12	-14.9108708443	1341712.16643
13	531.876981730	1342244.04341
14	-1719.08623687	1340524.95717
15	11280.9589680	1351805.91614
16	-104231.623763	1247574.29238
17	1254220.06652	2501794.35890

Table 5.8 Terms of the Asymptotic Series (5.22)

$\nu = 5.85,\ \ell = 2,\ \nu' = 4.85,\ \ell = 1,$

$s = 1,\ z = 1,\ r_0 = 1.0.$

(ii) Comparison with Bates-Damgaard Results

In order to appreciate the relationship between the Bates-Damgaard method and the asymptotic approximation (5.22), the individual terms of each approximation were computed for a range of values of ν, ℓ, ν', ℓ' ($\nu, \nu' < 20$, $\ell, \ell' = 0, 1$ or 2, $z = 1$ and $s = 1$). The terms $q_k b_k / q_0 b_0$ of (5.13) for the case $\nu = 5.85$, $\ell = 2$, $\nu' = 4.85$, $\ell' = 1$, $s = 1$, $r_0 = 1.0$, $z = 1$ are displayed in Table 5.9. The corresponding (but unscaled) terms $d_k b_k$ of (5.22) have already been displayed in Table 5.8. Another example of the terms of (5.22) for the case $\nu = 20.25$, $\ell = 2$, $\nu' = 19.25$, $\ell' = 1$, $r_0 = 10.0$, $s = 1$, $z = 1$ is given in Table 5.10. The corresponding Bates-Damgaard terms are displayed in Table 5.7.

It should be emphasised that it is the overall qualitative behaviour of the two pairs of series in Tables 5.7 - 5.10 that should be compared. We note that the individual terms of the series are not directly numerically comparable, since different scaling factors have been used.

This series of calculations lead to the following observations:

(a) with an appropriate choice of r_0 and scaling factor, the corresponding terms of (5.13) and (5.22) generally agree to within about 0.03%;

(b) the minimum term of (5.22) generally occurs 3 - 4 terms beyond the term $k = k_m$, the Bates-Damgaard truncation point.

It follows from (a) that when ν, ν' become large, the asymptotic expansion (5.22) suffers from rounding errors, similar to those of the Bates-Damgaard method.

k	$g_k b_k / g_o b_o$	$c_K = \sum_{i=o}^{K} g_i b_i / g_o b_o$
0	1.0000000	1.0000000
1	-3.4125165	-2.4125165
2	4.8833178	2.4708013
3	-3.7483051	-1.2775038
4	1.6157729	.33826911
5	-.36193797	$-.23668868 \times 10^{-1}$
6	$.28626357 \times 10^{-1}$	$.49574889 \times 10^{-2}$
7	$.84034729 \times 10^{-3}$	$.57978362 \times 10^{-2}$
8	$.10031567 \times 10^{-3}$	$.58981518 \times 10^{-2}$
9	$.28981276 \times 10^{-4}$	$.59271331 \times 10^{-2}$
10	$.17778882 \times 10^{-4}$	$.59449120 \times 10^{-2}$

Table 5.9 Terms of the Bates-Damgaard Series (5.13)
$\nu = 5.85$, $\ell = 2$, $\nu' = 4.85$, $\ell' = 1$,
$s = 1$, $z = 1$, $r_o = 1.0$.

k	$d_k b_k$	$s_k = \sum_{i=0}^{k} d_i b_i$	k	$d_k b_k$	$s_k = \sum_{i=0}^{k} d_i b_i$	k	$d_k b_k$	$s_k = \sum_{i=0}^{k} d_i b_i$
0	.52085035	.52085035	15	-103722.82	-42545.194	28	$.75458667 \times 10^{-1}$	$.91088332 \times 10^{-2}$
1	-9.4456424	-8.9247921	16	68975.950	26430.756	29	$-.10146858 \times 10^{-1}$	$-.10380225 \times 10^{-2}$
2	83.310418	74.385626	17	-41117.525	-14686.769	30	$.11333414 \times 10^{-2}$	$.95316941 \times 10^{-4}$
3	-467.09905	-401.71342	18	21990.268	7303.4987	31	$-.10205193 \times 10^{-3}$	$-.67349874 \times 10^{-5}$
4	1981.5217	1579.8083	19	-10553.136	-3249.6374	32	$.70731300 \times 10^{-5}$	$.33814259 \times 10^{-6}$
5	-6400.7376	-4820.9292	20	4542.1170	1292.4796	33	$-.34833628 \times 10^{-6}$	$-.10193698 \times 10^{-7}$
6	16699.030	11878.101	21	-1751.1877	-458.70815	34	$.10301996 \times 10^{-7}$	$.10830126 \times 10^{-9}$
7	-36154.315	-24276.214	22	603.59485	144.88671	35	$-.10229912 \times 10^{-9}$	$.60021397 \times 10^{-11}$
8	66237.395	41961.181	23	-185.46679	-40.580082	36	$-.10254215 \times 10^{-11}$	$.49767182 \times 10^{-11}$
9	-104192.56	-62231.376	24	50.609423	10.029341	37	$-.31379823 \times 10^{-13}$	$.49453383 \times 10^{-11}$
10	142296.17	80064.793	25	-12.202689	-2.1733480	38	$-.22562018 \times 10^{-14}$	$.49430821 \times 10^{-11}$
11	-170189.04	-90124.247	26	2.5828437	.40949573	39	$-.54287413 \times 10^{-15}$	$.49425393 \times 10^{-11}$
12	179473.70	89349.453	27	-.47584556	-.066349834	40	$-.43396562 \times 10^{-15}$	$.49424959 \times 10^{-11}$
13	-167770.91	-78421.455				41	$.35337960 \times 10^{-15}$	$.49425312 \times 10^{-11}$
14	139599.13	61177.678				42	$-.38090829 \times 10^{-16}$	$.49424931 \times 10^{-11}$

Table 5.10 Terms of the Asymptotic Series (5.22) (scaled by 10^{-49})

$\nu = 20.25$, $\ell = 2$, $\nu' = 19.25$, $\ell' = 1$,

$s = 1$, $z = 1$, $r_0 = 10.0$

(iii) Comparison with Gauss-Laguerre Quadrature

The accuracy of (5.22) was further assessed by computing the quantity*

$$\mathcal{I}_1 = \frac{2z}{3\nu_{l_>}\sqrt{\nu_{l_>}^2 - l_<^2}}\, J_1(\nu l; \nu' l'; r_0) \qquad (5.25)$$

by three methods: Gauss-Laguerre quadrature, the Bates-Damgaard method and the asymptotic method i.e. equation (5.22). $|\nu - \nu'|$ was fixed and $\mathcal{I}_1$ was computed for various values of $\nu_{l_<}$. The case $|\nu - \nu'| = 0.495$, $l = 0$, $l' = 1$, $z = 1$, $r_0 = 1.0$, $\nu_{l_<} = 1.65\ (0.25)\ 10.0$ is illustrated in graphical form in Fig. 5.4.

Fig. 5.4 shows that the three computed values of $\mathcal{I}_1$ agree very closely except when $\nu_{l_<}$ is close to an integer. The associated numerical values, which are given in Table 5.11, show further that the asymptotic method and Gauss-Laguerre quadrature always agree to within 2×10^{-4} if $\nu_{l_<}$ exceeds 3.0. However, the Bates-Damgaard results differ from the other two methods by as much as 5×10^{-3} when $\nu_{l_<}$ is within 0.15 of an integer. This anomalous behaviour of the Bates-Damgaard method diminishes as $\nu_{l_<}$ increases.

(iv) Variation of the Truncation Point of (5.22)

In order to gain further insight into the anomalous behaviour of the Bates-Damgaard method at small ν, ν' the integrals $\mathcal{I}_1$, $\nu_{l_<} = 2.65\ (0.25)\ 10.0$, were re-computed using (5.22) with four different truncation criteria:

(a) truncate immediately after the term of minimum absolute value;

---

* $l_> = \max(l, l')$, $l_< = \min(l, l')$

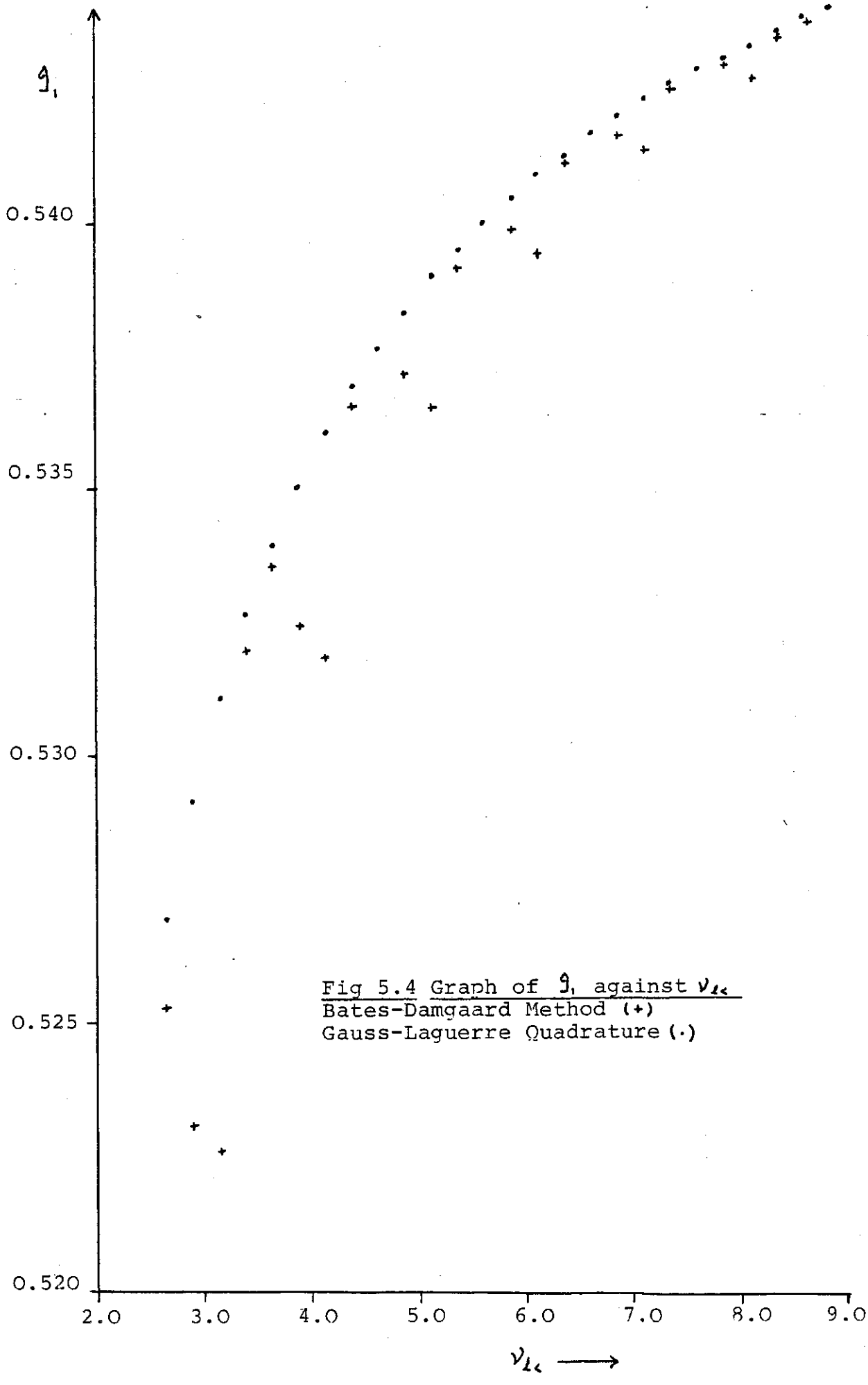

Fig 5.4 Graph of g_1 against ν_{LL}
Bates-Damgaard Method (+)
Gauss-Laguerre Quadrature (·)

(b) as (a), but include only half of the term of minimum absolute value;

(c) truncate immediately before the term of minimum absolute value;

(d) truncate according to the Bates-Damgaard criterion, i.e. include only those terms for which $k \leq \nu + \nu' + s - 2$.

The results of these calculations are shown in Table 5.11. In this case we find that if $\nu_{\ell\ell} \geq 6.5$, all computated values of g_1 agree to within three decimal places. However, if $\nu_{\ell\ell} \leq 6.5$, the values of g_1 obtained using criterion (b) show closest agreement with the values obtained using Gauss-Laguerre quadrature. On the other hand, the results obtained using criterion (d) are in complete agreement with those of the Bates-Damgaard method.

Calculations using other values of $|\nu - \nu'|$ have shown that the anomalous behaviour of the Bates-Damgaard method does not always occur at the integer values of $\nu_{\ell\ell}$. In general, it occurs at those values of $\nu_{\ell\ell}$ such that $(\nu + \nu')$ = ..., 2.5, 3.5, 4.5,.... This can be explained as follows. When ν, ν' are sufficiently large (≥ 6) the asymptotic series (5.22) "converges" reasonably fast and can normally be truncated before the Bates-Damgaard truncation point $k = k_m$. Since the minimum term of (5.25) usually occurs 3 or 4 terms beyond $k = k_m$, it is clear that the computed value of g_1 given by (5.22) is not strongly influenced by the truncation criterion.

For smaller values of ν, ν' the asymptotic series (5.22) "converges" slowly and the computed value of g_1 is sensitive to the truncation criterion. The results of Table 5.11 indicate that criterion (b) produces a minimum truncation error. Hence truncation according to the Bates-Damgaard criterion (d) introduces truncation errors in the third and fourth

ν_{lc}	GL	BD	Asy (a)	Asy (b)	Asy (c)	Asy (d)
2.65	.5270	.5253	.5254	.5253	.5253	.5253
2.90	.5292	.5231	.5280	.5289	.5297	.5231
3.15	.5311	.5226	.5306	.5311	.5316	.5226
3.40	.5327	.5320	.5329	.5327	.5326	.5320
3.65	.5340	.5336	.5334	.5335	.5336	.5336
3.90	.5351	.5325	.5353	.5349	.5345	.5325
4.15	.5361	.5319	.5358	.5361	.5363	.5319
4.40	.5370	.5366	.5369	.5370	.5371	.5366
4.65	.5377	.5377	.5378	.5377	.5377	.5377
4.90	.5384	.5372	.5386	.5383	.5381	.5372
5.15	.5391	.5366	.5389	.5390	.5392	.5366
5.40	.5396	.5394	.5396	.5396	.5397	.5394
5.65	.5401	.5402	.5401	.5401	.5400	.5402
5.90	.5406	.5399	.5407	.5406	.5404	.5399
6.15	.5410	.5395	.5409	.5410	.5411	.5395
6.40	.5414	.5412	.5414	.5414	.5415	.5412
6.65	.5418	.5419	.5418	.5418	.5417	.5419
6.90	.5421	.5417	.5422	.5421	.5420	.5417
7.15	.5424	.5414	.5424	.5424	.5425	.5414
7.40	.5427	.5426	.5426	.5425	.5424	.5426
7.65	.5430	.5431	.5430	.5430	.5430	.5431
7.90	.5432	.5430	.5433	.5433	.5432	.5430
8.15	.5434	.5428	.5435	.5435	.5435	.5428
8.40	.5437	.5436	.5436	.5436	.5435	.5436
8.65	.5440	.5440	.5439	.5439	.5439	.5440
8.90	.5441	.5439	.5442	.5441	.5441	.5439
9.15	.5442	.5438	.5443	.5443	.5444	.5438
9.40	.5445	.5444	.5444	.5444	.5444	.5444

Table 5.11 Dependence of g_1 on the Truncation Criteria (a) - (d), $|\nu - \nu'| = 0.495$, $\ell = 0$, $\ell' = 1$, $r_0 = 0.25$.

GL indicates Gauss-Laguerre quadrature, BD denotes the Bates-Damgaard method, and Asy (a) - Asy (d) denote the asymptotic method using truncation criteria (a) - (d).

decimal places of $\mathcal{J}_1$. Empirical calculations have shown that these errors are greatest when $\nu + \nu'$ lies half-way between successive integers.

A set of calculations of $\mathcal{J}_1$, similar to those outlined above, was performed by Friedrich et al. (1970) in an evaluation of Katterbach's method of computing radial integrals involving Coulomb wavefunctions. However, their calculations did not identify the anomalous behaviour of the Bates-Damgaard method. Indeed, their graphical results show some curious sharp kinks when ν, ν' is less than about 5. These may be due to truncation errors arising in the computation of the radial wavefunction, but this has not been investigated by the present author.

5.4 CONCLUSIONS

In this Chapter we have demonstrated that the author's method of computing radial multipole integrals in the Coulomb approximation is well suited to both exploratory and routine calculations, and is effective at large or small principal quantum numbers, ν, ν'. For $\nu, \nu' \lesssim 25$ the performance of the new method has been compared with the methods of Lindgård and Nielsen and Bates and Damgaard. For $25 \lesssim (\nu, \nu') \lesssim 55$ the main check used has been on the smooth variation of the integrals as functions of ν, ν', with the values for integer ν, ν' as fiducial marks. Our results have shown that the speed and accuracy of the new method compares favourably with the Bates-Damgaard method in the region where the latter is effective.

The general conclusion regarding the new method is that, by choosing appropriate values of r_0, N, n and M, results may always be obtained in which the computational errors are as small as desired, and thus negligible in comparison with the errors implicit in the assumptions of the Coulomb

approximation. Of course, even if the Coulomb approximation is inappropriate, the new method may still be an effective means of computing that part of the radial integral arising from large radial distances where Coulomb wavefunctions are valid; the remainder of the integral can then be computed by other means, using, for instance, Thomas-Fermi or self-consistent-field methods to determine the radial wavefunctions at small radial distances.

The most striking outcome of the tests on the new method is the relatively small number of abscissae needed to achieve a prescribed accuracy with Gauss-Laguerre quadrature. This is surprising in view of the fact that the integrands are strongly oscillatory and cannot, in general, be expressed in terms of finite polynomials.

The new method's main disadvantage is the necessity of preliminary setting of the parameters which control the precision of the computation. However, this problem has recently been alleviated by Pullen (1981), who has developed a technique for determining automatically the appropriate number of Chebyshev terms needed to compute the radial Coulomb wavefunctions.

The new method is especially suited to the calculation of radial quadrupole integrals in the context of the quadratic Zeeman effect, where very large values of ν, ν' may arise (see Chapter 6). The quadrupole operator r^2 emphasises the contribution to these integrals which arises from large radial distances.

CHAPTER 6

COMPUTATION OF THE PRINCIPAL SERIES OF Ba I

In this Chapter we assess the validity of the theoretical approach proposed in Chapter 2. The energy levels and associated intensities of Ba I in the presence of magnetic fields in the range of 10 - 70 kG are obtained by diagonalizing a truncated form of the Hamiltonian matrix $H_{nl,n'l'}$ (see equation 2.13). The physical significance of these results is discussed in the context of the experimental spectra of the $6s^2\ ^1S_0$ - $6snp\ ^1P_1$ principal series of Ba I obtained by Garton and Tomkins. The numerical methods described in Chapters 3 and 4 are used to compute the matrix elements of H.

This Chapter is organised as follows. In Section 6.1 we present a brief description of the Garton-Tomkins spectra. Then in Section 6.2 we discuss the methods used to overcome the computational problems associated with the construction and diagonalization of the truncated Hamiltonian matrix. In Section 6.3 we discuss the physical significance of the computed spectra. Finally, in Section 6.4, we draw some conclusions regarding the effectiveness of the free-field Coulombic wavefunctions as basis states.

6.1 THE SPECTRA OF GARTON AND TOMKINS

During the past twelve years a series of experiments has been performed at the Argonne National Laboratory, Illinois, concerned with the study of the absorption spectra of highly excited alkali and alkaline earth atoms in the presence of magnetic fields in the range 10 - 50 kG. According to Professor Garton, one of the principal investigators, only a small proportion of these results has been published because of the difficulty

of presentation in the absence of an adequate quantitative theoretical framework.

The first published results were of the principal series of Ba I in a magnetic field of 24 kG. A remarkably detailed set of observations of the $6s^2\ ^1S_0 - 6snp\ ^1P_1$ absorption spectrum was obtained, with separate measurements of the π and σ components. Garton and Tomkins (1969a) published a description of these results, including photographic prints of the whole spectrum, with and without the magnetic field, from n = 26 to a short distance beyond the series limit. Densitometer traces of the Zeeman σ components (n = 35 - 39) were also presented, although the σ^+ and σ^- components were not separated.

During the course of the research reported in this thesis the present author has also had access to the complete π and σ^+ densitometer traces of Ba I at 24 kG, made available by Professor Garton. Some of these results, together with other (σ^+) densitometer traces of Ba I and Sr I at magnetic fields of 17, 25, 32, 40 and 47 kG, have been published recently by Lu et al. (1978b). The densitometer traces for Ba I, taken from Lu et al. (loc. cit.), are reproduced in Fig. 6.1.

6.1.1 Characteristics of the Ba I Spectra

Both the π and σ spectra may be divided into regions with strikingly different characteristics. In the lower energy region, running from about n = 30 to n = 37, distinct groups of lines are seen which may be identified with successive principal quantum numbers. In addition to the quadratic shift, we have a breaking of the ℓ- degeneracy characteristic of hydrogenic spectra. The lines produced are easily distinguished and have, within each group, a roughly equal spacing. The members of each group in the π spectrum have roughly equal intensities, whereas in the σ spectrum

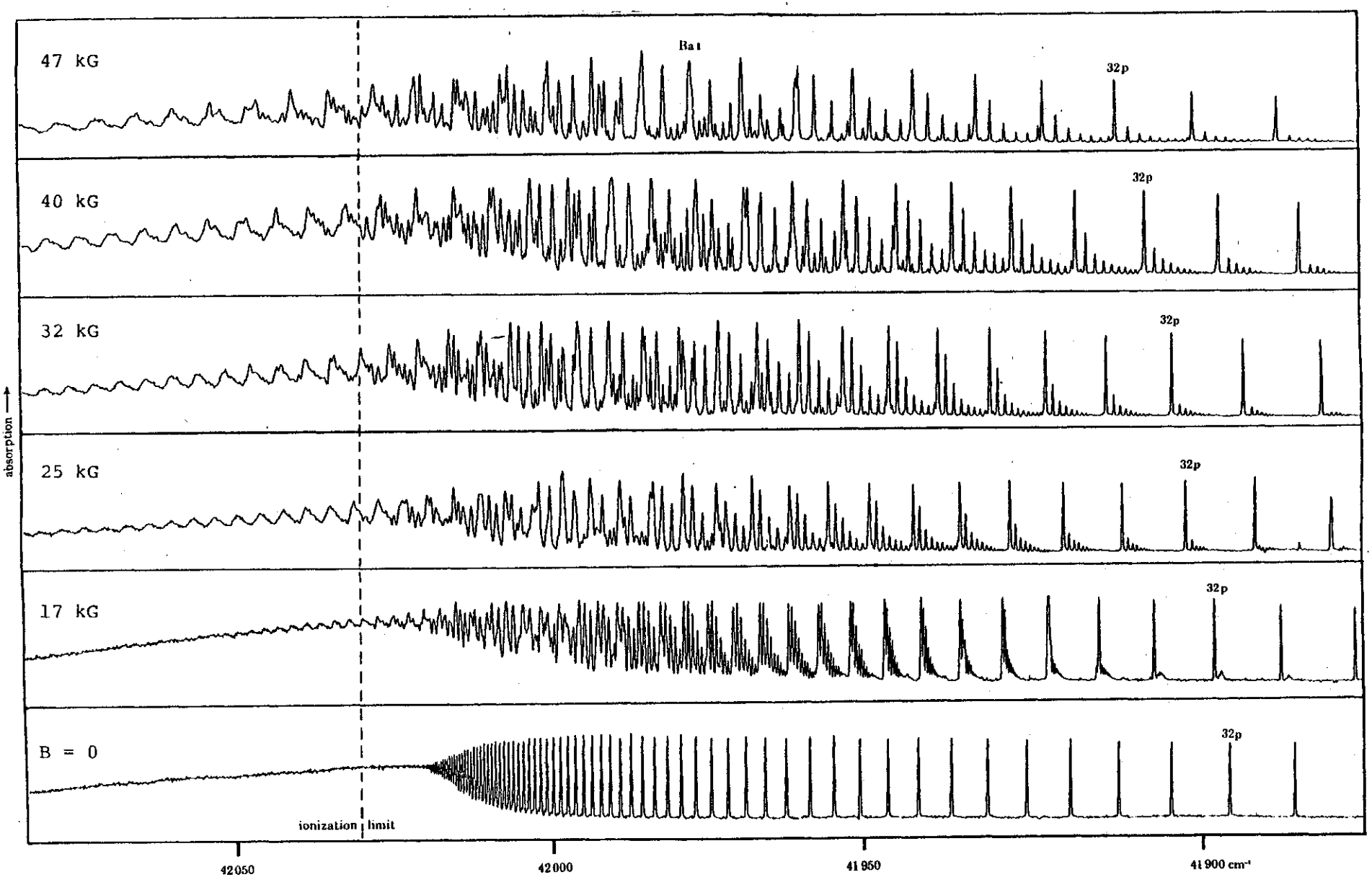

Fig. 6.1 Densitometer Traces of σ^+ spectra of Ba I; B = 47, 40, 32, 25, 17, 0 kG

(Reproduced from Lu et al. 1978b)

intensities within a group fall off rapidly, the strongest line being that with maximum displacement from the free-field position. Inter-ℓ mixing appears earlier (i.e. at smaller n) in the π series than in the σ series.

Towards the higher energy regions, both the π and σ spectra become more complex. Above about n = 37 inter-n mixing sets in, and above n = 40 there is little trace of the Rydberg structure remaining. However, there are other regularities that appear. In two distinct regions of the σ spectrum there are sequences of regularly spaced lines, the spacing being close to $\frac{1}{2}\hbar\omega$, where ω is the cyclotron frequency (see Section 2.1). Another system of very broad lines ("resonances") extends from a little below the free-field series limit into the continuum. The spacing is again regular and approximately equal to $\frac{3}{2}\hbar\omega$. The resonances start in the region n = 45 and about 15 of them are visible before the series limit. Regularities also appear in the π spectrum but, in this case, there is no detectable structure beyond the free-field series limit.

6.2 COMPUTATION OF ENERGY LEVELS AND INTENSITIES

We now describe the methods used to compute the quadratic Zeeman effect on the theoretical energy levels and intensities of the $6s^2\ {}^1S_0$ - $6snp\ {}^1P_1$ absorption spectra of Ba I, assuming magnetic fields in the range 10 - 70 kG. As outlined in Chapter 2 this involves the numerical computation of the eigenvalues and eigenvectors of a truncated form of the Hamiltonian matrix $H_{n\ell,n'\ell'}$. We denote the truncated matrix by $\bar{H}$, and assume $n_{min} \leq (n,n') \leq n_{max}$, $\ell_{min} \leq (\ell,\ell') \leq \ell_{max}$, $n_{max} - 2 \leq \ell_{max} < n_{max}$.

Of course, eigenvalues determined in this way are upper bounds to the true eigenergies of the atomic system. This is due not only to the truncation procedure but also to the fact that the selection of a basis of bound free-field states does not allow for mixing with the continuum.

In the general case we must solve the truncated form of equation (2.13) for given values of parity ($\tilde{\omega}$) and magnetic quantum number (m). $\tilde{\omega}$ takes the numerical values 0 and 1, corresponding to even and odd parity respectively. The angular momentum quantum number (ℓ) takes either even or odd values depending on the values of $\tilde{\omega}$ and m. The minimum value of ℓ, denoted by ℓ_{min}, is given by

$$\ell_{min} = |m| - \tilde{\omega} + 1, \qquad \text{if m is odd,} \qquad (6.1)$$

or

$$\ell_{min} = |m| + \tilde{\omega}, \qquad \text{if m is even.} \qquad (6.2)$$

When considering the particular case of Ba I with dipole transitions from the ground state ($6s^2\ {}^1S_0$) we shall only consider eigenvalues and eigenvectors of $\bar{H}$ which have odd parity ($\tilde{\omega} = 1$) and $m = 0, \pm 1$. In the π polarisation transition the magnetic quantum number does not change, and hence $\Delta m = 0$, whereas in the $\sigma^{\pm}$ polarisation transitions $\Delta m = \pm 1$.

The strength of the transition $i \rightarrow j$ (in atomic units) is given by

$$S_{ij} = \left| \langle \psi_i^{m\tilde{\omega}}(\underline{r}) \,|\, \underline{r} \,|\, \psi_j^{m\tilde{\omega}}(\underline{r}) \rangle \right|^2, \qquad (6.3)$$

where ψ_i and ψ_j represent the initial and final transition states (see equation 2.4). In the case of Ba I ψ_i may be taken as $|6s^2\ {}^1S_0\rangle$, i.e. the free-field ground state with negligible quadratic Zeeman effect.

Thus, from equations 2.5, 2.12 and 2.13, it follows that

$$S_{ij} \approx \left| \langle 6s^2\,{}^1S_0 | \underline{T} | \sum_{n'l'} C_{n'l'}^{m\tilde{\omega}} | n'l'm \rangle \right|^2. \qquad (6.4)$$

Thus the eigenvectors of $\bar{H}$, namely $C_{nl}^{m\tilde{\omega}}$, can be used to compute the approximate intensities of quadratic Zeeman spectral lines. We note that the selection rule on $|l - l'|$ implies that only the 'p' components of excited states contribute to intensity.

6.2.1 Construction of the Hamiltonian Matrix

As explained in Chapter 2, the construction of $\bar{H}$ for alkali and alkaline earth atoms must take account of the relevant quantum defects. Accurate experimental data are available for the 'p' states of Ba I up to n = 75 (Garton and Tomkins 1969b).

For the range of n-values of interest in the present study these quantum defects can be expressed as $4 + \alpha$, where α is a positive or negative quantity, small compared with one, although not small enough to be neglected: As n increases from 26 to 50, α increases monotonically from -0.1444 to +0.2500.

The quantum defects associated with 'f', 'h',... states are assumed to be negligible. This may not be justified in the case of 'f' states, but experimental data are not yet available.

In view of the large quantum defects of the 6snp $^1P_1$ terms of Ba I, it follows that, for any n, the energy level of the free-field 'p' state lies close to those of the (degenerate) 'd', 'f',.... states with principal quantum number n - 4. An applied magnetic field, not large enough to cause inter-n mixing, will therefore give rise to inter-l interactions between a given 6nsp $^1P_1$ term and 'f', 'h',.... terms corresponding to an n value

that is smaller by four. Therefore, when constructing $\bar{H}_{n\ell,n'\ell'}$ we use the free-field state $|n+4,\ell\rangle$ when the matrix element of $\bar{H}$ involves a 'P' state, i.e. if ℓ or $\ell' = 1$ (see equations 2.14, 2.15).

The numerical techniques used to compute the radial factors $\langle n\ell | r^2 | n'\ell' \rangle$ of $\bar{H}_{n\ell,n'\ell'}$ were described in Chapters 3 and 4, and need no further discussion. The angular factors $\langle \ell m | \sin^2\theta | \ell' m \rangle$ are easily determined by means of angular momentum algebra (see Edmonds 1968, p76):

$$\langle \ell m | \sin^2\theta | \ell' m \rangle = \frac{2(\ell^2 + \ell - 1 + m^2)}{(2\ell-1)(2\ell+3)} \quad \text{if } \ell = \ell', \tag{6.5}$$

$$= -\left[\frac{[(\ell_<+1)^2 - m^2][(\ell_<+2)^2 - m^2]}{(2\ell_<+5)(2\ell_<+3)^2(2\ell_<+1)}\right]^{\frac{1}{2}} \tag{6.6}$$

$$\text{if } |\ell - \ell'| = 2,$$

$$= 0 \quad \text{otherwise.} \tag{6.7}$$

In equations (6.5) and (6.6) $\ell_< = \min(\ell, \ell')$.

If we denote $n_{max} - \ell_{min}$, $n_{min} - \ell_{min}$ by a and b respectively, then the dimension, N, of $\bar{H}$ is given by

$$N = \tfrac{1}{4}[(a+1)^2 - b^2] \quad \text{(a odd, b even);} \tag{6.8}$$

$$N = \tfrac{1}{4}[a^2 + 2a - b^2] \quad \text{(a even, b even);} \tag{6.9}$$

$$N = \tfrac{1}{4}\left[(a+1)^2 - b^2 + 1 \right] \qquad \text{(a odd, b odd);} \qquad (6.10)$$

$$N = \tfrac{1}{4}\left[a^2 + 2a - b^2 + 1 \right] \qquad \text{(a even, b odd).} \qquad (6.11)$$

6.2.2 Computing Resources

In the present study we are interested in computing as many as possible of the energy levels and intensities of the σ and π series of Ba I from about n = 26 upwards, in magnetic fields ranging from 10 - 70 kG. In practice this involves the diagonalization of very large Hamiltonian matrices: as remarked earlier, the quadratic Zeeman energy shifts increase roughly as n^4, whereas the energy separation between successive free-field states decreases as n^{-3}. Consequently, the number of basis states needed in $\bar{H}$ to achieve an acceptable accuracy in the computed energy levels and intensities increases rapidly with n. For instance, if $n_{min} = 19$ and $n_{max} = 38$, the dimension of $\bar{H}$ is 280 x 280 (see equations 6.8 - 6.11); if $n_{min} = 31$ and $n_{max} = 44$ the corresponding dimension is 259 x 259 ($\ell_{min} = 1$ in both cases).

The calculations reported in this Chapter were conducted within the constraint of a fixed allocation of computing units on a time-shared CDC 6600 series computer at Imperial College. In addition to the restriction on the total number of units available, the processing power and memory available during each computer run was also limited. The appearance of large matrices thus presented serious computational problems, because of the large amount of computing power and memory required for their diagonalization. It was therefore necessary to devise an efficient and reliable computational scheme for diagonalizing $\bar{H}$.

These computational issues have not been so important in previous studies of the quadratic Zeeman effect since other investigations involving

free-field basis functions have not been concerned with inter-n mixing in highly excited states (see, for example, Kemic 1974).

6.2.3 Computation of Eigenvalues and Eigenvectors of $\bar{H}$

From the selection rule $|\ell - \ell'| = 0$ or 2 (see equations 6.5, 6.6, 6.7) it follows that, if the rows and columns of H are re-arranged in sub-matrices labelled by (ℓ, ℓ'), the resulting matrix, which we denote by A, has the block diagonal structure illustrated in Fig. 6.2. The rows and columns of each (ℓ, ℓ') sub-matrix are labelled by n and n' respectively. n takes the values $\bar{n}$, $\bar{n} + 1, \ldots, n_{max}$, where $\bar{n} = \max(n_{min}, \ell + 1)$; likewise n' runs from $\max(n_{min}, \ell' + 1)$ to n_{max}. Clearly the re-ordered matrix is symmetric and has a maximum of

$$w = 2n_{max} + 1 - \max(n_{min}, \ell_{min} + 1) - \max(n_{min}, \ell_{min} + 3) \quad (6.12)$$

non-zero elements to the right of the main diagonal (see Fig. 6.2). Thus

$$A_{ij} = 0 \quad \text{if} \quad |i - j| > w \quad (6.13)$$

A large number of numerical algorithms exist for the diagonalization of band symmetric matrices; a review of these techniques is given by Duff (1976). At first it seemed that one such method, that of Rutishauser and Swartz (1963), was well-suited for diagonalizing for our present purpose; a FORTRAN version of their algorithm, called LRCH, was easily available. Although LRCH could not compute eigenvectors, it seemed particularly attractive for determining eigenvalues, since these are determined one-by-one, and the algorithm can be interrupted after each eigenvalue has been computed. Thus, if the processing time available during one computer run

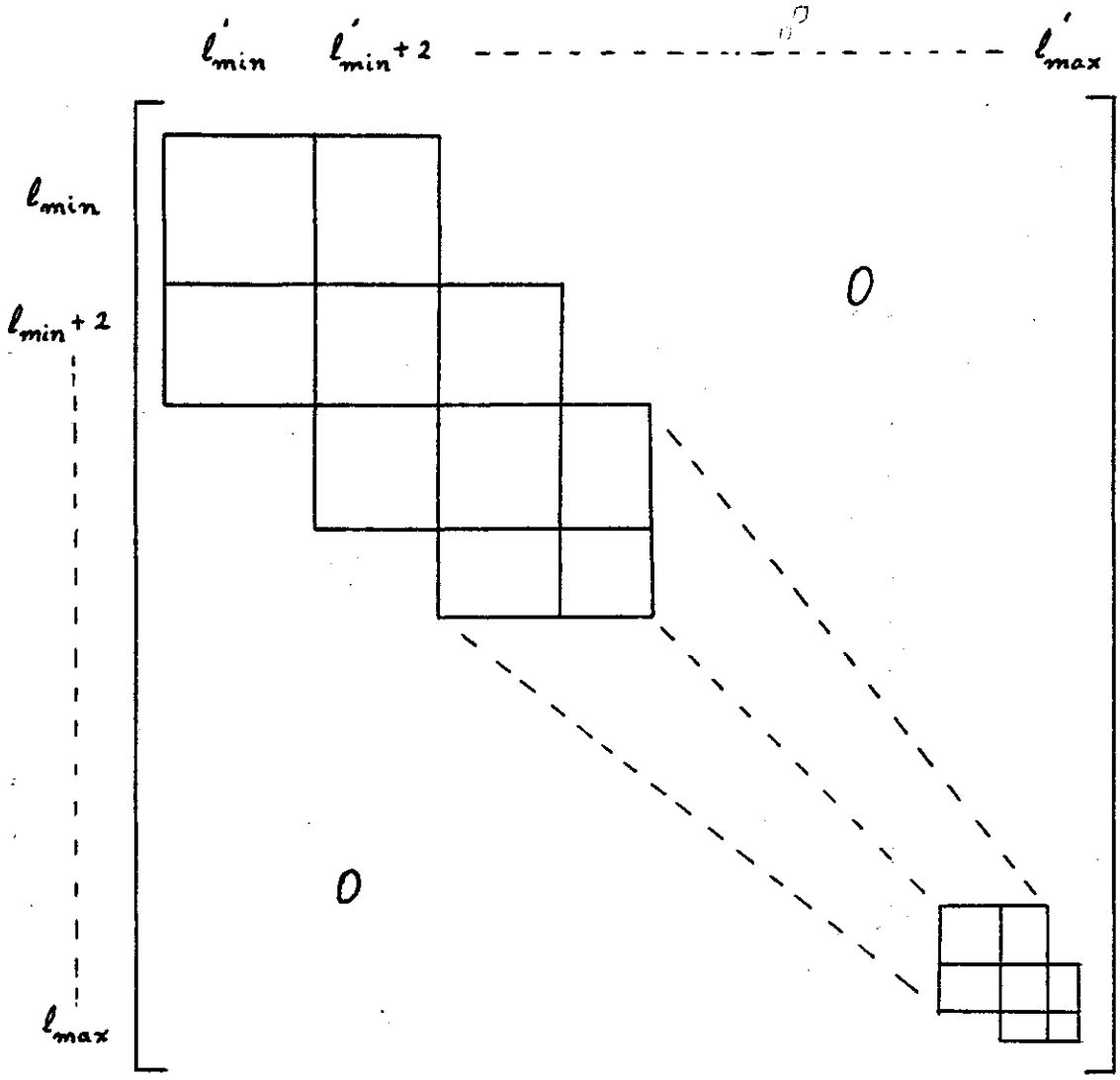

Fig. 6.2 Structure of the Truncated Hamiltonian Matrix

The diagonal sub-matrices are labelled by ℓ and ℓ'. The rows and columns of each sub-matrix are labelled by n and n', where $n = \max(n_{min}, \ell + 1), \ldots, n_{max}$ and $n = \max(n'_{min}, \ell' + 1), \ldots, n_{max}$.

was not adequate to diagonalize a complete matrix, the partially diagonalized matrix could be stored and the process completed during subsequent runs.

However, practical calculations later indicated that LRCH required a surprisingly large amount of computer processing time, and had to be abandoned.

By contrast, another algorithm, called SDIAG, which computes both eigenvalues and eigenvectors of any real symmetric matrix required much less computing time than LRCH. The SDIAG algorithm, which was acquired by Dr. Edmonds from the Argonne Computer Library, is based upon the work of Martin et al. (1968)*. The symmetric matrix is reduced to tridiagonal form by Householder's method. Then, by a sequence of QR transformations, the tridiagonal matrix is brought to almost diagonal form. Shifts are used to give an accelerated rate of convergence. An orthogonal set of eigenvectors is found for the original matrix A.

6.2.4 Application of SDIAG

The limitation of computing resources meant that the maximum size of truncated Hamiltonian matrix that could be diagonalized by SDIAG was 300 x 300. Thus the quadratic Zeeman effect on the energy levels and intensities of Ba I could only be determined using a "window" of basis states, including not more than 300 members. Of course, this restriction imposed a limitation on the domain of validity of the whole approach adopted by the author: at some point towards the higher energy region of any quadratic Zeeman spectrum, the diagmagnetic term eventually induces mixing between more than 300 free-field states.

---

* see Martin, R.S., Riensch, C. and Wilkinson, J.H. (1968), Num. Math. 11, pp 181-195.

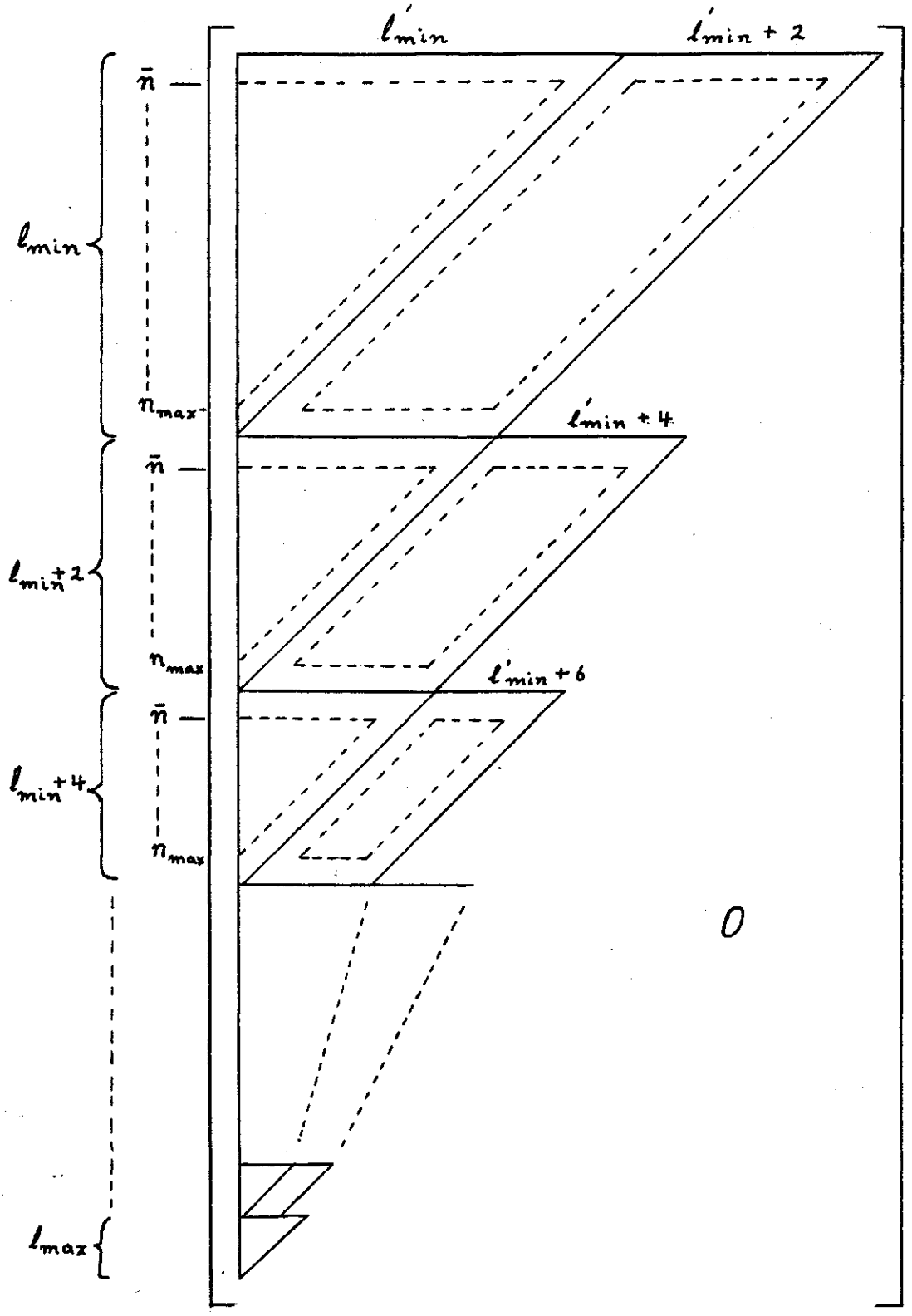

Fig. 6.3 Structure of the Matrix $\bar{A}$ of $\langle n l m | r^2 \sin^2\theta | n' l' m \rangle$

The matrix elements inside the dotted lines satisfy the condition $n_{min} \leq (n, n') \leq n_{max}$ ($20 \leq n_{min} < n_{max} \leq 60$). Only these sub-matrices are needed to construct a Hamiltonian matrix with given n_{min} and n_{max}.

In order to economize on computer processing time the field-independent parts of $Q_{nl,n'l'}$ were computed once, using extreme values of n_{max} and n_{min}, and stored for repeated use by SDIAG. Using $n_{min} = 20$ and $n_{max} = 60$, the values of $\langle nlm|r^2\sin^2\theta|n'l'm\rangle$ corresponding to the upper triangle of A (see Fig. 6.2) were stored as a band matrix, having N rows and w + 1 columns (see equation 6.13). The (i, j) element of this band matrix, which we denote by $\bar{A}$, contained the $\langle nlm|r^2\sin^2\theta|n'l'm\rangle$ associated with the (i, i + j) element of matrix A, (i = 1, 2,...., N; j = 0, 1,...., w). Thus, for any given values of n_{min}, n_{max}, and magnetic field B, the Hamiltonian matrix A to be input to SDIAG could be constructed easily from the matrix $\bar{A}$ and a table of quantum defects, using equations (2.13) - (2.16). The structure of $\bar{A}$ is illustrated diagrammatically in Fig. 6.3.

In practice it was found that this technique led to a 25% reduction in computer processing time. This resulted from the fact that each matrix was diagonalized several times in order to assess the effect of the truncation criterion.

6.3 RESULTS AND DISCUSSION

In this Section we discuss the results of numerical calculations of the principal series of Ba I, obtained using the computational methods described above. The ultimate objective of these calculations was to provide relevant data that could be compared with the spectroscopic results of Garton and Tomkins (1969a), since such a comparison would provide valuable insight into the general validity of the theoretical framework adopted by the present author. An important sub-objective, therefore, was to assess the accuracy of the energy levels and intensities obtained by diagonalizing a truncated Hamiltonian matrix constructed using free-field bound states.

Most of the results presented refer to the σ^+ and π spectra of Ba I in a magnetic field of 24 kG, since the experimental densitometer traces of these spectra were available for comparison. Nevertheless other magnetic fields are considered, notably 32 kG and 47 kG.

The strategy adopted in these calculations was to begin by computing the low-energy spectral lines, beginning at about n = 26, and moving progressively towards the higher energy regions of the spectrum. At each step of the process, a finite set of basis states, not exceeding 300 in number, was used to define the Hamiltonian matrix $\bar{H}$. Approximate energy levels and relative intensities were then determined, as explained earlier. The basis set was then changed to represent a neighbouring collection of free-field states, and the process repeated.

Since the above procedure yielded upper limits to the true energy levels of the system Hamiltonian H, the accuracy of the results obtained at each stage had to be assessed carefully. In particular, it was important to observe the variation of each computed energy level as the composition of the basis set was changed, i.e. as n_{min} and n_{max} were varied (see 6.3.4 below).

6.3.1 Labelling of States

Before presenting any computed results it is necessary to explain the method used to label the eigenstates of the system Hamiltonian H. The scheme used follows that of Kemic (1974), suitably modified to take account of the quantum defects of the 'p' states of Ba I. As remarked earlier the 'np' level of Ba I mixes with the 'f', 'h',... states associated with n - 4 when the magnetic field is not large enough to induce n-mixing. Therefore, before adopting Kemic's scheme we increase the n-value of 'f', 'h',... states by 4.

The ambiguity caused by the degeneracy amongst the re-labelled free-

field states (whose quantum defects are ignored) is overcome by invoking equation (1.1), which shows that, for fixed n and m_ℓ, the quadratic Zeeman shift is a decreasing function of ℓ. Thus it is possible to assign values of ℓ to the states of H according to their energy ordering among other states of the same n, m_ℓ and parity in the limit of low field, the state of highest energy in each group being assigned the lowest possible value of ℓ.

We note that this labelling scheme is still valid if the magnetic field becomes strong enough to induce n-mixing: since m_ℓ and parity are the only 'good' quantum numbers of the atomic system, energy levels having the same values of m_ℓ and parity cannot be degenerate, i.e. two such levels cannot "cross" as the field strength is varied (see Baldereschi and Bassani, 1970).

6.3.2 Computed Spectrum of Ba I

The results obtained for the σ^+ and π components of $6s^2\ ^1S_0 - 6snp\ ^1P_1$ principal series of Ba I in the presence of a uniform magnetic field of 24 kG are presented in graphical form in Figs. 6.4, 6.5 and 6.6. Fig. 6.4 shows that in both the σ^+ and π spectra the effect of the magnetic field is to broaden the free-field lines '28p',...,'32p' to form groups of lines, resembling band structures. Up to n = 31 the bands of both spectra have a similar structure. The strongest line of each group has the maximum displacement from the free-field position, and the intensities fall off rapidly towards longer wavelengths.

Beyond n = 31 the π and σ^+ spectra have distinctly different characteristics. In the π spectrum the leading line in each group loses its dominant position, and from n = 32 to n = 35 the groups consist of several components of comparable strength which increase in separation towards shorter wavelengths. Beyond n = 35 the groups of the π spectrum run together and no systematic structure is detectable thereafter.

By contrast, the bands of the σ^+ spectrum maintain an asymmetric structure as n increases. The intensity within each group falls off rapidly towards longer wavelengths, and the separation between component lines is greater that in the π spectrum. The groups of the σ spectrum begin to run together at n = 37 (later than in the π spectrum). However, the overlapping groups are still clearly discernible until n = 40. Indeed they do not lose their identity completely until n = 43.

Between n = 40 and n = 43 a new regularity appears in the σ^+ spectrum. This is illustrated on an expanded scale in Fig. 6.6. We note that the observable part of each (overlapping) group is characterised by a set of 4 or 5 strong lines of roughly equal separation, and decreasing slightly in intensity towards longer wavelengths. The separation between these lines is approximately 1.1 cm^{-1}, which equals $\frac{1}{2}\hbar\omega$, ω being the cyclotron frequency. About n = 43, however, additional lines appear and there are no systematic structures beyond this point.

6.3.3 Comparison with Experimental Results

The computed σ^+ and π spectra of Ba I have been compared with the experimental results of Garton and Tomkins.

In the spectral regions where the adjacent groups of lines associated with different n-values do not overlap the theoretical results show excellent qualitative agreement with the experimental values. For instance, in the region n = 26 to n = 37 of the σ^+ spectrum (see Figs. 6.4 and 6.5) the dominance of the lines of maximum quadratic shift over their associated groups of satellite lines, observed by Garton and Tomkins, is well reproduced.

In the spectral regions where adjacent groups overlap the large number of lines present and the absence of obvious regularities in either the theoretical or experimental spectra makes comparison difficult. However,

we note that the appearance of groups of regularly spaced lines, observed by Garton and Tomkins in the region of n = 43, have been reproduced in the theoretical results. The theoretical spacing of the 3 or 4 principal members of each overlapping n-group lies within 10% of $\frac{1}{2}\hbar\omega$ when $40 \leq n \leq 43$.

In order to check whether the regular spacing of $\frac{1}{2}\hbar\omega$ in the vicinity of n = 43 was due to chance coincidence, as Garton and Tomkins suggested it might be, the overlapping region of the σ^+ spectrum was also computed for magnetic fields of 32 and 47 kG. The results of these calculations, which are described in graphical form in Figs. 6.7 and 6.8, have confirmed the presence of regularly spaced lines of spacing $\frac{1}{2}\hbar\omega$ in the region where strong overlapping of groups sets in.

Fig. 6.6 shows clearly that the lines of the π spectrum are much more compressed than those of the σ spectrum - in agreement with the observations of Garton and Tomkins. We note that Jenkins and Segrè (1939) observed similar compression in the π spectra of Na I and K I; an explanation of this phenomenon was given by Schiff and Snyder (1939).

As a quantitative assessment of the accuracy of the theoretical energy levels of Ba I (B = 24 kG) the quadratic Zeeman energy shift of the leading line of each band was compared with the corresponding experimental value. These shifts could be identified up to n = 42 in the σ spectrum and up to n = 35 in the π spectrum. Comparison of these results has indicated that agreement between theory and experiment is within 5%. In the "worst" case, namely n = 42 of the σ spectrum, the theoretical shift exceeds the experimental value by 0.7 cm^{-1}. The variation of quadratic shift as a function of n is illustrated in Fig. 6.9.

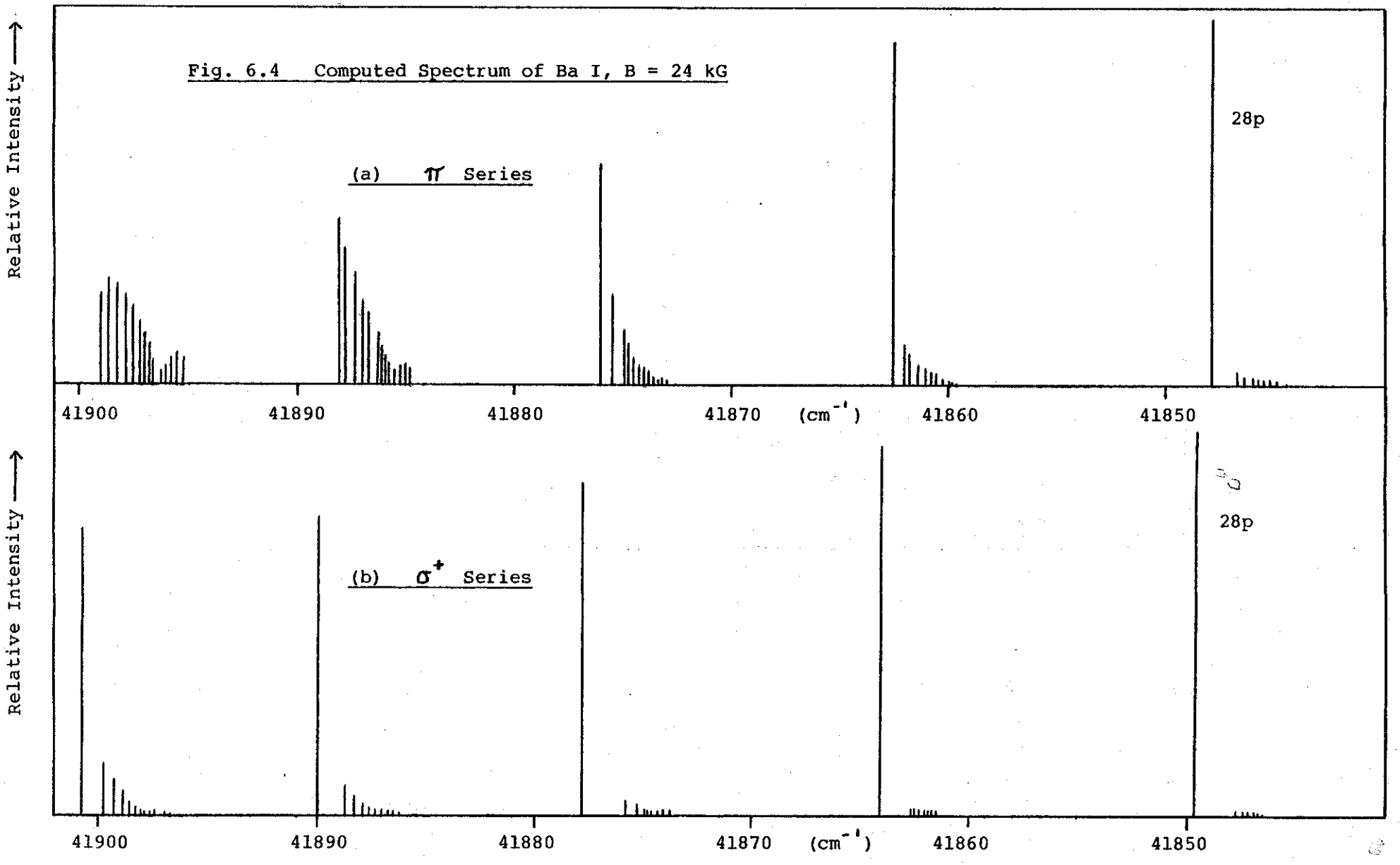

Fig. 6.4 Computed Spectrum of Ba I, B = 24 kG

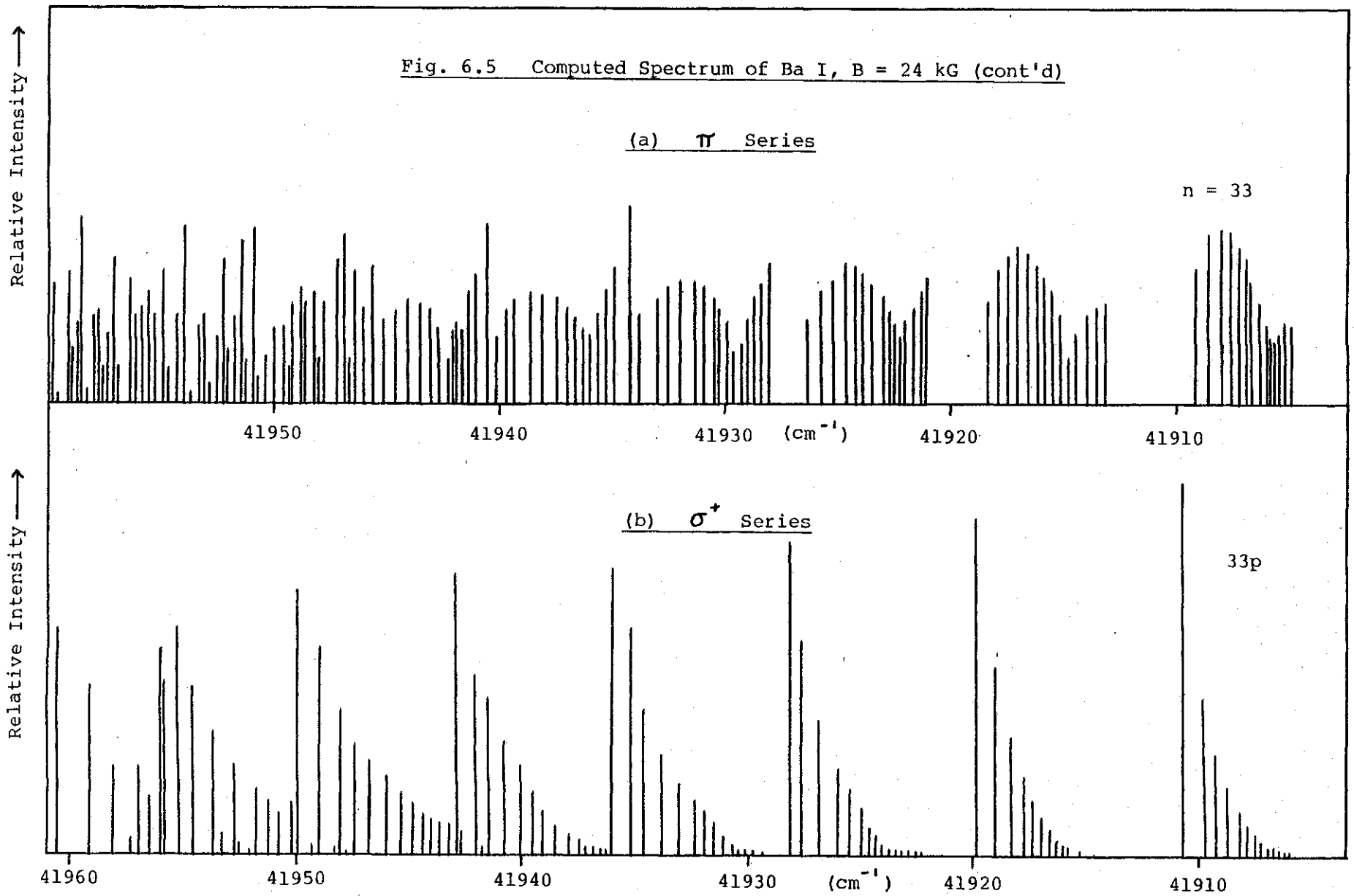

Fig. 6.5 Computed Spectrum of Ba I, B = 24 kG (cont'd)

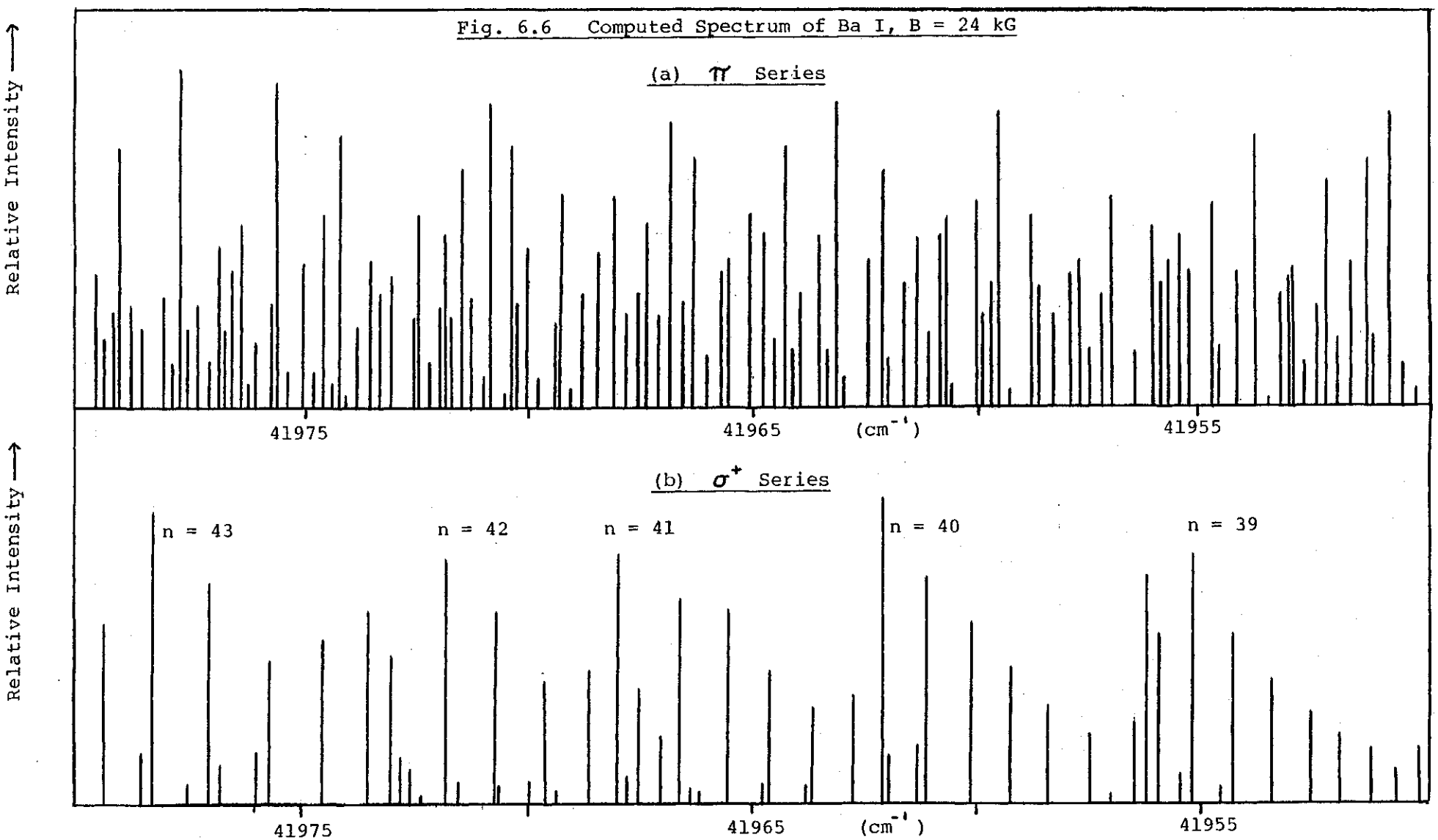
Fig. 6.6 Computed Spectrum of Ba I, B = 24 kG
(a) π Series
Relative Intensity
41975
41965
(cm⁻¹)
41955
(b) σ⁺ Series
Relative Intensity
n = 43
n = 42
n = 41
n = 40
n = 39
41975
41965
(cm⁻¹)
41955

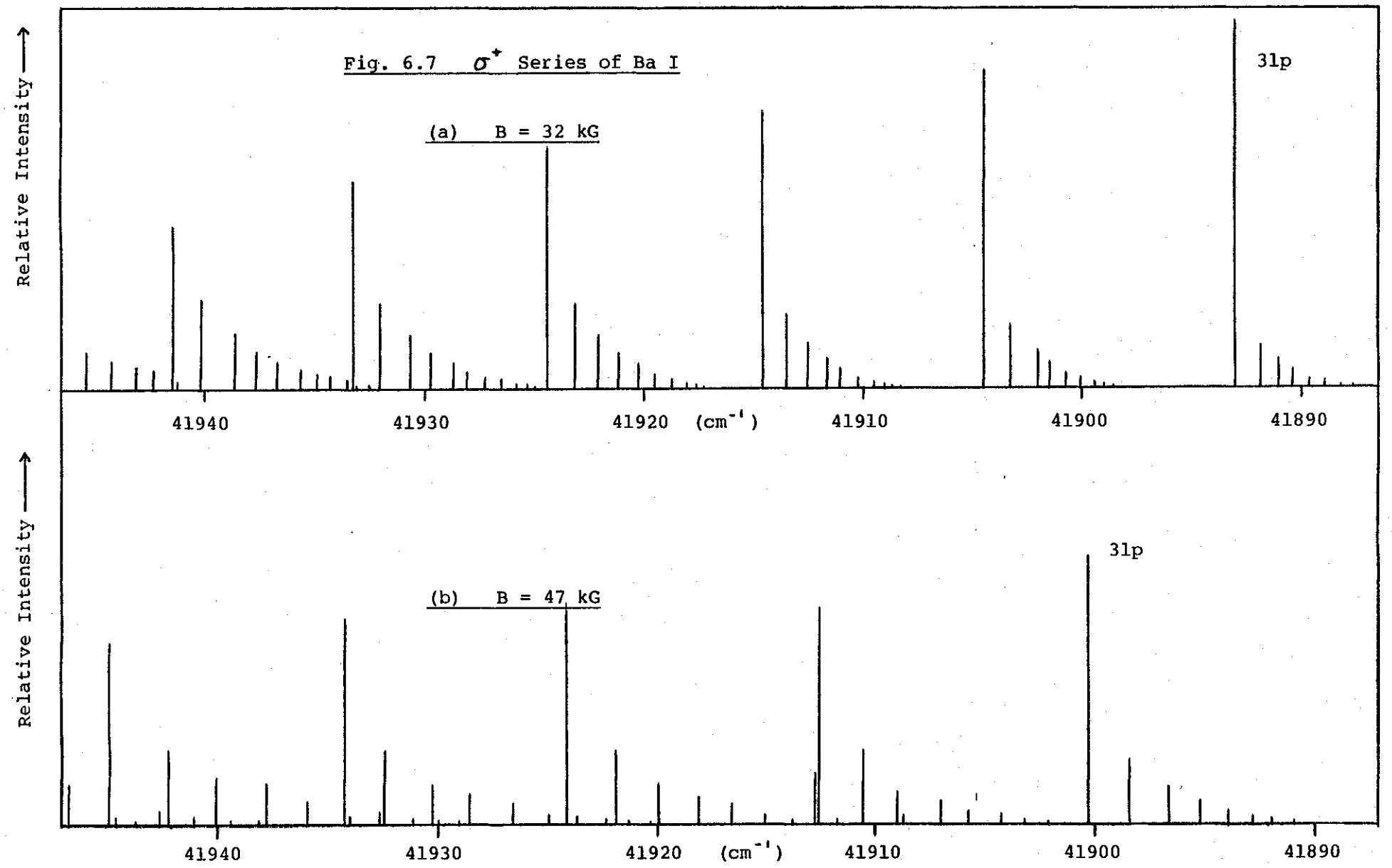
Fig. 6.7 σ^+ Series of Ba I
(a) B = 32 kG
31p
Relative Intensity
41940
41930
41920 (cm^{-1})
41910
41900
41890
(b) B = 47 kG
31p
Relative Intensity
41940
41930
41920 (cm^{-1})
41910
41900
41890

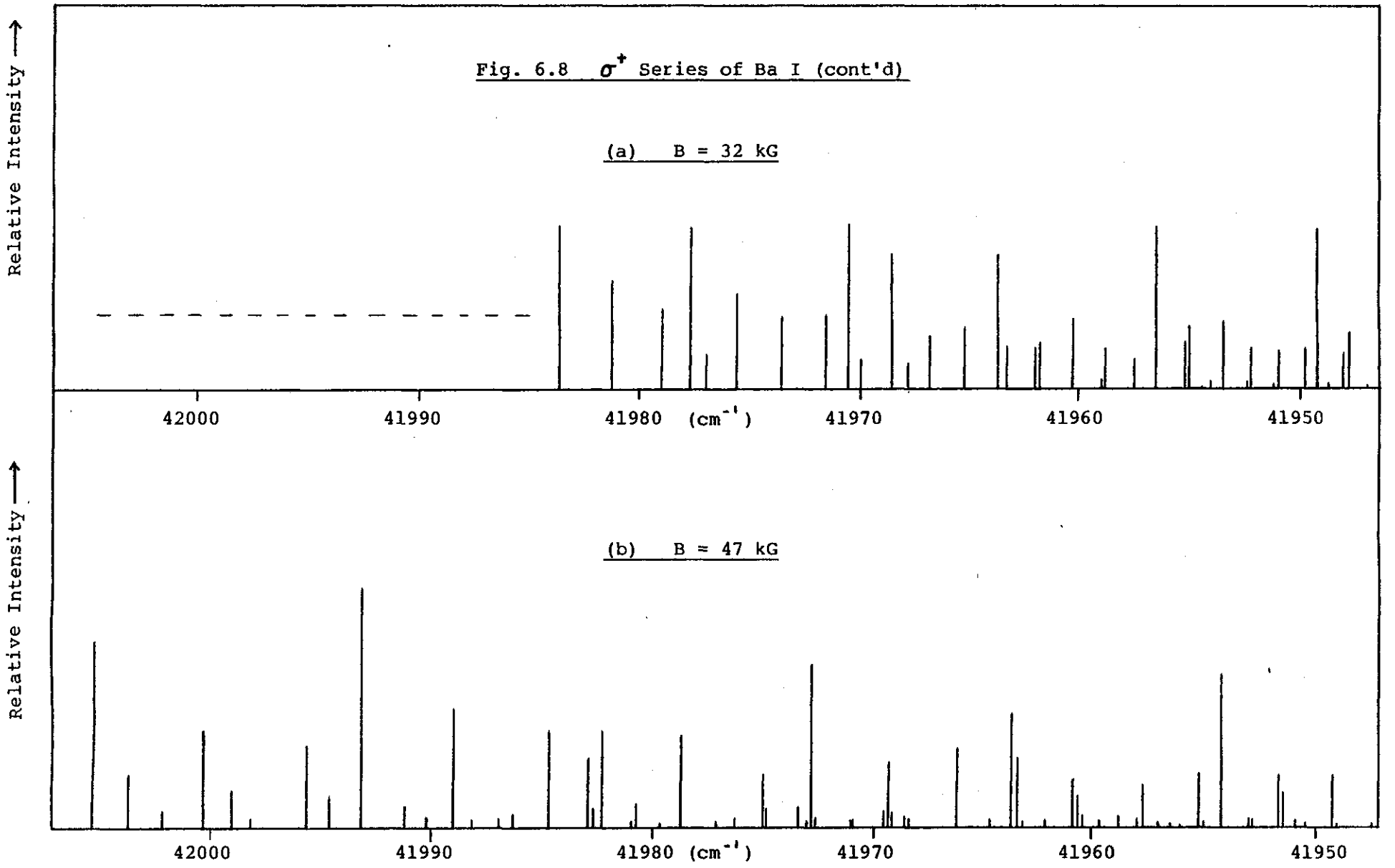

Fig. 6.8 σ^+ Series of Ba I (cont'd)

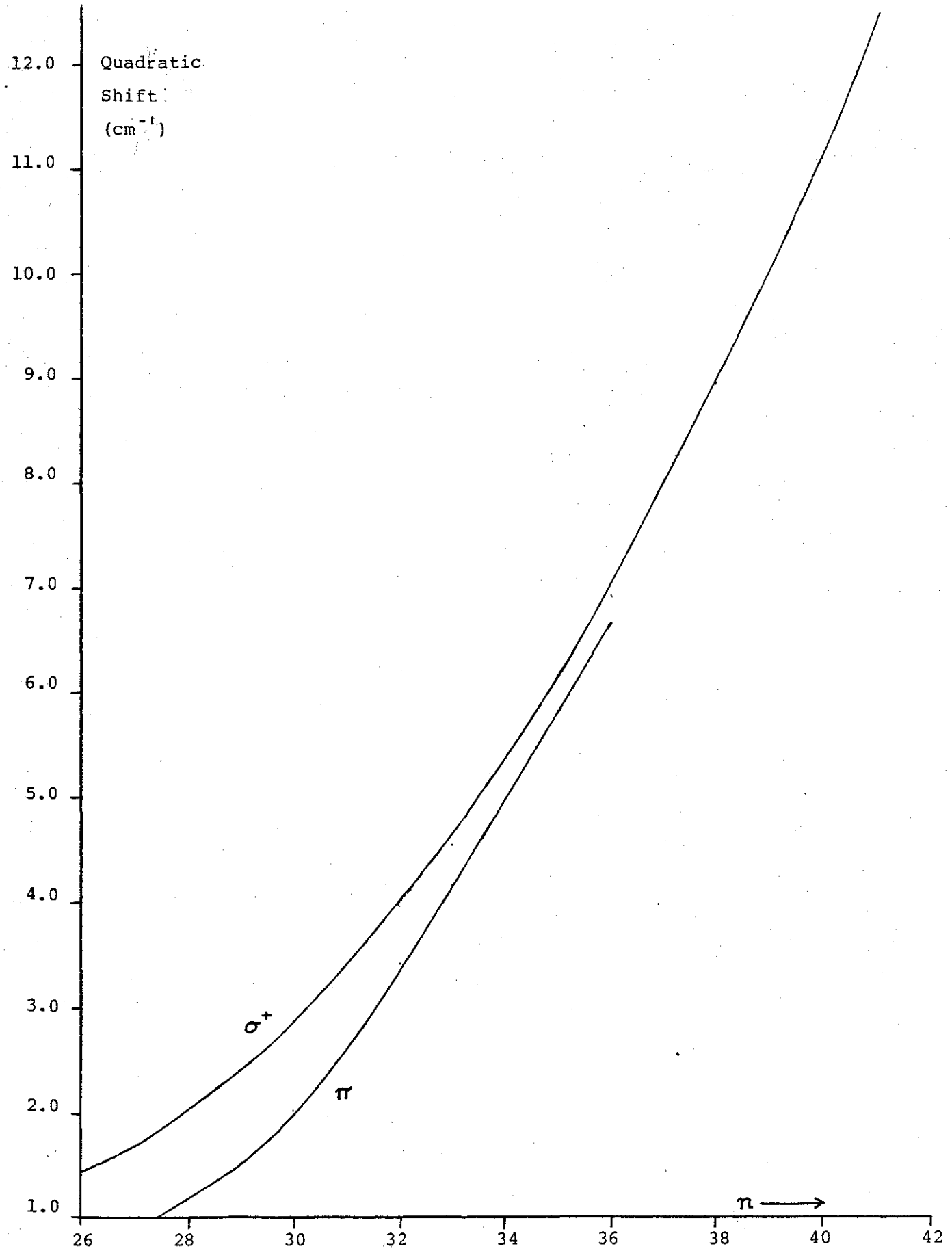

Fig. 6.9 Quadratic Zeeman Shift as a Function of n (B = 24kG)

6.3.4 Effect of Truncation

When computing the theoretical spectra of Ba I the effect of truncating the Hamiltonian matrix was assessed by varying n_{min} and n_{max} and observing the variation of the computed energy levels. This variation gave a rough estimate of the degree of interaction between the free-field states included in Hamiltonian matrix and those excluded by the truncation criterion.

In Table 6.1 we illustrate the variation of five energy levels computed using four pairs of values of n_{min}, n_{max}. These results indicate that, when n exceeds about 35 a rapid increase in matrix size is needed in order to maintain a given accuracy in the computed energy levels. We also note from Table 6.1 that the lines of the π spectrum are more sensitive to the truncation criterion than those of the σ spectrum, indicating that inter-n mixing sets in at longer wavelengths in the π spectrum (see Fig. 6.5).

6.3.5 Variation of Energy Levels with Magnetic Field

Once the accuracy of the author's methods were understood, a series of calculations was performed to assess the effect of variation of the magnetic field on the behaviour of the theoretical energy levels of the σ^+ spectrum. Some of the results are illustrated graphically in Fig. 6.10, in which the magnetic field varies between 25 and 70 kG. This diagram gives a good indication of the size of the quadratic Zeeman shifts compared with the inter-n differences of the free-field atom. It also illustrates the behaviour of the energy levels as ℓ varies. In order to simplify the diagram only a selection of the possible ℓ-values is represented.

Fig. 6.10 also demonstrates the type of interaction that occurs between states of different n-value when adjacent groups run together. We note that for a given value of n the quadratic shift is an increasing function of ℓ.

n_{max}	34	38	40	44
n_{min}	17	19	25	31
31p	41888.072	41888.072	41888.072	---------
35p	41926.777	41926.773	41926.773	41926.235
38p	41950.184	41946.708	41946.708	41946.708
41p	---------	41962.010	41961.587	41961.570
42p	---------	41975.906	41966.459	41966.246

(a) π Series

n_{max}	38	40	44
n_{min}	19	25	31
31p	41892.529	41892.529	---------
35p	41930.400	41930.400	41927.629
38p	41950.230	41950.222	41948.039
41p	41969.153	41966.387	41962.922
42p	41992.505	41971.938	41967.658

(b) σ^+ Series

Table 6.1 Effect of Matrix Truncation on Energy Levels, B = 24 kG

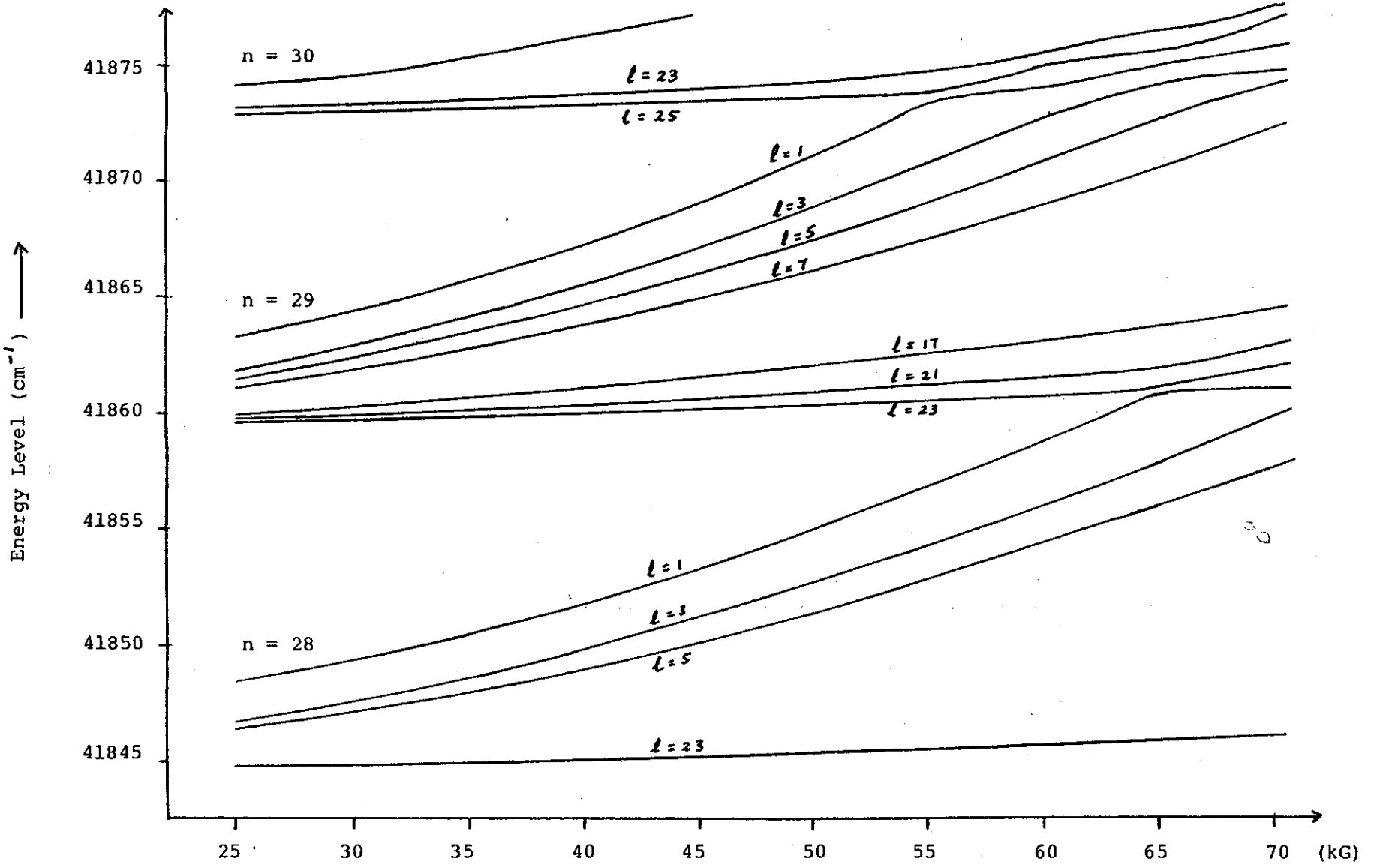

Fig. 6.10 Variation of Energy Levels with Magnetic Field

Hence the energy level of the state of smallest ℓ-value associated with n approaches that of the state of maximum ℓ-value associated with n + 1. For instance, the state (n = 28, ℓ = 1) tries to cross (n = 29, ℓ = 23) as the magnetic field strength approaches 65 kG. However, because of the "no-crossing rule" (see Section 6.3.1) these two states interact and therefore cannot cross. This interaction results in an exchange between the states of their characteristic eigenfunctions.

The exchange of eigenfunctions between interacting states has been investigated by Garstang and Kemic (1974) in the case of the hydrogen atom.

We note that the apparent overlapping of groups observed in the computed σ spectra of Ba I (see Figs. 6.5, 6.6) is a consequence of eigenfunction exchange between interacting states. However, it is not clear whether this phenomenon accounts for the regularly spaced lines ($\frac{1}{2}\hbar\omega$) which appear in the "overlapping" region of the σ^+ spectrum.

6.4 CONCLUSIONS

The results presented in this Chapter have demonstrated that the author's approach to determining theoretical energy levels and intensities is a valuable means of gaining insight into the quadratic Zeeman effect. However, it is only effective in regions where inter-n mixing is not too strong; under these circumstances the lack of completeness of the free-field basis wavefunctions does not introduce significant errors. The computed energy levels and intensities corresponding to the σ^+ series of Ba I in a magnetic field of 24 kG agree with the experimental results of Garton and Tomkins to within 1.0 cm^{-1} up to n = 43, representing agreement within 5% on the quadratic Zeeman energy shifts. The corresponding limit for the π series was found to be n = 35.

Beyond these limits the present approach is inadequate, since the Hamiltonian matrix becomes prohibitively large and hence the computing resources (memory and processing power) needed to perform such large calculations are not readily available. In principle matrix diagonalization techniques could be developed to use the computer's backing store, bringing rows/columns into the main memory only when needed. However, it is not clear how the computed results would be compared with the relatively featureless experimental spectra beyond n = 43 in the σ^+ spectrum and n = 35 in the π spectrum.

In the author's opinion there would not be much benefit derived from the use of more and more computing power, since this is unlikely to provide much insight into the physical mechanisms that give rise to the quadratic Zeeman spectra. It would seem more appropriate to investigate alternative approaches, as we shall outline in the following Chapter.

Finally, we note that the author's computational methods have been developed in the context of Ba I; they could be applied to other alkali or alkaline earth atoms, e.g. Li I, Na I, Sr, simply by changing the table of quantum defects.

CHAPTER 7

REVIEW

The research described in this thesis has been concerned with the development of computational techniques for use in the investigation of the quadratic Zeeman effect in alkali and alkaline earth spectra. This work began as an attempt to gain a theoretical understanding of the experimental spectra of the $6s^2(^1S_0) - 6snp(^1P_1)$ principal series of Ba I, produced by Garton and Tomkins (1969a,b). Most of the author's attention has been devoted to the spectral regions in which configuration mixing is appreciable. Hitherto this region has fallen between the domains of validity of the two main quantum mechanical approaches, namely perturbation theory (e.g. Schiff and Snyder, 1939), which is appropriate if inter-n mixing is negligible, and variational or adiabatic methods, which are valid if the magnetic field is large compared with the Coulomb force.

The approach adopted in this study follows that of Schiff and Snyder, but incorporates configuration mixing. The determination of energy levels and intensities involves the diagonalization of a truncated Hamiltonian matrix. The basis functions are the free-field Coulombic states, incorporating empirical quantum defects.

During the course of this research the author has concentrated on three main issues:

(i) computation of the radial quadrupole integrals of the Hamiltonian matrix which involve large principal quantum numbers and non-zero quantum defects;

(ii) computation of the eigenvalues and eigenvectors of the large structured Hamiltonian matrices which arise when configuration mixing is appreciable;

(iii) assessment of the effectiveness of the free-field basis states using the experimental spectra of Ba I obtained by Garton and Tomkins.

7.1 RADIAL INTEGRALS

In Chapters 3 and 4 a new method of computing radial multipole integrals involving Coulomb wavefunctions was presented. The development of this method was essential in order that the free-field basis states could be used to investigate the quadratic Zeeman effect in highly excited alkali and alkaline earth atoms, since configuration mixing and quantum defects had to be taken into account. The large principal quantum numbers involved in these calculations implied that the original approach of Bates and Damgaard would not be applicable. The author's method, which is based upon Gauss-Laguerre quadrature and Chebyshev expansions, has provided an efficient and reliable scheme for computing the required integrals.

As discussed in Chapters 4 and 5, the new numerical methods for evaluating radial integrals in the Coulomb approximation have been of interest to research workers in several other areas of atomic spectroscopy. In particular, the idea of using Chebyshev expansions for computing the Whittaker function $W_{\kappa,m}(x)$ has been adopted by Prof. Van Regemorter's group at the Meudon Observatory, Paris. They have been interested in extending the numerical techniques to compute $W_{\kappa,m}(x)$ and $M_{\kappa,m}(x)$, with large positive and negative κ, in the context of electron-atom scattering theory. Copies of the author's computer programs have also been distributed

to about a dozen other research centres, including the Universities of Reading, Caen and Rhur-Universitat, Bochum.

The author's method of computing radial integrals has recently been used in the development of alternative methods of computing similar integrals involving very high effective principal quantum numbers. One of these, Picart et al. (1978), was a method based upon a series expansion of the integral which gives accurate results for indefinitely large ν, ν', although there are restrictions on $|\nu - \nu'|$. In another case the author's method has been used to assess the accuracy of a new technique developed by Van Regemorter et al. (1979). The latter technique has, in turn, been used by Fonck and Tracy (1980) in the development of yet another method of calculating radial integrals involving moderately low to very high effective principal quantum numbers, using the WKB approximation to compute the radial wavefunctions.

7.2 AREAS FOR FURTHER RESEARCH

Interest in the quadratic Zeeman effect in neutral alkali and alkaline earth atoms has increased since the research described in this thesis was carried out. Considerable progress has been made in experimental techniques. Researchers at the Argonne Laboratory have recently published detailed densitometer traces of the σ^+ absorption spectra of Ba I, Sr I and Li I in magnetic fields ranging from 10 - 50 kG (Lu et al. 1978a,b).

However, the development of a satisfactory theory to explain these complex spectra has made relatively slow progress. A number of areas in which further research is needed are outlined below.

7.2.1 Free- Field Basis

As remarked in Section 6.4 further work is needed to investigate the domain of validity of the free-field basis. The author's research has provided most of the computational methods for such an investigation, but a practical method of computing lower bounds to eigenenergies still needs to be developed. Although a number of ideas for doing this have been outlined*, implementation in the form of computer programs has yet to be carried out.

We note that calculations of this large magnitude are becoming increasingly practical, due to the easy availability of cheap and powerful mini- and micro-computers.

7.2.2 Other Bases

Fano (1977) has suggested that spheroidal harmonics should be used in the expansion of the quantum mechanical wave function (cf. equation 2.5, in which spherical harmonics are used). This formulation has been extended by Lu et al. (1978b) but, to the author's knowledge, no numerical calculations have been performed using this approach.

7.2.3 Study of Hydrogen-Like Systems

Being given the experimental data relating to the quadratic Zeeman effect in alkalis and alkaline earths, one is naturally interested in the corresponding phenomena in the simpler system of a hydrogen atom. This question is also of interest to astrophysicists and students of certain effects in the solid state. Edmonds (1973) has suggested that the so-called Sturmian basis would be appropriate in such calculations. Since this basis is complete and discrete it may be useful in describing bound states in which the wavefunctions are grossly distorted by the magnetic

---

* see Bazley, N.W. and Fox, D.W., Phys. Rev. 124, pp 483-492, (1961).

field, and in dealing with the resonances in the continuum observed by Gross (1959) and others.

7.3 SEMI-CLASSICAL METHODS

All of the approaches outlined above are likely to give rise to problems of theoretical interpretation when applied to the spectral regions where configuration mixing is very strong. The fact that most quantum mechanical methods imply working with very large matrices, and the large size of electron orbits in this spectral region (measured in thousands of Bohr) indicate that semi-classical methods might be appropriate.

A semi-classical approach to the resonances in the region of the series limit of the Garton-Tomkins σ spectra was adopted by Edmonds (1970) and Starace (1973). Their approach, which used the Bohr-Sommerfeld quantization condition, was first developed by solid state physicists to explain the exciton spectra of semi-conductors in high magnetic fields (see the review by Baldereschi and Bassani 1970).

Connerade (1974) developed an extended Bohr model, incorporating Landau quantization, and used it to discuss the appearance of satellite lines in the Ba I spectra of Garton and Tomkins.

More recently Dr. Edmonds has applied semi-classical methods to the negative energy regions of the Garton-Tomkins spectra. This work is based on the ideas of Percival (1974), and involves numerical computation of the classical orbits of an electron moving in a central electrostatic and a uniform magnetic field. This problem can be formulated as as a dynamical system with only two degrees of freedom, and the technique of regularization can be used to remove the theoretical and computational difficulties raised by the central singularity. In this way the model

reduces to a system consisting of two harmonic oscillators coupled by a strong non-linear term.

The two major questions raised by this approach are:

(i) what are the important classical orbits of the excited electron, and what is their structure?

(ii) how can the characteristics of the classical orbits be used to give an approximation to the observed quantum mechanical spectra, in terms of energy values and estimates of relative intensities?

Some of these issues are discussed in a recent thesis by Pullen (1981), but much more research is needed.

A complete theoretical explanation of the quadratic Zeeman effect will require a combination of quantum mechanical and semi-classical methods.

REFERENCES

Abramowitz, M. and Stegun, I.A. (Eds) (1964).
"Handbook of Mathematical Functions"
(Washington D.C. : National Bureau of Standards).

Andersen, N., Jensen, K., Jepsen, J., Melskens, J. and Veje, E. (1975).
Z. Physik A, 273, pp 1-8.

Angel, J.R.P. and Landstreet, J.D. (1971).
Astrophys. J. Lett. 165, L71-5.

Angel, J.R.P. and Landstreet, J.D. (1972).
Astrophys. J. Lett. 178, L21-2.

Armstrong, B.H. and Purdum, K.L. (1966).
Phys. Rev. 150, p 51.

Baldereschi, A. and Bassani, F. (1970).
"Proc. 10th Int. Conf. on Physics of Semiconductors, Cambridge, Mass".
Eds: S.P. Keller, J.C. Hensel and F. Stern,
(AEC Oak Ridge CONF - 700801), pp 191-6.

Bates, D.R. and Damgaard, A. (1949).
Phil. Trans. Roy. Soc. A242, pp 101-22.

Brooks, H. and Ham, F.S. (1958).
Phys. Rev. 112, pp 344-61.

Burgers, J.M. (1919).
"Het Atoomodel van Rutherford-Bohr"
(Haarlem: De Erven Loosjes).

Burgess, A. and Seaton, M.J. (1960).
Monthly Notices Roy. Astron. Soc. 120, pp 121-51

Cabib, D., Fabri, E. and Fiorio, G. (1971).
Solid St. Commun. 9, pp 1517-20.

Canuto, V. and Kelly, D.C. (1972).
Astrophys. Space Sci. 17, pp 277-91.

Clenshaw, C.W. (1955).
Math. Tab. Wash. 9, p 118.

Clenshaw, C.W. (1957).
Proc. Camb. Phil. Soc. 53, pp 134-149.

Clenshaw, C.W. (1962).
"Chebyshev Series for Mathematical Functions"
NPL Math. Tab. Vol. 5
(London: HMSO).

Condon, E.U. and Shortley, G.H. (1963).
"The Theory of the Atomic Spectra"
(Cambridge: Cambridge University Press).

Connerade, J.P. (1974).
Proc. Roy. Soc. A339, pp 127-32.

Crossley, R.J.S. (1969).
Advances Atom. Molec. Phys. 5, pp 237-96.

Curtis, A.R. (1964).
"Coulomb Wave Functions"
Royal Society Mathematical Tables, Vol. 11
(Cambridge: Cambridge University Press).

Ducas, T.W., Littman, M.G., Freeman, R.R. and Kleppner, D. (1975).
Phys. Rev. Lett. 35, pp 366-9.

Duff, I.S. (1976).
"A Survey of Sparse Matrix Research"
Harwell Technical Report (HL 76/485).

Edmonds, A.R. (1968).
"Angular Momentum in Quantum Mechanics"
(Princeton: Princeton University Press).

Edmonds, A.R. (1970).
J. Physique, 31, Colloq. C4, pp 71-4.

Edmonds, A.R. (1973).
J. Phys. B : Atom. Molec. Phys. 6, pp 1603-15.

Elliot, R.J. and Loudon, R. (1959).
J. Phys. Chem. Solids, 8, pp 382-8.

Erdélyi, A. (Ed) (1953).
"Higher Transcendental Functions", Vol. 1
(New York: McGraw-Hill).

Fano, U. (1977).
Colloque International, No. 273,
C.N.R.S., pp 127-37.

Foldy, L.L. (1958).
Phys. Rev. 111, p 1093.

Fonck, R.J. and Tracy, D.H. (1980).
J. Phys. B : Atom. Molec. Phys. 13, L101-4.

Fox, L. and Parker, I.B. (1968).
"Chebyshev Polynomials in Numerical Analysis"
(Oxford: Oxford University Press).

Friedrich, H., Katterbach, K. and Trefftz, E. (1970).
J. Quant. Spectry. Radiative Transfer, 10, pp 11-16.

Garstang, R.H. (1977).
Rep. Prog. Phys. 40, pp 105-154.

Garstang, R.H. and Kemic, S.B. (1972).
In "The Structure of Matter"
Ed: B.G. Wybourne,
(Canterbury, New Zealand: University of Canterbury Press), pp 396-404.

Garstang, R.H. and Kemic, S.B. (1974).
Astrophys. Space Sci. 31, pp 103-15.

Garton, W.R.S. and Tomkins, F.S. (1969a).
Astrophys. J. 158, pp 839-45.

Garton, W.R.S. and Tomkins, F.S. (1969b).
Astrophys. J. 158, pp 1219-30.

Gautschi, W. (1967).
SIAM Review, 9, pp 24-82.

Gautschi, W. (1975).
"Computational Methods in Special Functions".
In "Theory and Application of Special Functions"
Ed: R.A.Askey,
(New York: Academic Press).

Gordon, W. (1929).
Ann. d. Physik, 2, pp 1031-56

Gross, E.F. (1959).
J. Phys. Chem. Solids, 8, p 172.

Guth, E. (1929).
Z, Phys. 58, pp 368-72.

Haidemenakis, E.D. (Ed) (1969).
"Physics of Solids in Intense Magnetic Fields"
(New York: Plenum Press).

Halpern, O. and Sexl. T. (1929).
Annalen d Physik, 3, p 565.

Harting, D. and Klinkenberg, P.F.A. (1949).
Physica, 14, pp 669-83.

Hartree, D.R. (1928).
Proc. Camb. Phil. Soc. 24, pp 89-110.

Hasegawa, H. and Howard, R.E. (1961).
J. Phys. Chem. Solids, 21, pp 179-98.

Herzfeld, K.F. (1914).
Phys. Z. 15, pp 193-8.

Jeffreys, H. (1962).
"Asymptotic Approximations"
(London: Oxford University Press).

Jenkins, F.A. and Segrè, E. (1939).
Phys. Rev. 55, pp 52-8.

Kemic, S.B. (1974).
Joint Institute for Laboratory Astrophysics,
Report No. 113, pp 1-27.

Kemic, S.B. (1975).
Astrophys. Space Sci. 36, pp 459-66.

Kemp, J.C., Swedlund, J.B., Landstreet, J.D. and Angel, J.R.P. (1970).
Astrophys. J. Lett. 161, L77-9.

Kohn, W. and Luttinger, J.M. (1955).
Phys. Rev. 98, p 915.

Krylov, V.I. (1962).
"Approximate Calculation of Integrals"
(New York: Macmillan).

Lamb, F.K. and Sutherland, P.G. (1974).
In "Physics of Dense Matter"
Ed: C.J. Hansen,
(Dordrecht, Holland: Riedel), pp 265-85.

Landau, L.D. (1930).
Z. Phys. 64, pp 629-37.

Landstreet, J.D. and Angel, J.R.P. (1971).
Astrophys. J. Lett. 165, L67-70.

Larsen, D.M. (1968).
J. Phys. Chem. Solids, 29, pp 271-80.

Layzer, D. and Garstang, R.H. (1968).
Ann. Rev. Astron. Astrophys. 6, pp 449-94.

Le Dourneuf, M. and Vo Ky Lan, (1977).
J. Phys. B : Atom. Molec. Phys. 10, L35-42.

Lindgård, A. and Nielsen, S.E. (1975).
J. Phys. B : Atom. Molec. Phys. 8, pp 1183-99.

Lisitsa, V.S. and Sholin, G.V. (1972).
Sov. Phys. JETP, 34, p 484.

Littman, M.G., Zimmerman, M.L., Ducas, T.W., Freeman, R.R. and Kleppner, D.
Phys. Rev. Lett. 36, pp 788-91, (1976).

Lu, K.T., Tomkins, F.S., Crosswhite, H.M. and Crosswhite, H. (1978a).
Phys. Rev. Lett. 41, pp 1034-6.

Lu, K.T., Tomkins, F.S. and Garton, W.R.S. (1978b).
Proc. Roy. Soc. A362, pp 421-4.

Luke, Y.L. (1959).
Math. Comp. 13, pp 261-71.

Luke, Y.L. (1969).
"The Special Functions and their Approximations: Vol. II"
(New York: Academic Press).

Luke, Y.L. and Wimp, J. (1963).
Math. Comp. 17, pp 395-404.

Miller, G.F. (1966).
SIAM J. Numer. Anal. 3, pp 390-409.

Norcross, D.W. (1973).
Phys. Rev. A7, pp 606-16.

O'Connell, R.F. (1974).
in "Physics of Dense Matter"
Ed: C.J. Hansen,
(Dordrecht, Holland: Riedel), pp 287-300.

Oertel, G.K. and Shomo, L.P. (1968).
Astrophys. J. Suppl. 16, pp 175-217.

Olver, F.W.J. (1974).
"Asymptotics and Special Functions"
(New York and London: Academic Press).

Peach, G. (1965).
Monthly Notices Roy. Astron. Soc. 130, pp 361-77.

Peach, G. (1967).
Memoirs Roy. Astron. Soc. 71, pp 1-11.

Percival, I.C. (1974).
J. Phys. A : Math. Gen. 7, p 794.

Percival, I.C. and Pomphrey, N. (1976).
Molec. Phys. 31, p 97.

Picart, J., Edmonds, A.R. and Tran-Minh, N. (1978).
J. Phys. B : Atom. Molec. Phys. 11, L651-4.

Praddaude, H.C. (1972).
Phys. Rev. A, 6, pp 1321-4.

Preston, G.W. (1970).
Astrophys. J. Lett. 160, L143-5.

Pullen, R. (1981).
Ph.D Thesis, University of London.

Risberg, P. (1955).
Ark. Fys. 9, pp 483-94.

Risley, J.S. and Jebule, R. (1975).
"Abstracts of 9th International Conference on the Physics of Electronic and Atomic Collisions, Seattle, 24-30 July, 1975"
(Seattle: University of Washington Press).

Rutishauser, H. and Schwartz, H.R. (1963).
Numer. Math. 5, pp 273-289.

Schiff, L.I. and Snyder, H. (1939).
Phys. Rev. 55, pp 59-63.

Seaton, M.J. (1958).
Monthly Notices Roy. Astron. Soc. 108, pp 504-18.

Seaton, M.J. (1966).
Proc. Phys. Soc. 88, pp 801-15.

Shao, T.S., Chen, T.C. and Frank, R.M. (1963).
Math. Comp. 18, pp 598-616.

Slater, L.T. (1960).
"Confluent Hypergeometric Functions"
(Cambridge: Cambridge University Press).

Smith, E.R., Henry, R.J.W., Surmelian, G.L., O'Connell, R.F. and Rajagopal, A.K. (1972).
Phys. Rev. D, 6, pp3700-1.

Sobel'man, I.I. (1972).
"Introduction to the Theory of Atomic Spectra"
(Oxford: Pergamon Press).

Starace, A.F. (1973).
J. Phys. B : Atom. Molec. Phys. 6, pp 585-90.

Stebbings, R.F., Latimer, C.W., West, W.P., Dunning, F.B. and Cook, T.B. (1975).
Phys. Rev. A12, pp 1453-8.

Stroud, A. and Secrest, D. (1966).
"Gaussian Quadrature Formulas"
(Englewood Cliffs, N.J.: Prentice Hall).

Sturmelian, G.L., Henry, R.J.W. and O'Connell, R.F. (1974).
Phys. Lett. 49A, pp 431-2.

Tran-Minh, N., Feautrier, N. and Van Regemorter, H. (1976).
J. Quant. Spectry. Radiative Transfer, 16, pp 849-59.

Van Regemorter, H., Hoang, Binh Dy and Prud'homme, M. (1979).
J. Phys. B : Atom. Molec. Phys. 12. pp 1053-61.

Van Vleck, J.H. (1932).
"Theory of Electric and Magnetic Susceptibilities"
(Oxford: Oxford University Press).

Whittaker, E.T. and Watson, G.N. (1946).
"Modern Analysis"
(Cambridge: Cambridge University Press).

Wiese, W.L., Smith, M.W. and Glennon, B.M. (1966).
"Atomic Transition Probabilities", Vol. 1,
NSRDS - NBS 4,
(Washington, D.C.: National Bureau of Standards).

Wilkinson, J.H. (1960).
Numer. Math. 2, pp 319-340.

Wilkinson, J.H. (1963).
"Rounding Errors in Algebraic Processes",
NPL Notes on Applied Science No. 32,
(London: HMSO).

Wimp, J. (1967).
Math. Comp. 21, pp 639-46.

Wimp, J. (1970).
SIAM Studies in Appl. Math. 6, pp 110-23.

Yafet, Y., Keyes, R.W. and Adams, E.N. (1956).
J. Phys. Chem. Solids, 1, pp 137-42.

Zhilich, A.G. and Monozon, B.S. (1967).
Sov. Phys. - Solid State, 8, pp 2846-50.